1971

Hydrogenation of ethylene on iridium thin films

Paul Bruce Masterson
Iowa State University

Hydrogenation of ethylene on iridium thin films

by

Paul Bruce Masterson

A Dissertation Submitted to the
Graduate Faculty in Partial Fulfillment of
The Requirements for the Degree of
DOCTOR OF PHILOSOPHY

Major Subject: Physical Chemistry

Approved:

Signature was redacted for privacy.

In Charge of Major Work

Signature was redacted for privacy.

Head of Major Department

Signature was redacted for privacy.

Dean of Graduate College

Iowa State University
Of Science and Technology
Ames, Iowa

1971

TABLE OF CONTENTS

INTRODUCTION

It is well known that most transition metals, including iridium, will catalyze the hydrogenation of C_2H_4 to C_2H_6 (1). In recent years R. S. Hansen and students have extensively investigated the adsorption and thermal decomposition of C_2H_4 on Ir using both field ion microscopy and the flash filament technique (2-5). They found that when an Ir filament, covered with a monolayer of chemisorbed C_2H_4 (or any other simple hydrocarbon), was flash heated hydrogen was virtually the sole desorption product (Figure 1).

Concurrently, R. W. Roberts of the General Electric Research Laboratory published studies of C_2H_4 and C_2H_6 adsorption on evaporated thin films of Ir (6, 7). Figure 2 is illustrative of his results, showing C_2H_6 and CH_4 as the principal products from the isothermal adsorption of C_2H_4 on Ir at 100° C. From other experiments he concluded that the CH_4 resulted from decomposition of C_2H_6.

While this difference in results may appear surprising at first glance, there were major differences in the experimental techniques and conditions employed in the two studies. The number of molecules of C_2H_4 adsorbing or reacting per unit area was roughly the same in both types of experiments, but Roberts' films had a geometric area of 300 cm^2 and a microscopic area available for adsorption (as measured by low temperature oxygen adsorption) of about

2100 cm^2, compared to an adsorption area of 1-2 cm^2 for flash filament. The C_2H_4 dose on a film (admitted "instantaneously") corresponded to an initial dose pressure of about 30 μ in the one-liter reaction volume, whereas C_2H_4 was dosed in a flow system at a pressure on the order of 10^{-7} torr (10^{-4} μ)--some five orders of magnitude lower--and required several minutes to achieve monolayer coverage. Perhaps the most significant difference is that the film reactions were isothermal while the flash filament desorption products were observed as the filament was heated (flashed) after the C_2H_4 flow had been discontinued.

Hansen et al. (3) have proposed that a reaction mechanism whereby C_2H_4 from the gas phase reacts directly with hydrogen of an adsorbed species so that no C_2H_6 is formed on the surface, accounting for the absence of C_2H_6 in the flash desorption products.

The present study was undertaken in an effort to correlate the results of these two sets of experiments and verify or disprove the mechanistic proposal. The thin film experimental method was chosen because it appeared that it could better be adapted to approach flash filament conditions than vice versa.

In the course of the investigation, significant information concerning hydrogen adsorption and C_2H_6 decomposition on Ir was obtained and will be presented herein.

EXPERIMENTAL

Introduction

Experimental work in this study consisted primarily of dosing a known amount of a high purity gas onto a freshly prepared iridium surface in a closed reaction volume and measuring the gas adsorption and product evolution as functions of time. The basic components of the vacuum system constructed to accomplish this purpose were: a) a thermostated ultrahigh vacuum cell for deposition of Ir thin films; b) a capacitance manometer for measuring the gas dose and the total pressure throughout the course of an experiment; c) a quadrupole mass spectrometer connected to the reaction cell through a suitable leak for determination of gas composition during reaction.

Instrumentation and Calibration

The complete vacuum system (shown in Figure 3 except for traps and pumps) consisted of four vacuum lines. The bakeable portion, lines 1 and 2, were constructed of Pyrex glass and stainless steel and employed metal valves throughout, while greased stopcocks were used on lines 3 and 4.

The reaction cell and mass spectrometer on line 1 were pumped by a three-stage mercury diffusion pump backed by two liquid nitrogen traps. Except for valve C2 and its connecting tubulation, the entire line (including one trap)

was mounted on the front of the supporting rack (Figure 4) where it could be readily enclosed with a portable oven and baked to 400° C. A vacuum of 10^{-9} torr or better was achieved on this line prior to the beginning of each experiment.

Line 2, pumped by a two-stage mercury diffusion pump and a single liquid nitrogen trap, served primarily as a gas handling line, so that large amounts of gas did not have to be pumped away through the ultrahigh vacuum line. When the system was initially put into operation this line, including the capacitance manometer, was baked to 350° C with a small oven. Subsequently, the glass tubulation and valves that could be left open (C2 and C5) were routinely baked to 300° C with heating tapes. The gas reservoir valves attained temperatures of 100-150° C during bakeout. The manometer was not baked after the initial bakeout. The background pressure at the beginning of each experiment was 10^{-7} torr or lower. No pressure buildup was detectable on the manometer if the volume V3 was closed off for several hours, so it was assumed that any contamination from background gases in line 2 was negligible.

The backside of the capacitance manometer (line 3) was maintained at a pressure below 10^{-5} torr by a single-stage mercury diffusion pump and a single liquid nitrogen trap. This line was completely isolated from lines 1 and 2 (except

that lines 2 and 3 shared a common mechanical forepump) obviating any possibility of mercury or stopcock grease contamination from the McLeod gauge. A liter of argon at atmospheric pressure was stored behind valve A3 for periodic checks of the capacitance manometer calibration against the McLeod gauge.

The fourth line was used only during these periodic checks for raising and lowering the mercury in the McLeod gauge.

The capacitance manometer (Granville-Phillips, Boulder, Colo.) was used for all experimental dosing and reaction pressure measurements. Its head was a stainless steel cylindrical chamber divided into two sections by a thin metal diaphragm which comprised one side of a parallel plate capacitor; the other side was a fixed probe sealed into the head through an electrically insulating feedthrough. The position of the diaphragm relative to the probe, and hence the capacitance, was determined by the pressure differential across it--that is, the pressure differential between lines 2 and 3. This capacitor, together with balancing capacitors mounted on a detachable (for bakeout) portion of the head, formed one arm of a capacitance bridge. The audio-oscillator, detector, and associated circuitry were mounted on a remote, rackmounted chassis. The minimum sensitivity of the unit was 5×10^{-5} torr and the reference side of the

head (line 3) was maintained at a pressure well below this figure in normal operation, so that absolute pressure was being measured in line 2. The dc output from the detector was normally recorded on a Moseley X-Y recorder, operated in time sweep mode (Figure 5).

To minimize zero drift the head was thermostated by circulating water from a constant temperature bath through Tygon tubing closely wrapped around the head, which was then covered with glass wool and aluminum foil. It was found that a one-degree change in head temperature resulted in a zero drift equivalent to a 13 μ pressure differential. Thermostating reduced drift below .05 μ over a 15 minute period, and it seldom exceeded 0.2 μ over several hours.

The manometer had five readout pressure ranges with nominal full-scale values of 10, 30, 100, 300, and 1000 μ. Absolute calibration of the 1000 μ range sensitivity (in μ/scale division) was determined against the McLeod gauge by admitting argon into V3 to a given manometer reading, then nulling the manometer to give a zero pressure differential by admitting argon into the backside common to the McLeod gauge. The pressure was then determined on the McLeod gauge and divided by the manometer reading to obtain the sensitivity. Periodic checks over several months showed variations of about 3% in the calibration. The manufacturer's (Consolidated Vacuum Corporation,

Rochester, New York) calibration of the McLeod gauge was assumed accurate and no independent check was made of it.

The sensitivity ratio of each pair of adjacent ranges was determined in the following manner. Argon from a one-liter (STP) reservoir was leaked into the closed volume V3 at a rate such that 2 to 5 minutes were required to reach full scale on the less sensitive range. During this period the output (followed on a recorder) was switched repeatedly between ranges so that the recording gave a determination of both slopes. The sensitivity ratio was given by the inverse ratio of the slopes. This method proved to be much more precise than calibration of each range individually against the McLeod gauge.

It was observed that the linearity of these pressure-time recordings was excellent from 0 to 50 scale divisions (full scale = 100 divisions) on each range, but above 50 the curves fell off in a pattern common to all ranges. Since, at most, 150 μ-liters of argon was leaked from the 7×10^5 μ-liters (one liter-atmosphere) reservoir on a given determination, the decrease in leak rate should have been less than .05%, assuming constant temperature. In Figure 6 the quantity $\epsilon = d'-d$ is plotted against d for all five ranges, where d is the number of scale divisions read at a given pressure (time) and d' is the number read from the extrapolation of the linear portion of the curve

at the same pressure (time). The fact that all ranges can be fit with a single correction curve indicates that the linearity of capacitance with pressure from 0 to 1000 μ is excellent (0.5%), and that the nonlinearity must originate in an amplification stage of the output. Reproducibility of the sensitivity ratios between ranges was about 1%. The relationship used in this work to convert a manometer reading d_R on range R to pressure P was

$$P = s_R(d_R + \epsilon) \qquad (1)$$

where s_R is the sensitivity of range R (μ/division). For $d_R > 50$, ϵ was read from Figure 6, and for $d_R < 50$, $\epsilon = 0$.

The manometer response time, limited chiefly by the conductance of the system, was of the order of 1 second (see Figure 7). The conductance between the head and reaction cell through 95 cm of 1.2 cm i.d. tubulation was calculated to be 0.23 l/sec (8), and was found to be 0.18 l/sec experimentally in the following manner. When a leak rate of .052 μ-liter/sec was established through valve C1 for an experiment in which C_2H_4 was dosed on a clean Ir film, a steady pressure of 0.28 μ was observed on the manometer. It was assumed that the clean film pumped well enough to maintain the pressure below 0.01 μ in the reaction cell, so that the pressure difference was essentially 0.28 μ. The conductance is defined as the quotient of the flow rate

divided by the pressure difference responsible for the flow.

To estimate the response time of the system from conductance considerations alone, consider an idealized system of two volumes V_1 and V_2 which are connected by tubulation of conductance F and negligible volume. If a pressure $P = P_0$ is established in V_1 at time $t = 0$ with zero pressure in V_2, the pressure will decay according to the equation

$$P = P_e + e^{-\alpha t} (P_0 - P_e) \qquad (2)$$

where $P_e = P_0 V_1/(V_1 + V_2)$ is the equilibrium value of P and $\alpha = F(V_1 + V_2)/V_1 V_2$. Taking F = 0.2 l/sec, V_1 = 0.15 l, and V_2 = 0.80 l for values corresponding to the real system, α is calculated to be 1.6 sec^{-1}. The half-life for the decay is given by $t_{1/2} = (1/\alpha) \ln 2 = 0.43$ sec, while 90% equilibration requires 1.4 sec, in good agreement with the observed response. This treatment is strictly valid only for pressures in the molecular flow region, which for this system was 5 μ and below. The conductance should increase with pressure when the pressure is greater than 5 μ.

Partial pressure analysis of the reaction mixtures was made from mass spectra (Figure 8) of the gas mixtures leaked through valve A1. The mass spectrometer (Electronic Associates, Inc., Palo Alto, California, model Quad 150) consisted principally of three sections: ionizing region,

quadrupole mass filter, and ion detector. Gas molecules were ionized in the first section by 70-volt electrons from an emission current variable from 0.25 to 3.0 mA, but normally set at 1.0 mA. The ions were drawn into the mass filter (a high frequency electrical quadrupole field which oscillated perpendicularly to the initial ion trajectory) with constant voltage (energy). For given amplitude of the quadrupole field, only ions of a single mass-per-charge (m/e) ratio were able to pass through the field without striking the electrodes and becoming neutralized.

These emerging ions were accelerated and then impinged upon the first dynode of a 14-stage electron multiplier which amplified the resulting current with a gain greater than 10^8, when the standard 3000-volt potential drop was used across the multiplier. At fixed emission current (e.g., 1.0 mA), the ion current i_m for a species of mass m was proportional to the pressure p of the parent species

$$i_m = q_m p \tag{3}$$

where the sensitivity q_m is a constant. The ion current is defined herein as the electron multiplier output (although, strictly speaking, it is the unamplified current at the first dynode of the multiplier); hence q_m depended directly on the multiplier gain, and accurate pressure measurement depended on a stable gain. At 3000 volts the multiplier

saturated (gain decreased) when the output current reached 100 μA, which put too low a limit on the maximum pressure that could be measured. Consequently the 3000 volts furnished from the power supply was reduced to 2200 volts (by installing a 5-megohm resistor in series with the 14 megohms of the electron multiplier) thereby reducing the gain of the multiplier more than an order of magnitude and increasing the upper pressure limit correspondingly. (Saturation current dropped to about 80 μA.) Under these conditions the useful range of the spectrometer was about 10^{-12} to 10^{-6} torr.

The mass range of the instrument was 150 amu, and any portion of this range from 4 to 150 amu wide could be swept continuously at a sweep rate variable from 0.01 to 10 cycles per second. The rate was uniform across any range chosen, so that mass (m/e, actually) was a linear function of time for each sweep. Alternatively, the spectrometer could be operated such that the ion current of a single mass was constantly monitored.

In normal operation the ion current was fed into an operational amplifier (Tetronix "Type O") having a one-megohm feedback resistor to give a 1.0 volt/μA conversion of current to voltage (Figure 5). The resulting signal was connected to both channels of a two-channel, time-drive chart recorder (Brush Instruments, Cleveland, Ohio, model Mark 280).

The sensitivity of one channel was set from 4 to 20 times that of the other so that mass peaks (ion currents) in a given spectrum differing by four orders of magnitude or more could be detected. Figure 8 shows a typical experimental recorder trace with a sweep width of 0 to 44 amu and a sweep rate of one cycle every 8 sec or about 5.5 amu/sec. Sweep rates as high as 25 amu/sec were used with little deterioration in the recorder signal.

During partial pressure determinations the mass spectrometer was pumped continuously as gas from the reaction cell was leaked into it. As discussed in Appendix A, the pressure of a given gaseous species in the mass spectrometer ideally will be directly proportional to its pressure in the reaction cell if the leak and pumping are strictly molecular flow phenomena. When this is true

$$i_m = s_m P_m \qquad (4)$$

which is the same as Equation 3 except that here P_m represents the pressure of species of mass m in the reaction cell (some 4 to 5 orders of magnitude greater than that in the mass spectrometer) and consequently s_m is 4 to 5 orders of magnitude smaller than q_m.

The validity of this equation in the case of argon is illustrated in Figure 9. The dimensionless parameter a_m plotted as the ordinate is defined by the equation

$$s_m = a_m \sigma_m \tag{5}$$

where σ_m is a constant with units the same as s_m. Essentially a correction factor for nonlinearity, a_m was experimentally determined from the equation

$$a_m = \frac{i_m P_m^o}{P_m i_m^o} \tag{6}$$

which is derived by setting a_m equal to unity at some arbitrary value of $i_m = i_m^o$, for which $P_m = P_m^o$. In Figure 9 $i_m^o = 1.0$ uA (m = 20, 40) and $\sigma_{40} = 0.255$ uA/u. With a fixed leak valve setting i_m was measured for argon pressures (determined with the capacitance manometer) ranging from 0.4 μ to 500 u in the reaction cell. The graph shows that the deviation from linearity (deviation of a_m from 1.0) is slight over three orders of magnitude of ion current. The sharp drop-off at 80 μA is caused by electron multiplier saturation.

In Figure 10 the sensitivity for C_2H_6 relative to argon (f_{30}) is plotted against i_{30}. In general the relative sensitivity f_m may be defined as

$$f_m = a_m \sigma_m / \sigma_{40} . \tag{7}$$

In practice it was determined from the equation

$$f_m = \frac{i_m}{i_{40}} \frac{P'_{40}}{P'_m} \sigma_{40} \tag{8}$$

where P'_{40} and P'_m are fixed pressures of argon and gas of mass m (C_2H_6 in Figure 10) in the reaction cell, and i_m (i_{30}) and i_{40} were measured for different settings of the leak valve A1. It is assumed in this method that f_m and a_m are functions of i_m only, requiring that the leak rate for given valve setting be strictly proportional to the partial pressure of an individual species throughout the pressure range used, regardless of the gas composition. Representative values of f_m are given in Table 1.

Although the variation in sensitivity of C_2H_6 was more pronounced than that of argon, it was still less than 10% ($\pm$ 5% from the mean) for an order of magnitude change in ion current. Constant sensitivity values were generally assumed in the partial pressure analysis.

The f_m determinations were made under steady-state flow conditions in the mass spectrometer. It was found that argon, H_2, C_2H_6, and CH_4 achieved steady state (95% equilibrium) within 2-3 seconds, but as shown in Figure 11, C_2H_4 was much slower to reach steady state. Approximately equal pressures of C_2H_6 and C_2H_4 were established in the reaction cell and A1 was then opened at t = 0. (Tailing at the beginning was caused by the time required to open A1 to the desired setting--the rise time of C_2H_6 is less than might be inferred from this graph.)

There is no mass species in the cracking pattern of

C_2H_4 which does not also appear in the C_2H_6 cracking pattern, but i_{30} appears only from C_2H_6 and is equal to i_{26} (within 2%). Hence, for a mixture of C_2H_4 and C_2H_6, C_2H_4 could be determined from the equation

$$i_{26} - i_{30} = s_{26} P_{26}$$

where P_{26} is used to represent C_2H_4 pressure for the sake of uniformity in the subscripts, although the mass number of C_2H_4 is 28. In the cracking patterns of both hydrocarbons i_{28} is the major peak, while i_{30} is 25% of i_{28} for C_2H_6 and i_{26} is 60% of i_{28} for C_2H_4.

Procedure

The general experimental procedure for dosing C_2H_6 or C_2H_4 on a bare or hydrogen-covered Ir film is outlined below.

1. Reduce background pressure in volumes V1 and V2 to 10^{-9} torr or lower and in V3 to 10^{-7} or lower.
2. Establish the pressure ratio P(V2 + V3)/P(V3) by argon expansion with cell at reaction temperature.
3. Adjust valve A1 for a suitable leak rate with argon; pump argon away.
4. Set C_2H_6 or C_2H_4 dose rate and freeze reservoir (low pressure doses only).
5. Deposit Ir film with cell at 100° C.
6. (Optional) Dose film with hydrogen and pump away excess.

7. Admit measured hydrocarbon dose to V3 (high pressure experiments only).
8. Start recorder systems.
9. Dose hydrocarbon on film by opening valve C2 (high pressure) or by thawing hydrocarbon reservoir (low pressure), and simultaneously start timer.

The volumes V2 and V3 were estimated to be 800 $\pm$ 50 cm^3 and 150 $\pm$ 10 cm^3, respectively, by measurement of their linear dimensions. The ratio V3/(V2 + V3) = 150/950 = 0.158 agreed excellently with the experimental value of 0.162 determined by gas expansion (assuming the ideal gas law valid). At room temperature the number of molecules per unit pressure N/P = V/(RT) for V = 150 cm^3 is 5.0 x 10^{15} molecules/μ; all dosing measurements were based on this figure. The dimensions of V3 were unchanged throughout the study; the cell in V2 was replaced frequently, but the change in volume was probably never more than 30 cm^3. Prior to each experiment, argon was expanded from V3 into V2 (second step in the above outline) with the cell thermostated at the reaction temperature to determine the number of molecules per unit pressure for the entire reaction volume (V2 + V3). For the cell at 100° C, for example, this figure varied from 0.029 x 10^{18} to 0.030 x 10^{18} molecules/μ. At all cell temperatures used, the calculated value, assuming 500 cm^3 at reaction temperature and 450 cm^3 at room temperature, agreed well

with the experimentally determined figure, indicating that there was no significant thermal transpiration effect.

With argon in the cell at a pressure comparable to the anticipated reaction pressure, the leak valve was set to give an ion current (i_{40}) on the order of 5 uA. This typically resulted in an s_{40} value of 0.25 uA/μ (i.e., P_{40} = 20 μ). The time required for 1% of the argon to leak away under these conditions was found to be about 4000 seconds; for the same valve setting hydrogen would leak out 4.5 times as fast. In all cases the amount of gas leaked out during reaction was ignored in mass balance calculations. For long reactions (over 1000 seconds), sampling was done intermittently.

As implied in the outline above, two principal dosing techniques were used. In the "high pressure" doses, a measured amount of the dosant was admitted into V3 from its reservoir and the experiment was initiated by opening valve C2 rapidly (1 to 2 seconds required) with a ratchet wrench. For a monolayer dose, the initial pressure over the film was of the order of 30 μ (3×10^{-2} torr).

If a gas is introduced at a constant rate L (molecules/sec) into an idealized closed system where pumping by surface adsorption is characterized by a constant sticking coefficient σ, then a steady-state pressure P will be established over the surface such that, from the laws of

gas kinetics,

$$L = \sigma A P (2\pi mkT)^{-1/2} \qquad (9)$$

where A is the surface area, m the mass of the gas molecule, k Boltzmann's constant, and T the absolute temperature. At 300° K for m = 28 amu, the pressure P is given in microns by the equation

$$P = \frac{L'}{\sigma} (1.8 \times 10^{-3} \text{ μ-sec/monolayer}). \qquad (10)$$

L', having units of monolayer/sec, is defined by $L' = L/(An_s)$, where n_s is the number of sites per cm^2 on iridium and was taken as 0.7×10^{15} on the basis of two surface Ir atoms per C_2H_4 site.

The second principal dosing technique--"low pressure" dosing--involved dose rates of this nature. Monolayer quantities of the dosant were leaked in over a period of from 500 to 6000 seconds, equivalent to dosing pressures of 10^{-8} to 10^{-9} torr, if the sticking coefficient σ is of the order of 0.1. The leak rate was set by adjusting the valve to the reservoir to allow a slow leak into V3 while monitoring the rate of pressure increase on the capacitance manometer (step 4 of the experimental procedure outline). The leak was effectively turned off by condensing the gas in the reservoir with liquid nitrogen (reducing the pressure by 10^6), and turned on to give reproducibly the

initially set rate in 2-3 seconds by thawing the reservoir.

The Ir films (averaging about 100 Å in thickness) were deposited by evaporation from a filament heated with a current of about 5.5 amps in a 6 seconds on/6 seconds off cycle to minimize the heating of the leads. The filament, 10 mil in diameter and about 10 cm long, was helically wound in 3 to 4 turns and supported at the ends by spot welds to 40-mil Ni leads 20 cm long. Deposition occurred on the inner wall of a spherical 500 cm^3 Pyrex cell having an interior area of 300 cm^2 and thermostated at 100° C with a boiling water bath. In general a new cell was used for each film, although in some cases two films, and in one case four films, were deposited in the same cell. The filament was outgassed by heating during bakeout of the system and further heating to just below deposition temperature for an hour or more before deposition. Deposition required 15 to 60 minutes, but generally most of the film was laid down in the final 10 to 15 minutes. (The filament heating current was increased in steps of about 0.1 amp every few minutes until the rate of evaporation from the filament was sufficient to give appreciable deposition as detected by darkening of the cell walls.) Pressure rose as high as 5×10^{-8} torr (measured on gauge G1) during initial deposition but usually was not over 10^{-8} torr. Pressure decreased with further deposition indicating some gettering

may have occurred. The principal species observed during deposition, in order of decreasing ion currents, were CO_2, CO, and H_2. Gettering of H_2 was judged to be slight from the fact that when D_2 was dosed on the film in excess, no significant H-D exchange was noted.

In those experiments employing hydrogen-predosed (H_2 or D_2) films, hydrogen isotherms were obtained by admitting fractional monolayer doses of hydrogen until no further adsorption occurred. If the reaction temperature was to be different from 100° C, adsorption was first measured at 100° C, and then the isotherm was measured at the reaction (lower) temperature. The excess hydrogen was pumped away before the hydrocarbon was dosed leaving an ambient pressure on the order of 10^{-5} torr over the film. As discussed in the next section, it was found that the adsorption was partially reversible under these conditions.

Just before the hydrocarbon was dosed the two recorder systems (Figure 5) were started. An electric digital timer was started simultaneously to opening the valve or thawing the reservoir. Time marks were made on the recorder traces at frequent intervals for time correlation between ion currents and total pressure.

To resolve the raw data into partial pressures, generally time plots of the pertinent ion currents were first constructed from the ion current peaks and smooth lines were

drawn through the points. Then partial pressures were determined as functions of time from the equation

$$P_m = P \frac{i_m/f_m}{\Sigma\, i_k/f_k} \qquad (11)$$

where m, k = 2, 16, 30, and if necessary 26; i_{26} is understood to be the corrected value obtained after subtracting out i_{30} as discussed above. P is the total pressure as measured with the capacitance manometer.

In the experiments where the surface was predosed with deuterium, time plots of i_M and i_E were used in place of i_{16} and i_{30}, where

$$i_E = \sum_{24}^{36} i_m \; ; \qquad i_M = \sum_{12}^{20} i_m - .058\, i_E \; .$$

The .058 i_E term corrects for the ethane cracking contribution. If P_E represents the sum of the deuterated ethane partial pressures and P_M the sum of the deuterated methane partial pressures, then

$$P_E = i_E/f_E \; ; \qquad P_M = i_M/f_M \; .$$

The relative sensitivities f_E and f_M were determined by the equations

$$f_E = f_{30} \frac{i_E(C_2{}^1H_6)}{i_{30}} \; ; \qquad f_M = f_{16} \frac{i_M(C^1H_4)}{i_{16}} \; .$$

The subscripts m and k in Equation 11 then take on the

"values" 2, 3, 4, M, E, and 26 where practical. In the few instances where C_2H_4 appeared in the gas phase in deuterated experiments it was negligibly deuterated. C_2H_4 and C_2H_6 ion currents could be resolved to a fair degree by applying liquid nitrogen to the cold finger; the C_2H_6 spectrum disappeared in 2 to 3 seconds while the C_2H_4 spectrum was much slower to decay.

This method of analysis for the deuterated hydrocarbons assumes that all species in the cracking patterns of C_2H_6 or CH_4 which differ only by substitution of D for H have identical sensitivities. Correlation of the total pressure increase with i_M increase while CH_4 isotopic composition was markedly changing showed this to be a reasonable assumption. D_2, HD, and H_2 sensitivities, however, differed appreciably, as seen in Table 1.

In general this method could resolve partial pressures to about 0.1 μ; detection of traces below .01 u was possible in the absence of interfering background species. Uncertainty in hydrogen pressures in the presence of large hydrocarbon pressures was somewhat higher because of appreciable interference from hydrocarbon cracking, and in the case of H_2, a rather high background current.

It was found that the relative sensitivities f_m were not absolute values but showed variations of as much as 20% from one experiment to another--presumably because of

aging of electronic components in the mass spectrometer. Often f_m values could be adequately determined during an experiment by applying liquid nitrogen to the cold finger. If C_2H_6 were the only condensable gas, its sensitivity could be determined from the resultant change in pressure of i_{30} or i_E. The noncondensable portion could be attributed to H_2 and CH_4, one of which often predominated. (The C_2H_6 vapor pressure under these conditions was about 0.2 μ.) In no case were ion currents observed which could not be attributed to mixtures of C_2H_6, C_2H_4, CH_4, H_2 and their deuterated isotopes.

Several different methods were used in determining the thickness of the Ir films. For the thinner films, the metal could be scraped off the Pyrex and weighed, after the cell had been cut off the system and cut into sections of measured area. Thicker films could not be scraped off and it was necessary to analyze by other means. Single cell sections of 2 to 4 cm^2 were sealed into Vycor tubes (13 mm o.d. and 13 cm long) together with 5 grams dried $K_2S_2O_7$ and 0.5 gram dried NaCl and fused at 600° C for 6 hours (9). This produced a water soluble chloroiridate which was colorimetrically analyzed (402 mμ) after heating with $SnCl_2$ and HBr (10). If the film is assumed to be uniform throughout with the same density as the bulk metal (most likely a false assumption) a weight per unit area of 1.0 μgram/cm^2

corresponds to a film thickness of 4.46 Å. The samples analyzed varied from 4 to 32 μgram/cm^2 (18 to 140 Å). Subsequent film thicknesses were estimated by the amount of light (from a flashlight in a darkened room) absorbed by a given film compared to that absorbed by sections of the previously analyzed films.

Many of the films were manifestly not uniform (on a macroscopic scale). The helical filament configuration tended to favor deposition perpendicular to the axis of the helix over that along the axis. More seriously, the filament sagged in some cases during deposition, resulting in a thicker film at the bottom of the cell. Overall precision in thickness determinations was estimated to be 30%.

Materials

The C_2H_4 used in this study was furnished by Air Products and Chemicals, Inc. (Emmaus, Pa.) and was specified as "Research Grade." The C_2H_6 was Phillips Research Grade, specified 99.98% pure. Both gases were supplied in steel cylinders under pressure. Each was further purified upon loading into its system reservoir by first trapping any condensable contaminants with a dry ice-acetone trap, then freezing a measured amount (enough to give an atmosphere pressure at room temperature) of the hydrocarbon in the reservoir with liquid nitrogen and pumping off any noncondensable contaminants (with a liquid nitrogen-trapped

mechanical pump) before sealing the reservoir. Just before the beginning of each experiment, the gas to be used was frozen again and the ambient pumped for about two minutes. The closed reservoir was then thawed and the procedure repeated (once or twice) until the vapor pressure over the condensed gas in a closed system measured less than 1.0 μ on the capacitance manometer. No impurities were evident in the mass spectra of the gases.

D_2 was supplied by Volk Radiochemical Co. in a 100 ml (STP) glass flask with a break-seal. The supply, after being sealed to the system, was found to contain 2% H on an atomic basis and about 2% N_2 mass spectrometrically. It was evident, however, that N_2 did not adsorb on Ir and this impurity presumably had no effect on the reactions.

H_2 from a standard high pressure steel cylinder was diffused through a palladium-silver tube into the glass reservoir. No impurities were evident in the mass spectrum.

Argon was supplied by the Linde Division of Union Carbide in one-liter (STP) glass flasks with break-seals. No impurities were evident in the mass spectrum.

The Ir wire was obtained from Engelhard Industries and was specified 99.9% pure with Pd, Pt, Rh, and Fe as the major impurities.

RESULTS

Hydrogen

A composite isotherm for hydrogen (D_2 in most cases) adsorption on Ir films at 100° C is shown in Figure 12. The data were obtained in the process of preparing surfaces for hydrogen-predosed experiments. In Figure 13 the thickness of each film used for hydrogen adsorption at 100° C is plotted against the amount of adsorption measured for an equilibrium pressure of 20 μ--or, as in several cases where the adsorption was measured at a pressure less than 20 μ, the saturation adsorption for 20 μ was calculated on the basis of the isotherm. Within experimental error film thickness was linear with hydrogen adsorption; 4.0×10^{15} H_2 molecules adsorbed per angstrom of film thickness.

Figure 14 shows the 100° isotherm together with lower temperature isotherms; each of the latter was obtained on a separate film. Hydrogen adsorption was first determined with the film at 100° (as a measure of film thickness); it was then cooled to the temperature of interest and more hydrogen was added to obtain the low temperature isotherm.

The Langmuir adsorption model (1) is

$$\theta = \frac{bP^x}{1 + bP^x}, \qquad (12)$$

where θ is the fractional surface coverage for pressure P,

b is a constant which generally is temperature dependent, and the exponent x in the case of hydrogen is equal to 1 for molecular adsorption and 1/2 for atomic adsorption. This model predicts the same limiting value for surface coverage at all temperatures, which obviously is not the case for the data shown in Figure 14. If, however, Θ_T is substituted for Θ, where Θ_T is Θ divided by the limiting value of Θ at temperature T, Equation 12 is a valid analytical representation of the data. To show this the equation is rearranged in the form

$$\frac{P^x}{\Theta_T} = P^x + \frac{1}{b}, \qquad (13)$$

according to which a plot of P^x/Θ versus P^x should give a straight line with a slope of unity. The intercept on the ordinate gives 1/b. Plots for $x = 1/2$ are shown in Figure 15; the slopes and values of b are listed in Table 2. (There were insufficient data to test the 0^o isotherm.) Plots for $x = 1$ were not so linear and generally had slopes of about 2.

A value of 250 on the left-hand ordinate of Figure 14 was chosen to correspond to maximum adsorption of hydrogen ($\Theta = 1$), as this gave reasonable agreement with the variation of coverage versus temperature for flash filament results (Figure 16). (Note, however, that neither the linearity nor the slopes of the test plots (Figure 15) are

affected by this choice.) On this basis the amount of low temperature hydrogen adsorption was 2.0×10^{16} atoms per angstrom of film thickness, or 6.7×10^{13} atoms per cm^2 of Pyrex film support for each angstrom of film thickness. The adsorption per unit weight of Ir was 3.0×10^{14} atoms/ug. If each adsorption site represented one Ir surface atom, 9.6% of the Ir atoms were at the film surface.

Of the hydrogen adsorbed at 100° and 20 u, it was found that 40 to 45% could be pumped off in the time required to reduce the hydrogen ambient pressure to about 0.2 u (~ 30 seconds). At the end of several experiments in which C_2H_4 or C_2H_6 was dosed on a D_2-predosed surface, the amount of deuterium in the gas phase (as hydrogen--usually small--and as hydrocarbon) was calculated. Then by assuming that the hydrogen remaining on the surface was of the same H-D composition as the gas phase hydrocarbons after reaction (including H-D exchange) had apparently ceased, it was possible to calculate the amount of deuterium in the system at the beginning of the reaction. This amount is of course identical to that remaining after pumping the D_2 ambient off the D_2-dosed surface.

An example of this sort of calculation is given in Table 3. It can be seen that the assumption of equilibrium between gas phase and surface H-D composition is not critical because of the relatively small amount of hydrogen on the

surface relative to that in the gas phase.

Whether the 55-60% of the hydrogen saturation dose remaining at 100° after reducing the ambient to 0.2 torr was irreversibly adsorbed (at least in the sense that its desorption half-life was very large compared to the experimental time scale), or was simply the amount expected to be in equilibrium with a hydrogen pressure of 0.2 μ, cannot be resolved from the information obtained. The second possibility is not inconsistent with Equation 12 using the values of b in Table 2. On the other hand, flash filament studies suggest that this order of magnitude of hydrogen coverage is also retained at 10^{-8} torr (10^{-5} μ), which would not be consistent with the second hypothesis.

Figure 16 shows the dependence of hydrogen surface coverage on temperature for Ir for both flash filament (5) and thin films. Coverage is assumed to be a monolayer at 100° K (-173° C) in both cases. The data for film adsorption were taken from the saturation values of the isotherms in Figure 14 and can be fairly accurately represented by the linear equation

$$\theta_{max} = 1 - \beta\,(T + 173^{\circ}\,C) \qquad (14)$$

where $\beta = 2.2 \times 10^{-3}$ monolayer/deg for T in the range -130 to 100° C. While the film data were obtained under equilibrium conditions as described above, the flash fila-

ment curve represents the coverage during a flash with a heating rate of approximately 50°/sec. θ_{max} was calculated from the relation $\theta_{max} = 1 - P/P_{max}$ where P is the desorption pressure (corrected for pumping, and P_{max} represents the maximum value of P, corresponding to complete desorption.

In view of this difference and the 5-6 orders of magnitude pressure difference the agreement in general slope of the two curves is rather surprising.

Ethane

Adsorption of C_2H_4 on 100° C Ir films under some conditions causes the production of CH_4 as well as C_2H_6. The CH_4 may arise from re-adsorption and decomposition of C_2H_6 or directly from adsorbed C_2H_4 decomposition. To clarify the mechanism and kinetics of the C_2H_6 decomposition itself, four C_2H_6-dose experiments (Table 4) were conducted at 100° C.

The first of these (Figure 17) was a "low pressure" dose, where the C_2H_6 was administered at a constant rate over a 6300 second period. (Since the total C_2H_6 dose was about 0.5 monolayer, the dose rate L' was 8×10^{-5} monolayer/sec. Substituting this value into Equation 10 in the Experimental section yields a steady-state C_2H_6 pressure of 2×10^{-4} μ for an assumed sticking coefficient of 10^{-3}.) The other three experiments (Figures 18-20) were "high pressure" doses meaning that all the C_2H_6 was dosed

at the beginning of each reaction--in a quantity corresponding to an initial C_2H_6 pressure ranging from 7 to 35 μ.

CH_4 was produced from the high pressure doses at a rate which appeared to be zeroth order in H_2 and C_2H_6 pressures (when greater than 0.1 μ) and first order in surface area. That is,

$$r_M = k_M s \qquad (15)$$

where r_M is the CH_4 rate of production on a film having s atomic hydrogen sites, and the rate constant $k_M = r_M/s$ (Table 4, line 14) was found to have the value $(2.0 \pm .3) \times 10^{-3}$ molecule $(\text{sec-site})^{-1}$.

For high pressure doses on a hydrogen-predosed surface the number of CH_4 molecules produced is 1.50 times the number of C_2H_6 molecules dosed (Table 4, line 12), and the net change in the amount of hydrogen on the surface is slight from the beginning to the end of the reaction. Stoichiometrically the reaction may be written

$$2\ C_2H_6\ (g) \rightarrow 3\ CH_4\ (g) + C\ (a) \qquad (a)$$

In the low pressure dose (hydrogen-predosed surface), where the C_2H_6 dose rate was slow enough to be rate limiting (Experiment XII), the CH_4 rate of production r_M was about 1.5 times the dose rate. (The r_M/(dose rate) ratio was found to be 1.65 following a short induction period and

gradually decreased to 1.37 as the carbon surface coverage reached 0.14 atom/H site.)

When C_2H_6 was dosed on a bare Ir film, the reaction--initially rapid--slowed appreciably with time; after 1000 seconds 16% of the C_2H_6 dose remained in the gas phase (Figure 20). Although the carbon coverage was comparatively high at this point (0.38 atom/H site), it is clear that the reaction slowed from lack of hydrogen since addition of D_2 (1100 seconds after the C_2H_6 dose) restored the initial CH_4 rate (Figure 21).

The results indicate that the amount of CH_4 that will be produced from a C_2H_6 dose (on a bare or on a hydrogen-covered surface) will be equal to the number of carbon atoms dosed, or to 1/4 the number of hydrogen atoms dosed, whichever is smaller--after allowing about 0.28 hydrogen atom/site for surface saturation. Thus with a hydrogen predose the surface is initially hydrogen-saturated (at 0.2 μ) and all the hydrogen dosed as C_2H_6 is available for CH_4 production, as indicated by Reaction (a). In Experiment XV a total of 8.00×10^{18} hydrogen atoms was dosed (6.00×10^{18} as C_2H_6 and 2.00×10^{18} as D_2). At the end of the reaction there were 1.84×10^{18} molecules of methane and $.05 \times 10^{18}$ of hydrogen, or a total of 7.46×10^{18} hydrogen atoms. The amount of hydrogen remaining on the surface is thus 0.54×10^{18} atoms or 0.34 atom/site, with an uncertainty of

.08 atom/site when the uncertainty in both partial pressure and film thickness determinations are considered. The similarity of this value to the predose coverages of Experiments XIII and XIV and the invariance of the latter values (Table 4, lines 3 and 11) indicate that the amount of hydrogen on the surface is for most part independent of the amount of carbon adsorbed. This may be rationalized by postulating that hydrogen adsorbs on sites not available to carbon or that an adsorbed CH_2 species occupies the same sites as do two hydrogen atoms.

The data collected suggest that an unlimited amount of a 1:1 mixture of C_2H_6 and H_2 could be converted to CH_4 on a hydrogen-predosed Ir surface at 100° C, but with C_2H_6 alone 25% of the carbon from the C_2H_6 which disappears from the gas phase would accumulate on the surface and would thus eventually poison the reaction--at a carbon coverage comparable to the 0.38 atom/H site of Experiment XV (t = 1000 sec).

C_2H_6 was found to adsorb dissociatively at 100° C, by evidence of H_2 evolution:

$$C_2H_6 \rightarrow C_2H_n\,(a) + (6 - n)\,H\,(a) \qquad (b)$$

$$2\,H\,(a) \rightleftharpoons H_2\,(g)\,. \qquad (c)$$

Judging from Figures 18 and 19, n is about 2 or 3 if it is assumed that none of the preadsorbed hydrogen was displaced

by C_2H_6 and that all dissociated hydrogen evolved as gas. The value of n for adsorption on the bare surface of Experiment XV (Figure 20) is greater (smaller apparent dissociation) because the bare surface was able to adsorb more of the hydrogen originating from C_2H_6 dissociation than a predosed one.

As stated above the rate of CH_4 production was found to be zeroth order in C_2H_6 and H_2. The kinetics of C_2H_6 adsorption observed in this study may be represented by a complex first-order adsorption model:

$$-dN_E/dt = sk_AN_E (1 - \theta_A) + sk_BN_E (1 - \theta_B) \qquad (16)$$

where N_E is the number of gaseous C_2H_6 molecules at time t; θ_A, θ_B are the fractional coverages of two kinds of sites designated (A) and (B); k_A and k_B are the respective rate constants; and s is the number of low temperature atomic hydrogen sites of a given film.

Semilog plots of N_E against t for Experiments XIII, XIV, and XV are shown in Figures 22, 23, and 24, respectively. In Figure 25 the plots of all three experiments are shown through the first 35 seconds. The t = 0 intercepts of Experiments XIII and XV differ from the corresponding doses, and in each case the difference (initial C_2H_6 adsorption) divided by s shows an adsorption of .088 $\pm$ .002 carbon atom/H site (Table 4, lines 15 and 16). This fast initial

adsorption, assigned to the (A) sites, represents 23% of the carbon coverage found at t = 1000 seconds in Experiment XV--the highest carbon coverage from C_2H_6 encountered in this study.

If it is assumed that $\theta_A = 1$ and θ_B is small compared to 1.0 at 10 seconds after the dose, then from Equation 16 k_B is equal to (-)slope/s = (d ln N_E/dt)/s. Within experimental error the two curves give the same value of k_B (Table 4, line 18).

The experimental error in Experiment XIV was considered too great for a meaningful determination of the amount of fast adsorption. Moreover, the slope divided by the number of sites in the region of 10 to 35 seconds is much greater (negatively) for XIV than that found for XIII and XV (Table 4, line 18), indicating that θ_A in this region of Experiment XIV is considerably less than 1.0. (For this reason (-)slope/s is not a valid approximation of k_B in XV.)

As the reactions of XIII and XIV proceed, the slopes (Figures 22 and 23) become sharply steeper, reflecting a decreasing value of θ_A as the reactions exhaust the C_2H_6 supply while CH_4 production continues. On the other hand, carbon coverage in Experiment XV, where there is a hydrogen deficiency, is increasing with time; the (negative) slope (Figure 24) is steadily decreasing indicating that θ_A = 1.0 and that θ_B is also appreciable compared to 1.0 and is increasing.

Ethylene

The gas phase products obtained from the hydrogenation of C_2H_4 on Ir are C_2H_6, CH_4, and H_2 in amounts and proportions which vary with time and dosing conditions. Two series of experiments were conducted in this study to investigate the quantitative dependence of products on time and conditions. The first series, Experiments I to VII, were "high pressure" doses--meaning that a given amount (on the order of a monolayer) of C_2H_4 was dosed at the beginning of each reaction in quantity corresponding to an initial pressure of about 5 to 50 μ--at temperatures ranging from 100° C down to -140° C. The second series, Experiments VIII to XI, were "low pressure" doses, where the C_2H_4 was leaked in at a constant rate for 500 to 3000 seconds. The amount dosed in each case was roughly a monolayer. (Equation 10 in the Experimental section gives dosing pressures ranging from 3.6×10^{-5} to 6.0×10^{-6} μ for these leak rates when a sticking coefficient of 0.1 is assumed.) All four low pressure experiments were run at 100° C; both bare and hydrogen-predosed Ir films were used.

The high pressure dose results are given in Table 5 and time plots of the gas phase products for selected experiments are shown in Figures 26-29. In each case there was rapid adsorption of all or part of the C_2H_4 dose accompanied by rapid production of C_2H_6 (and H_2 at 100° C). In some

instances slow CH_4 production was noted--in others there was none. This result will be discussed more fully below. (In the absence of an Ir film and filament in the cell at 100° C, no C_2H_6 or CH_4 was detected during a 90-minute period following the introduction of a charge of 1×10^{18} C_2H_4 molecules. The detection limit for the presence of the two products was about 1×10^{15} molecules.)

The low pressure dose experiments are summarized in Table 6 and time plots of the gas phase composition of each experiment are shown in Figures 30-33. These plots exhibit a common pattern consisting of four time periods delineated as follows.

Period 1 extends from $t = t_0$ (essentially $t = 0$) to $t = t_1$, where t_0 is the time at which the C_2H_4 leak was begun (by removing liquid nitrogen from around the frozen reservoir--see Experimental section for details) and t_1 is time value obtained from extrapolation of the linear, sloped portion of the CH_4 curve to the time axis. (In Experiments VIII and X, t_0--given by the intersection of extrapolation of the dose curve with the time axis--differs from the time at which C_2H_4 was actually introduced to the film. A small amount of C_2H_4 was allowed to accumulate in volume V3 to check the dose rate and was then introduced to the film at the time indicated by the dose curve. It is assumed that the results are essentially the same as if C_2H_4 were

dosed on the surface at $t = t_0$ with no accumulation in V3). This period is characterized by C_2H_4 adsorption with only trace amounts of products, except in Experiment X where substantial H_2 was evolved. The period is markedly shorter (relative to the overall reaction period) in the hydrogen-predosed experiments (X and XI).

Period 2 extends from t_1 to t_2 where t_2 is the time obtained from extrapolation of the linear, sloped portion of the C_2H_6 curve to the time axis. CH_4 was produced at a constant rate initially in this period but the rate fell off as C_2H_6 showed a concomitant increase.

Period 3 extends from t_2 up to the somewhat ill-defined time t_3 at which C_2H_4 first becomes evident in the gas phase. Experiments VIII and X were terminated prior to t_3.

Period 4 begins at t_3 and extends to the end of the other two experiments (IX and XI).

It was found that the self-hydrogenation reaction ceased in the presence of excess C_2H_4 at 100° C when the carbon surface coverage was $0.65 \pm .07$ atom/H site (average of Experiments I and XI). Roughly half of the C_2H_4 consumed in the reactions where an excess was dosed was hydrogenated to C_2H_6, leaving a surface residue consistent with the reaction

$$2\ C_2H_4\ (g) \rightarrow C_2H_6\ (g) + C_2H_2\ (a)\ . \qquad (d)$$

A more striking result, evident from both low pressure and high pressure doses, was the poisoning of CH_4 production at a carbon coverage of about 0.4 atom/H site--substantially less than the coverage required for poisoning the self-hydrogenation. In Experiment I, where an excess of C_2H_4 was dosed, there was no CH_4 produced. In Experiment III, following the first dose a slow rate of production of CH_4 was noted as shown in Table 5, line 14. This figure gives the CH_4 rate r_M as a fraction of $k_M s$, the CH_4 rate that would have been expected if C_2H_6 rather than C_2H_4 had been dosed (see Equation 15). As Figure 27 and Table 5 show, the CH_4 production all but stopped when the second charge of C_2H_4 was introduced.

In the low pressure dose experiments the carbon surface coverage n_c/s (Table 6, line 12) was .41 $\pm$ .07 atom/H site at $t = t_2$, approximately where CH_4 production stopped.

About this same coverage was required for blocking CH_4 production at 100° in the high pressure doses, as best as can be inferred from the available data; and the coverage of 0.38 atom/H site found in Experiment XV when C_2H_6 decomposition had nearly stopped is nearly the same.

It is not clear, however, whether or not the CH_4 observed in the low pressure doses originates from the decomposition of C_2H_6. Line 27 of Table 6 shows that in no case did the rate of CH_4 production r_M exceed the

theoretical maximum rate $(r_M)_{max}$ where

$$(r_M)_{max} = k_M s \, [1 - n_c(t_1)/n_c(t_2)] \, . \qquad (17)$$

The term $k_M s$ is of course the rate expected for CH_4 production from an excess of C_2H_6 on a surface of s H sites and the term in brackets corrects for the fraction of sites that are carbon covered (and therefore possibly not available for the reaction) when CH_4 evolution begins. Thus it is conceivable that in Period 2, C_2H_6 was produced at a rate slow enough to be adsorbed and decomposed to give CH_4 as fast as it was produced.

The alternative source of the CH_4 is direct decomposition of adsorbed C_2H_4. This appears to be more consistent with the results, as will be made clear in the Discussion section. According to this interpretation, the low pressure results imply that the surface must be covered with C_2H_4 (to the extent of 0.4 C atom/H site) before C_2H_6 will be produced at an appreciable rate. The rate of adsorption of C_2H_4 must therefore be large compared to its rate of decomposition at low coverage; this in turn (given the dosing pressures and times required for appreciable C_2H_6 production rates to develop) implies that the sticking coefficient of C_2H_4 on Ir at low coverages must be moderately high (~ 0.1).

If it is assumed that the CH_4 in Experiments VIII to XI originates from C_2H_4 decomposition rather than C_2H_6

decomposition, or in other words, that no C_2H_6 is produced that does not stay in the gas phase, then a theoretical model which accounts for the kinetics of low pressure C_2H_6 production may be constructed on the basis of the reactions

$$C_2H_4\ (g) \rightarrow C_2H_4\ (a) \qquad (e)$$

$$C_2H_4\ (a) + C_2H_4\ (g) \rightarrow C_2H_6\ (g) + C_2H_2\ (a)\ . \qquad (f)$$

Since Reaction (f) does not change the carbon surface coverage, we may write

$$d\theta/dt = k_1\ (1 - \theta)\ x/x_m \qquad (18)$$

$$dy/dt = k_2\ x\ (\theta x_m - y) \qquad (19)$$

where x and y are the numbers of gas phase C_2H_4 and C_2H_6 molecules, respectively; x_m is the number of C_2H_4 molecules required for a monolayer, and θ is the fractional monolayer coverage at time t. The variables x and t may be eliminated by dividing Equation 18 by Equation 19 to give

$$\frac{d\theta}{d(\frac{y}{x_m})} = \frac{a\ (1-\theta)}{\theta - \frac{y}{x_m}} \qquad (20)$$

where $a = k_1/k_2$.

Values of y/x_m as a function of θ may be calculated by numerical integration of Equation 20 for given values of a. For comparison of this function with the experimental

C_2H_6 (g) curves, however, it is preferable to have y as a function of t. The total dose according to the model is $L't = x/x_m + y/x_m + \theta$ (L' = dose rate of C_2H_4 in monolayers /sec). If x/x_m is small compared to $y/x_m + \theta$ (amount of C_2H_4 (g) small compared to amount of C_2H_6 (g) plus C_2H_4 (a)), then $L't = y/x_m + \theta$, and $y(L't) = y(\theta + y/x_m)$. (Considering the pumping of C_2H_4 from adsorption only, with a sticking coefficient of 0.1 for $0 \leq \theta < 1$, it can be shown from gas kinetics that x will not exceed .01 monolayer--equivalent to 0.3 μ C_2H_4 or less--for typical film thickness during gradual C_2H_4 introduction until $\theta \geq 0.99$. In other words, C_2H_4 pressure should be negligible until the surface is 99% covered. Consideration of C_2H_4 "pumping" by hydrogenation as well as by adsorption would reduce the theoretical C_2H_4 pressure yet farther for a given value of θ.)

Plots of y/x_m as a function of L't are shown in Figure 34 for a = 10 and a = 100, which brackets the range of a that appears to give best agreement with experimental C_2H_6 curves. It is evident that the time defined as t_2 in the experimental plots (extrapolation of the C_2H_6 curve) is equivalent to the t at which a monolayer has been dosed (i.e., $\theta + y = 1$). Table 7 shows the results of calculation of experimental values of a for two experiments. For y/x_m small compared to θ Equation 20 integrates to give

$$a = [- \ln (1 - \theta) - \theta] x_m/y \qquad (21)$$

To evaluate θ and y, a monolayer was taken to be the sum of the number of surface carbon atoms $n_C(t_2)$ (Table 6, line 12) plus twice the number of C_2H_6 (g) molecules at $t = t_2$, so that

$$\theta = n_C/[n_C(t_2) + 2\,N(C_2H_6)_{t_2}]$$

and

$$y/x_m = 2\,N(C_2H_6)/[n_C(t_2) + 2\,N(C_2H_6)_{t_2}] .$$

As shown in Table 7, θ, y, and a were determined at $t = t_2$ and at a smaller, arbitrary value of t.

While the agreement between determinations of a within each experiment is excellent, the agreement between experiments is not good. The results may possibly have been affected by adsorption of C_2H_6, giving a low result for y. The effect presumably should have been greatest on the slower Experiment XI, and since a varies inversely with y (at a given time), a correction for this effect should result in better agreement.

Aside from possible C_2H_6 adsorption the experiments deviated from the model in the following respects. First, C_2H_4 adsorbed dissociatively (e.g., Figures 31 and 32) at 100°, in a step such as

$$C_2H_4\ (a) \rightleftharpoons C_2H_2\ (a) + H_2\ (g) \qquad (g)$$

and hence Reaction (f) was not the only one by which C_2H_4 (a) was consumed. Secondly, Experiment XI was predosed with hydrogen and this would tend to shift the above equilibrium, and also produce other effects discussed below. Thirdly, the reaction produced an appreciable amount of CH_4 which resulted in a reduction of the H/C ratio on the surface. At $t = t_2$ the amount of carbon in the gas phase as methane is 13% of the carbon dosed up to that time in Experiment IX and 30% of that in XI. It is to be expected that the higher the hydrogen concentration on the surface the higher the rate of Reaction (f). (Within the limits of the model, the term $(\theta x_m - y)$ in Equation 17 is essentially a measure of the hydrogen available for reaction. Hence, the higher the ratio n_H/n_C for a given carbon coverage, the greater ought to be the rate of Reaction (f).)

On the basis of the relatively large H_2 pressure at t_2 in Experiment IX (about 3 times that of Experiment XI at t_2) it is reasonable to assume that the n_H/n_C ratio is greater than in XI, leading to a larger value of y, and hence (by Equation 19) the observed smaller value of a. The relative magnitude of the ratio n_H/n_C measured at $t = t_2$ (Table 6, line 15), however, is the opposite of that deducted above. The cause of the discrepancy may be that the predosed hydrogen (or a portion of it) adsorbs in a manner such that C_2H_4 will neither displace it nor react with it.

Since the CH_4 production rate is much more sensitive to temperature (at least for CH_4 produced from C_2H_6 decomposition) than is the hydrogenation reaction, a better test of the model could be obtained by running the low pressure dose experiments at lower temperature (e.g., 40° C).

The results of dosing hydrogen at 100° C on the residues from two different C_2H_4 doses at 100° on films of comparable area (Experiments VIII and IX) are shown in Figure 34. The ambient in each case (Figures 30 and 31) was pumped away before the hydrogen was introduced. The initial dose pressure in VIII was about 25 μ which decreased to 5 μ at 1200 sec; in IX the initial 40 μ of H_2 decreased to 25 μ at 1200 sec. In both cases CH_4 and C_2H_6 were slowly evolved with initial rates that reflected the relative amounts of the respective hydrocarbon (CH_4 or C_2H_6) that had been pumped away from the preceding C_2H_4 doses. For example, CH_4 pressure at the end of VIII was greater than the C_2H_6 pressure, and the CH_4 rate was greater than the C_2H_6 rate upon dosing H_2. In IX the roles of CH_4 and C_2H_6 were just the opposite. This relationship may be the consequence of a slow equilibrium between the gas phase hydrocarbons and H_2 and adsorbed species (e.g., CH_3 and C_2H_5), or it may be an indirect result of the higher surface coverage concomitant with the higher C_2H_4 dose in Experiment IX (i.e., implying that higher carbon surface coverage favors desorption of C_2H_6

or hinders decomposition of adsorbed C_2 units).

It should be noted that the rate of CH_4 evolution increased with time from both the residues, most likely as a result of decreasing carbon coverage accompanied by a higher coverage of adsorbed hydrogen (as distinguished from hydrogen bonded to adsorbed carbon).

The results in Figure 36 show that C_2H_4 can be hydrogenated rapidly on a carbon-covered surface. In regard to the history of the surface, 0.755×10^{18} molecules C_2H_4 were dosed at t = 0 on the hydrogen-predosed surface at -78° C (Experiment VI). The dose was completely consumed producing 0.44×10^{18} C_2H_6 molecules and leaving a surface that was approximately half-covered with a carbon residue. Addition of H_2 ($.75 \times 10^{18}$ molecules) at t = 425 in presence of the ambient resulted in very fast adsorption of 0.20×10^{18} H_2 molecules and a slow evolution of C_2H_6 (at a rate not very much less than that seen at 100° C in Figure 35). The fraction of C_2H_6 formed subsequent to H_2 addition was about 2% of the total C_2H_6 in the gas phase at t = 900. (No CH_4 is to be expected at -78°.)

Upon the addition of C_2H_4 (0.765×10^{18} molecules) at t = 950 sec (Figure 36) about 90% of it was rapidly hydrogenated (compared to 58% the initial, nearly equal-sized C_2H_4 dose). This result and others of a similar nature lead to the conclusion that an indefinite amount of a 1:1

mixture of C_2H_4 and H_2 will readily react to form C_2H_6 over a carbon covered Ir surface at temperatures as low as -78° (and probably much lower).

Note that the C_2H_6 increase in Figure 36 was 0.2 x 10^{18} molecules greater than the decrease in H_2--a difference equivalent to the amount of H_2 adsorbed at t = 425 sec. Note also that the H_2 decay apparently was slower than the C_2H_6 rise (even if the initial 0.2 x 10^{18} molecules increase is first discounted) indicating that C_2H_4 was reacting with hydrogen on the surface, and that H_2 from the gas phase was replenishing the surface supply, at a slower rate.

In the presentation of the foregoing results, it has been assumed for the sake of simplicity that C_2H_4 dosed on an Ir surface first adsorbs to monolayer coverage as per Reaction (e), giving rise to an equilibrium such as Reaction (g) (at 100° C) followed by hydrogenation as indicated by Reaction (f). In full consideration of the experimental evidence it is obvious that the overall reaction cannot be this simple.

First, adsorption occurs beyond the "monolayer" coverage assumed by the model for Equations 18 and 19 (0.4 carbon atom/H site) up to 0.65 carbon atom/H site.

Second, it may be that there is some initial inactive adsorption--that is, adsorbed C_2H_4 that will not support hydrogenation either by furnishing hydrogen or by adding

hydrogen. This quantity (number of carbon atoms), designated n_C^* (Table 5, line 10), was experimentally determined from the expression

$$n_C^* = 2 [\Delta N(C_2H_4) - 2 N(C_2H_6)] \quad (22)$$

where $\Delta N(C_2H_4)$ is the number of C_2H_4 molecules consumed in the reaction (difference between dose and remainder in gas phase) and $N(C_2H_6)$ is the number of C_2H_6 molecules produced. The average value of n_C^* is 0.16 $\pm$ .04 atom/H site at 100°. This average does not include Experiment IV; it is a special case because (1) the surface was hydrogen predosed and (2) it is not clear how much of the C_2H_6 produced subsequently decomposed to CH_4.

If n_C^* does actually represent inactive carbon initially absorbed, Equations 18 and 19 would require revision to allow for n_C^*/s inactively adsorbed carbon atoms per hydrogen site.

It may be that what appears to be inactively adsorbed C_2H_4 is better explained by postulating that on a bare surface C_2H_4 adsorbs dissociatively (as in Reaction (g)) and the hydrogen arising thereby adsorbs irreversibly so that it is not available for support of hydrogenation.

The significance of the values of n_C^* calculated in the experiments run below 100° is ambiguous because of the hydrogen predoses on these films. It is of interest, how-

ever, that the carbon coverages (Table 5, line 13) on the low temperature films were substantially lower than those of the 100° experiments even though the C_2H_6 production is comparable. This may be because the hydrogen predose is not easily displaced by C_2H_4 at lower temperatures.

Comparison of Figures 30-33 shows that CH_4 production begins at a considerably lower coverage when the surface is hydrogen predosed (Figures 32 and 33) indicating that perhaps a certain minimum hydrogen coverage is required before reaction (other than adsorption and decomposition) occurs--whether the reaction be hydrogenation (followed by C_2H_6 decomposition) or C_2H_4 decomposition to give CH_4 directly.

There is an interesting relationship in the C_2H_4 low pressure dose series of experiments between the dose rate r_d, the methane production rate r_M (both taken in molecules per second), and the hydrogen pressure. For the two slowest dose rates (Experiments VIII and XI) the ratio r_M/r_d (Table 6, line 25) was $0.70 \pm .01$, while for the two fastest rates (IX and X) the ratio was $0.44 \pm .03$. Note that only one experiment in each of the pairs was run on a hydrogen-predosed surface, so this condition apparently had no effect on the ratio. Examination of Figures 30-33 shows that a low, steady-state hydrogen pressure was established in the early part of the two slower doses, while in the two faster doses the hydrogen pressure rose continuously to a maximum

(although there is a slight shoulder in IX). There were also hydrogen pressure maxima in the slow doses, but much less pronounced. It is striking that in each of the four experiments the hydrogen maximum coincided with the onset of a constant rate of C_2H_6 production (which very nearly coincided with the end of CH_4 production).

The exact mechanism responsible for these relationships is obscure, but it seems clear that with the slower dose rates, the excess hydrogen was "burned" in CH_4 production, while at the faster dose rates, the reaction step responsible for methane production was not fast enough to burn the excess hydrogen--perhaps because the carbon coverage on the surface was too high.

In the application of the model implied by Reactions (e) and (f) to the kinetics of the high pressure C_2H_4 doses, the assumption that $\theta = 1$ before hydrogenation begins ought to be a good approximation. (This is equivalent to assuming that $a = k_1/k_2$ is very much greater than unity.) Substitution of $\theta = 1$ in Equation 19 gives

$$dy/dt = k_2\, x(x_m - y) \qquad (23)$$

Since the model considers C_2H_4 and its residue C_2H_2 to be the only adsorbed species, and C_2H_4 (x) and C_2H_6 (y) to be the only gaseous species, x and y are related by the mass balance equation

$$x_d = x_m + x_i + x + y \qquad (24)$$

where x_d is the number of C_2H_4 molecules dosed at t = 0, x_m is here defined as the number of molecules of C_2H_4 constituting a "monolayer" of actively adsorbed (reactive) C_2H_4, and x_i is the number of inactively adsorbed (non-reactive) C_2H_4 molecules and is equal to 1/2 n_C^*. With the assumption that adsorption is rapid compared to hydrogenation, the total number of molecules x_0 in the gas phase will be constant, such that

$$x_0 = x_d - (x_m + x_i) = x + y \qquad (25)$$

This relationship is used to eliminate x in Equation 23 which then integrates to give

$$\ln \frac{1 - y/x_0}{1 - y/x_m} = (x_0 - x_m)k_2 t \qquad (26)$$

for $x_0 \neq x_m$.

Figure 37 shows data from Experiment I (Figure 26) plotted to test the fit with Equation 26. Values of the constants used were: x_m (taken as y at $t = \infty$), 0.39×10^{18}; x_0 (x + y at $t = \infty$), 0.91×10^{18}; and x_i, 0.20×10^{18}. From the break in this plot and the shape of the C_2H_6 curve in Figure 26 it was considered likely that there was a fast initial hydrogenation process which exhausted itself in about 100 seconds while a slower one continued. Assuming this fast process to be responsible for all the C_2H_6 present at t =

80 sec, it should produce a total of 0.25×10^{18} molecules at $t = \infty$. Using $x_m = 0.25 \times 10^{18}$ the data were again tested for fit with Equation 26; the results are shown in Figure 38 ($x_0 = 0.91 \times 10^{18}$, $x_i = 0.34 \times 10^{18}$). The data give a reasonably linear plot with a slope corresponding to $k_2 = 0.035 \times 10^{-18}$ (molecule-sec)$^{-1}$. The plot, however, fails to pass through the origin, having a $t = 0$ intercept corresponding to $y = 0.07 \times 10^{18}$ C_2H_6 molecules, which may represent production from a yet faster reaction.

When the magnitude of the C_2H_4 dose x_d is such that $x_0 = x_m$, the corresponding form of Equation 23 is

$$\frac{y}{x_m - y} = x_m k_2 t \ . \qquad (27)$$

In Experiment VII $x_d = 0.83 \times 10^{18}$, $x_0 = x + y = 0.46 \times 10^{18}$ (at $t = 500$), and it was estimated that y would have increased from 0.41×10^{18} at $t = 500$ to 0.43×10^{18} molecules at $t = \infty$. Thus x_0 is very nearly equal to x_m. A plot of the left-hand side of Equation 27 against t is shown in the upper curve of Figure 39. The plot is fairly linear, with a slope that gives a value for the rate constant k_2 of 0.079×10^{-18} (sec-molecule)$^{-1}$. The plot, however, fails to pass through the origin as agreement with the model would require; the intercept at $t = 0$ corresponds to $y = 0.18 \times 10^{18}$ molecules.

If this quantity, defined as $y = y_0$, is produced by

a separate, fast reaction, then the following quantities, using the subscript s to denote slow reaction, may be defined: $y_s = y - y_0$; $x_{ms} = x_m - y_0$, which is the number of adsorbed C_2H_4 molecules remaining on the surface following the fast reaction; and $x_{is} = y_0 + x_i$, which is the amount of inactive C_2H_4 on the surface (inactive because it has reacted to leave a C_2H_2 residue, according to the model); and $x_{os} = x_0 - y_0$. Thus if $x_0 = x_m$, then $x_{os} = x_{ms}$ and the condition necessary to justify use of Equation 27 is satisfied for the slow reaction. Putting the s subscript variables into this equation yields

$$\frac{y_s}{x_{ms} - y_s} = \frac{y - y_0}{x_m - y} = (x_m - y_0)k_s t \qquad (28)$$

where k_s is the rate constant for the slow reaction. The lower curve of Figure 39 is a plot of $(y - y_0)/(x_m - y)$ against t for $y_0 = 0.18 \times 10^{18}$ molecules. The value of k_s calculated for this curve is $.076 \times 10^{-18}$ $(\text{sec-molecule})^{-1}$. (It can be shown mathematically from Equations 27 and 28 that $k_2 = k_s$, in the case where arbitrary intercepts are allowed.)

It should be noted that a model in which the rate is second order in C_2H_4 pressure over a surface covered with C_2H_4 gives a rate expression identical to that of Equation 26, but such a model would be inconsistent with results

such as those of Experiment I.

Figure 40 shows the results of slowly heating the film and reaction residue from Experiment II after the ambient pressure had been reduced to about 0.1 μ. The ion currents shown have been corrected to compensate for the effect of temperature change on the pressure, so that i_m in the figure is proportional to the number of gas phase molecules of the respective species in the reaction volume (V2 + V3). At t = 45 min the pressure (corrected to a cell temperature of 100° C) is 18.2 μ and the number of gas molecules is 0.43×10^{18}. Since the mass spectrometer sensitivities of H_2 and CH_4 are comparable (see Table 1), it is evident that hydrogen is by far the major desorption product. Moreover, much of the CH_4 production may be a consequence of the relatively high (compared to flash filament experiments) H_2 pressure and slow heating rate. In other words, if the products had been pumped away as they desorbed to more closely simulate flash filament conditions, it is not unlikely that CH_4 production would have been substantially less. Only a trace of i_{30} (.005 μA--about 0.02 μ C_2H_6) was present when heating was begun, and it never was above the detection limit (about 0.1% of i_2) in the latter part of the desorption.

As it turned out, predosing the films with D_2 afforded a means of comparing the amount of hydrogen dosed at a

given pressure with the amount left on a given film after the ambient had been virtually pumped away; these results (presented above in the Hydrogen section) showed that the hydrogen adsorption was at least partially reversible. But for most part D_2 predosing was not particularly useful in elucidating any reaction mechanisms. The composition of the deuterated products (at 100° C) indicated rapid scrambling of H and D on the surface when C_2H_6 or C_2H_4 was dosed, with slower exchange in the gas phase, particularly over a surface highly covered with carbon.

DISCUSSION

Film Thickness and Surface Area

As discussed in the Results section hydrogen adsorption data indicated that the surface area of the Ir films in this study was proportional to film thickness. The variation in zeroth-order CH_4 production as well as first-order C_2H_6 adsorption tend to support this conclusion. Roberts, however, states, "The thickness of the iridium film did not appear to have much effect on the decomposition of ethane (Experiments 2, 3; Table I). This is in agreement with our observations on rhodium films" (6). The results cited by him for iridium are reproduced in the first two columns of Table 8. Two Ir films, differing in thickness by a factor of 3, were dosed with equal amounts of C_2H_6 at 27° C; the resulting surface residues, determined after reaction had ceased, were nearly equal in amounts of adsorbed carbon and hydrogen. No kinetic data were obtained in these experiments. The third column of Table 8 shows the results of a later experiment reported by Roberts (Figure 1 of Reference 7) in which gas phase composition was followed as a function of time. The data tabulated are taken from the final data points on the graph, although it is apparent that at this time (1500 min) the reaction was still proceeding, particularly with respect to CH_4 production. While the amount of carbon on the surface is remarkably similar for

the three experiments, there are significant differences in the amounts of CH_4 produced, and these show a weak correlation with film thickness.

The criterion Roberts used in judging that the thickness of his Rh films had little effect on C_2H_6 decomposition is puzzling. He maintains that "plotting the log of the ethane pressure against time yielded a straight line for the initial 10% of the reaction, indicating that initially the rate of disappearance of ethane obeys a first-order law" (11)--at four different temperatures ranging from 0 to 100° C. The first three columns of Table 9 are taken directly from Roberts' Table 2 (11) in which he gives his first-order rate constants (k) for disappearance of C_2H_6 on Rh at 100°. He chooses to ignore the k value for Experiment D4 because of the small film thickness, and because of the small variation in k for large variation in thickness of the three other films, he concludes that "these films have about the same available surface area on which the reaction can occur"--not an unreasonable conclusion from the evidence presented.

In Roberts' Figure 3 (11) the C_2H_6 decay is plotted against time for Experiment D3, the only one of the four 100° adsorptions on Rh for which such data were given. It is readily apparent from this graph that no kinetic data could have been obtained from "the initial 10% of the reaction" because about 75% of the C_2H_6 dose had disappeared

in two minutes, the time at which the first data point subsequent to dosing was taken.

In Figure 41 the C_2H_6 data from Roberts' Figure 3 have been replotted on a log scale. It can be seen that they fall reasonably well on a straight line (curve A) with a slope of -0.30 min^{-1}, but the t = 0 intercept corresponds to only about 40% of the C_2H_6 dose. Curve B, with a slope of -0.56 min^{-1}, has been drawn through the dose point to correspond to Roberts' k value of 0.56 min^{-1}. Apparently there was fast initial adsorption which consumed about 60% of the dose in less than two minutes by a process different than that responsible for slower adsorption.

This result suggests a reinterpretation of Roberts' kinetic data. Assume for purposes of argument that the k values Roberts reported for Experiments D1, D2, and D4 actually were measured for the initial 10% of the C_2H_6 adsorption, in contrast to what was apparently measured for D3; assume also that the initial adsorption rate is first order and directly proportional to film thickness. Then the rate constant per unit film thickness is .0143 $(min\text{-}\mathring{A})^{-1}$ (average calculated from D1 and D2 data). In the last column of Table 9 the first-order rate constants obtained by multiplying the film thickness in each experiment by .0143 are tabulated. There is necessarily good agreement between these values and Roberts' experimental k for D1 and

D2. For D3 the value is 2.50 min^{-1}, which corresponds to curve C in Figure 41. It is not unreasonable to suppose that the adsorption in D3 follows curve C initially and then slows to follow curve A after the intersection of the two. The fast adsorption could represent selective adsorption on one type of adsorption sites, which quickly saturate, while the slower adsorption may represent adsorption on other sites or adsorption that is controlled by the rate of evolution of CH_4 (from C_2H_6 decomposition) from the surface. Much the same behavior--fast initial adsorption of C_2H_6 followed by slow first-order adsorption--was noted on Ir at 100° in the present study. Furthermore, in this interpretation the agreement of Roberts' result with the calculated value of k for Experiment D4 in Table 9 is probably very nearly within experimental error, and it is not necessary to discard this result.

If Roberts' Experiments D1, D2, and D4 also showed fast initial adsorption similar to that of D3, the reinterpretation is not valid of course. But whether it is or not, Roberts' conclusion that the rate of C_2H_6 adsorption on Rh was independent of film thickness appears doubtful.

Roberts' Figure 2 (11) shows C_2H_6 adsorption on Rh at 27° C, and in this case also a substantial fraction (more than 40%) of the C_2H_6 dose disappeared before the following data point was taken. The close spacing of the data points

on this graph make it impractical to check the rate constant of 3.3×10^{-3} min^{-1} tabulated for "the initial 10% of the reaction" in this experiment, to see if it corresponds to the rate of adsorption following the fast initial adsorption.

Most of the transition metals for which evaporated films have been studied have produced film surface areas that are proportional to the weight (thickness) of the film. Beeck (12), for instance, found a nearly linear relationship between surface area and deposited weight of Ni films for thicknesses as great as 10^4 atomic layers. (The Ir films of this study were less than 100 atomic layers thick.) This relationship was the same for area as determined by H_2 adsorption, by CO adsorption, and by the activity of the film for C_2H_4 hydrogenation. Similar results were found for other metals, but copper was a notable exception; Beeck reported that ". . . no measurable internal surface could be observed . . ." for copper. Because of its relatively low melting point (1083° C) it can be expected to sinter more readily than other transition metals.

Roberts found that on a 166 Å Ir film at 100° C, 1.5×10^{18} molecules of oxygen adsorbed "instantaneously" and an additional 0.3×10^{18} molecules adsorbed more slowly. Thus for the total adsorption (on 300 cm^2 geometrical area) there were 22×10^{15} oxygen atoms/Å compared to 20×10^{15} hydrogen atoms/Å (also on 300 cm^2 geometrical area) found

for low temperature adsorption in this study. Assuming that the oxygen adsorption was proportional to film thickness (only the single experiment was reported) and that each Ir surface atom adsorbed one atom of oxygen or of hydrogen, the agreement in specific area (area per unit weight or unit thickness) is very good.

Other comparisons, however, indicate that Roberts' films may have had a somewhat higher specific area than the films of this study. Roberts' data show an initial CH_4 rate from C_2H_6 decomposition at 100° C on Ir of 6.1×10^{13} molecules $(\text{Å-sec})^{-1}$; the comparable value in this study is 4.2×10^{13} molecules $(\text{Å-sec})^{-1}$. For an excess dose of C_2H_4 on Ir at 100° C, the amount of carbon adsorbed per unit thickness was 3.4×10^{16} atom/Å in Roberts' Experiment 8, Reference 6 compared to $(1.2 \pm .2) \times 10^{16}$ atom/Å in the present study for comparable experiments.

Roberts' Ir films were deposited at 27° C and consequently can be expected to have a somewhat greater area than films deposited at 100° C. Trapnell (13) has shown that for Ni, Fe, Rh, Mo, Ta, and W, a larger film area is formed when the temperature of the film support is at a lower temperature during deposition. The specific area deposited at -183° C was greater than that deposited at 0° C by factors ranging from 8.5% (Ta) to 160% (Fe). The increase for Rh was 35%. The films (13) deposited at either

temperature were sintered at 23° C prior to determination of area (at -183° C by O_2 or H_2 adsorption).

Ethane

The kinetic results of adsorption and decomposition of C_2H_6 on Ir at 100° C showed three major characteristics:

A. A fast initial adsorption process (Figure 25, Experiments XIII and XV) accounting for a small fraction of saturation carbon coverage;

B. A slow first-order adsorption process (Figure 25, Experiments XIII and XV) accounting for the bulk of the total adsorbed carbon at high coverages;

C. A zeroth-order production of CH_4 with no induction time (Figures 18-20).

These characteristics suggest three kinds of adsorption sites on Ir, namely:

(A) sites which show high activity for C_2H_6 adsorption;

(B) sites which show low activity for C_2H_6 adsorption;

(C) sites which are responsible for CH_4 production by virtue of C-C bond breaking.

The proposed mechanism which occurs on these sites begins with the adsorption of C_2H_6, followed by a multistage dissociation

$$C_2H_6\ (g) \rightleftharpoons C_2H_5\ (a) + H\ (a) \qquad (h)$$

$$C_2H_n\ (a) \rightleftharpoons C_2H_{n-1}\ (a) + H\ (a) \qquad (i)$$

where n = 1, 2, . . . 5. The amount of H_2 evolved initially in the experiments

$$2\ H\ (a) \rightleftharpoons H_2\ (g) \qquad (c)$$

indicates an average initial value for n of 2 or 3, if little of the dissociated hydrogen remains behind as H (a). Reactions (h) and (i) may occur--at different rates--on any of the three sites, but the initial adsorption is due principally to (A) sites.

The principal role of the (C) sites is breaking the C-C bond--probably by the splitting of a diadsorbed species

$$\underset{**}{C_2H_n} \rightarrow \underset{*}{CH_p} + \underset{*}{CH_q} \qquad (j)$$

where p + q = n. (Each star (*) represents a carbon-surface bond.) Adsorption on (C) sites may occur directly from the gas phase or by migration from (A) and (B) sites. Reaction (j) is followed by rapid hydrogenation of the single-carbon fragments to give CH_4

$$\underset{*}{CH_p} + (4 - p)\ H\ (a) \overset{\text{fast}}{\rightarrow} CH_4\ (g)\ , \qquad (k)$$

so that C-C bond breaking is seen as the rate-limiting step, in the presence of sufficient hydrogen. The (C) sites--small in number compared to the (A) and (B) sites--are filled in preference to the other sites, whether by migration or adsorption. A central hypothesis of the

mechanism is that since the (C) sites are continually saturated, the rate of Reaction (j) and hence the rate of CH_4 production (with sufficient hydrogen) then depends only on the number of these sites (or the film thickness), and is consequently zeroth order in C_2H_6 and H_2 partial pressures.

The initial adsorption accounts for 23% of the maximum carbon coverage encountered from C_2H_6 adsorption (0.38 atom/H site--although this was less than the maximum of 0.65 atom/H site observed from C_2H_4 adsorption.) Since it has been postulated that (C) sites are filled in preference to (A) sites, this means that the initial adsorption is a measure of the total number of (A) and (B) sites. It is necessary to make a distinction between the (A) and (C) sites, however, because of the results of Experiment XIV. In this (relatively small) C_2H_6 dose the fast adsorption sites never became saturated, but even so, CH_4 production was first order with the same rate per hydrogen site (or per unit film thickness) as the other high pressure C_2H_6 doses (Table 4, line 14).

The exact nature of the different sites is of course unknown. They may correspond to different crystal faces, different spacings on the same face, or defects (e.g., crystal face boundaries or lattice dislocations) that occur in a reproducible concentration from film to film.

Since the proposed mechanism implies that single-carbon fragments are rapidly hydrogenated to CH_4, the

stoichiometry of Reaction (a) (for a hydrogen-predosed surface) might be better represented as

$$4\ C_2H_6\ (g) \rightarrow 6\ CH_4\ (g) + C_2\ (a)\ . \qquad (1)$$

The stoichiometry can be justified by assuming that adsorption on (A) and (B) sites forms a pool of mobile hydrogen adatoms which maintain Reaction (k). The H/C atomic surface ratio was about 1.0 at the end of both the hydrogen-predosed experiments (XIII and XIV), indicating that perhaps C_2 species were adsorbed on sites unavailable to hydrogen at 100°. Alternatively, the adsorbed carbon species may be C_2H_2, each of which would occupy the sites of two predosed hydrogen atoms.

In Experiment XV (Figure 20) in which no hydrogen was predosed the reaction slowed before the C_2H_6 was consumed, probably because the hydrogen originating from the dissociation of adsorbed C_2H_6 was adsorbed in preference to reacting via Reaction (k). The addition of hydrogen to this reaction (Figure 21) restored the zeroth-order CH_4 rate after a 60-second induction period. The reason for the induction period is not clear, but two causes based on the mechanism are offered. 1) It may be that there is a disproportionation among the adsorbed CH_n fragments (n = 0 to 3) in the presence of a hydrogen deficiency. If the reverse reaction is slow in the presence of excess hydrogen,

the (C) sites may be temporarily poisoned. 2) The hydrogen deficiency may promote formation of a polymeric species, such as $\underset{*}{(CH)}_n$, which is more resistant to C-C bond breaking than is C_2H_n (a).

It is interesting to note in regard to Roberts' results for C_2H_6 adsorption kinetics on Rh discussed above that although the surface areas are comparable in Experiments XIV and XV, the rate constants for disappearance of C_2H_6 (ignoring any fast initial adsorption) differ by a factor of 6 (Table 4, line 16). This difference is primarily a function of the ratio of amount of C_2H_6 dosed to area of the surface. Presumably, much the same result could have been obtained by dosing equal amounts of C_2H_6 on surface areas differing by a factor of 6.

Ethylene

Two broad types of mechanisms for catalytic reactions are the Langmuir-Hinshelwood (reaction of two adsorbed species) and Rideal-Eley (reaction of an adsorbed species with an impacting gas molecule) mechanisms. A priori, three of the latter type and two of the former appear to be reasonable possibilities for the formation of C_2H_6 from C_2H_4 and H_2. These are

$$C_2H_4\ (g) + C_2H_4\ (a) \rightarrow C_2H_6\ (g) + C_2H_2\ (a) \qquad (m)$$

$$C_2H_4\ (g) + 2\ H\ (a) \rightarrow C_2H_6\ (g) \qquad (n)$$

$$H_2\ (g) + C_2H_4\ (a) \rightarrow C_2H_6\ (g) \qquad (o)$$

$$C_2H_4\ (a) + 2\ H\ (a) \rightarrow C_2H_6\ (g) \qquad (p)$$

$$2\ C_2H_4\ (a) \rightarrow C_2H_6\ (g) + C_2H_2\ (a) \qquad (q)$$

The major portion of the C_2H_6 production in high pressure dose (i.e., fast initial dose) experiments is first order in C_2H_4 pressure (see Figure 29 and ethylene portion of Results section), with a substantial amount of carbon-containing species on the surface. This result is consistent with Reaction (m) (provided the sites capable of adsorbing C_2H_4 are nearly saturated) or with Reaction (n) (provided the sites capable of adsorbing hydrogen are nearly saturated) but not with Reactions (o), (p), or (q).

Reaction (m) is favored over (n) by the results of the low pressure (slow leak) doses by C_2H_4 on hydrogen-covered surfaces. In these experiments (X and XI) CH_4 production began soon after the introduction of C_2H_4 to the surface, indicating either that C_2H_4 was hydrogenated to C_2H_6, which in turn adsorbed and decomposed to give CH_4, or that C_2H_4 decomposed directly to CH_4 with the implication that C_2H_4 does not readily react with hydrogen adsorbed directly to the surface to form C_2H_6. If C_2H_4 did indeed decompose directly to CH_4, Reaction (m) must be favored over Reaction

(n) as the hydrogenation pathway. If, on the other hand, the CH_4 originated exclusively from decomposition of C_2H_6, the rate of CH_4 production should have been 1.5 times the rate of C_2H_4 hydrogenation according to the experimentally determined stoichiometry of C_2H_6 decomposition (Reaction (a))--so long as the C_2H_4 dose rate was slow enough to be rate limiting. But the experimental evidence (Table 6, line 25) shows the CH_4 rate was at most 0.70 times the dose rate, indicating that less than half the C_2H_4 is hydrogenated on the hydrogen-covered surface--a result which also favors Reaction (m) over Reaction (n).

The results of hydrogenation of C_2H_4 on a carbon-covered surface, such as shown in Figure 36 also tend to support Reaction (m) since the rate of hydrogenation shows no appreciable decrease as would be expected if most of the adsorbed hydrogen were displaced by adsorbed carbon (leaving hydrogen bonded to adsorbed carbon rather than directly to the surface). It is understood that in the most general case C_2H_4 (a) in Reaction (m) is to be taken as any hydrocarbon adsorbate which meets the requirements of having labile hydrogen atoms for C_2H_4 hydrogenation and readily accepting replacement of these atoms by gas phase hydrogen or mobile surface hydrogen. If there are hydrogen sites on the surface, however, that are unavailable for carbon adsorption Reaction (n) is still a valid possibility. It

may be that hydrogenation can proceed equally well by either reaction.

Gardner and Hansen have recently proposed (14) trans diadsorbed C_2H_4 on the 4.47-Å spacing of tungsten as the active site or species for hydrogenation. After an impinging gaseous (or physically adsorbed) C_2H_4 molecule captures two hydrogen atoms from this adsorbed species it leaves trans diadsorbed C_2H_2. Upon addition of hydrogen (from the gas phase or adsorbed hydrogen) it reverts back to trans diadsorbed C_2H_4.

The metal-metal spacing required for strain-free trans diadsorption of C_2H_2 is about 5.0 Å for either W or Ir. Diadsorbed C_2H_4 can be accommodated on spacings of about 3.0 to 5.0 Å, depending on the orientation of the carbon-metal bonds relative to the C-C axis. The 4.47-Å spacing occurs on the 111 and 211 planes of W, which has a body-centered-cubic structure. The longest spacing (of adjacent atoms) on the densest planes of Ir (100, 110, 111--which probably comprise the largest part of the surface) is 3.82 Å on the 110 plane; for this reason the trans diadsorbed species would to be less important for hydrogenation on Ir than on W.

Polymerized adsorbed hydrocarbons offer interesting possibilities for active hydrogen donor sites in the hydrogenation reaction in much the same way as does the

proposed trans diadsorbed C_2H_4. The distance between alternate carbon atoms in an alkyl chain is 2.50 Å, while the closest-packed spacing of Ir atoms is 2.71 Å. The similarity of these distances leads to the suggestion that C_2H_4 may form polymer chains of indefinite length on the surface, with alternate carbons bonded to adjacent Ir atoms. A C_2H_4 trimer model adsorbed on the 110 face of Ir is shown in Figure 42. The six carbon atoms lie in a single plane which presumably may rotate about the axis of the bonding Ir atoms within the obvious steric limitations. The carbon plane is shown parallel to the surface plane for simplicity in depicting the model. An infinitely long polymer with the distance of alternate carbons expanded from 2.50 to 2.71 Å to match the Ir spacing would require distortion of the C-C-C angle from the normal 109° to 122°. The distance between the hydrogens (above the plane of the carbons) on carbons 1 and 2 is 2.5 Å, while that between hydrogens on carbons 1 and 3 varies from 2.5 to 2.7 Å depending upon the distortion of the carbon skeleton. These spacings are viewed as favorable for C_2H_4 hydrogenation. (The most favorable spacing would presumably be slightly less than the 2.25 Å spacing of eclipsed hydrogen atoms on C_2H_6, for best overlap of C_2H_4 (g) π-bonding p orbitals with the hydrogen σ orbitals in the transition intermediate.) Thus a pair of hydrogens presumably could be readily abstracted

from the surface polymer by an impinging C_2H_4 molecule and replaced by hydrogen from the gas phase or elsewhere on the surface.

For the concerted reaction of gaseous C_2H_4 with the hydrogens ~ 2.7 Å apart on carbons 1 and 3, there is essentially a plane of symmetry passing thrcugh carbon 2, equidistant from carbons 1 and 3, and perpendicular to the surface. The assumed approach of the C_2H_4 molecule is such that the plane defined by its hydrogen atoms is parallel to the carbon plane, and its double bond is bisected by the plane of symmetry (Figure 43a). Such a reaction should conserve orbital symmetry. Although the application of the orbital symmetry conservation rules in this instance is of somewhat dubious validity because of the necessity of considering an orbital of a surface iridium atom, a discussion of the conservation rules as applied to a hypothetical reaction is given in Appendix B. It is shown that symmetry conservation can be observed if certain restrictions are met by the metal orbital involved.

In the initiation of a chain reaction for formation of a polymer on the surface, vacant surface sites may function much as do free radicals in homogeneous reactions. The first step in the chain could well be

$$*\cdot + C_2H_4\,(g) \rightarrow \underset{*}{CH_2CH_2}\cdot \qquad (r)$$

where the symbol (*·) denotes a vacant surface site with an unpaired electron. The chain may be extended by

$$2\ \underset{*}{CH_2CH_2}\cdot \rightarrow \underset{*}{CH_2CH_2}\underset{*}{CHCH_2}\cdot + \underset{*}{H}\cdot \qquad (s)$$

or by

$$C_2H_4 + \underset{*}{CH_2CH_2}\cdot \rightarrow \underset{*}{CH_2CH_2CH_2CH_2}\cdot\ . \qquad (t)$$

Two possibilities for termination of the chain are

$$\underset{*}{RCHCH_2}\cdot + \underset{*}{H}\cdot \rightarrow \underset{*}{RCHCH_3} \qquad (u)$$

and

$$\underset{*}{RCHCH_2}\cdot + *\cdot \rightarrow \underset{* *}{RCHCH_2} \qquad (v)$$

where R denotes a hydrocarbon group or a hydrogen atom. A third possibility for termination is

$$2\ \underset{*}{CH_2CH_2}\cdot \rightarrow \underset{*}{CH_2CH_2CH_2}\underset{*}{CH_2}\ . \qquad (w)$$

The 4-carbon skeleton could take on conformations to accommodate a wide variety of site spacings.

The relative probabilities of Reactions (s) and (w) would depend on the distance between adsorbed free-radical ethylenes, longer distances favoring Reaction (w) over Reaction (s). The species $\underset{*}{C_2H_4}\cdot$ is viewed as a relatively short lived one which goes to the diadsorbed species $\underset{*}{CH_2}\underset{*}{CH_2}$ on a sparsely covered surface.

While this study furnished nc direct evidence for polymer formation (i.e., none was found in the gas phase) and little work has been done with hydrocarbons on Ir, production of small amounts of polymers has been observed on other transition metals. For example, Beeck (15) found that hydrogenation of an C_2H_4 residue on Ni film at 23° C, 20% of the residue could be reacted off in one hour as "about 90% saturated polymers (C_4 to C_8 and higher) and 10% ethane." Similar experiments with Rh yielded mostly ethane with only a few percent polymer, with 60% of the adsorbed carbon desorbed in one minute. Rh resembles Ir chemically and has nearly the same closest-packed spacing--2.69 Å. The Ni spacing (2.49 Å) is nearly identical to the 1, 3 carbon distance. The lack of polymerized desorption products from Ir does not necessarily rule out polymer formation but may instead indicate reversibility of polymer formation upon treatment with excess hydrogen.

Block (16), using field desorption from the carbon-covered 211 plane of Pt, has reported desorption of products with masses corresponding to C_{2n} hydrocarbon species following C_2H_4 doses.

CONCLUSIONS AND SUMMARY

In conclusion, it can be seen that there is no reason why the C_2H_4 results of Roberts and Hansen need to be considered contradictory to each other. If the basic hydrogenation mechanism involves direct reaction of a gas phase C_2H_4 molecule with surface hydrogen, any C_2H_6 production on a filament at low pressure ($< 10^{-6}$ torr) would more likely occur during C_2H_4 dosing rather than during flash desorption when there is no C_2H_4 gas present.

Rye (17) has shown that on both bare and hydrogen-predosed tungsten filaments at room temperature, C_2H_6 can be detected if C_2H_4 is dosed slowly in a closed system. (The subsequent flash desorption results are similar to those for Ir in that H_2 is by far the predominant desorption product.)

The role of hydrogen pressure in the hydrogenation reaction as well as in the C_2H_6 decomposition is not yet fully understood and invites further study. In nearly all the experiments in this study it was noted that cessation of reaction (i.e., of production of CH_4 or C_2H_6) was accompanied by a decrease in H_2 pressure to about 0.2 μ. In contrast, H_2 pressure during flash filament dosing is typically less than 10^{-9} torr during flashing.

In relation to the above hydrogen pressure effect, it has been pointed out (in the Results section) that the

hydrogen isotherms found to be valid for the films of this study in the pressure region above 0.05 μ predict hydrogen coverages on the order of 0.01 monolayer at the pressures used in flash filament experiments. Coverages this low are clearly in contradiction with the known facts. Either the extrapolation of the isotherm to low pressure (on both films and filaments) is not valid or there are significant differences in the surface structures of the two forms of the metal.

The major findings of this study may be summarized as follows:

1. The microscopic surface area of Ir films, evaporated on 100° C Pyrex to average thicknesses of 30 to 200 Å, was found to be proportional to film thickness, as determined by low temperature hydrogen adsorption. There were 6.7×10^{13} atomic hydrogen sites per cm^2 of film support (Pyrex) for each Å of film thickness (or 3.0×10^{14} sites/μg Ir). If each adsorption site represented one Ir surface atom, 9.6% of the Ir atoms were at the film surface.

2. Saturation hydrogen adsorption (at 20 μ) increased with decreasing temperature according to the relationship

$$\theta_{max} = 1 - \beta (T + 173^\circ C)$$

for T in the range -143 to 100° C, where $\beta = 2.2 \times 10^{-3}$ monolayer/deg. Hydrogen adsorption isotherms at several

temperatures were found to follow the model

$$\theta_T = \frac{bP^{1/2}}{1 + bP^{1/2}}$$

where θ_T is the fractional coverage at pressure P, temperature T, divided by the saturation coverage at temperature T. Values of b are given in Table 2.

3. Initial adsorption of C_2H_4 or C_2H_6 on a hydrogen-predosed surface at 100° C was dissociative with about 2 or 4 hydrogen atoms evolved, respectively, per adsorbed hydrocarbon molecule.

4. C_2H_6 decomposed on Ir at 100° C to give CH_4 at a rate proportional to the microscopic area of the film--2.0×10^{-3} molecule (hydrogen site-sec)$^{-1}$--but zeroth order in C_2H_6 and H_2 partial pressures in the range 0.1 μ to ~ 20 μ. Breaking of the C-C bond was most likely the rate-limiting step.

5. Self-hydrogenation of C_2H_4 at 100° C was initially rapid, but finally self-poisoning, consistent with the reaction

$$C_2H_4\ (g) + C_2H_4\ (a) \rightarrow C_2H_6\ (g) + C_2H_2\ (a)\ .$$

6. Alternate dosing of H_2 and C_2H_4 indicated that an indefinite amount of a 1:1 mixture of C_2H_4 and H_2 will readily react to form CH_4 at temperatures from -143 to 100° C on a carbon-covered surface.

7. For low surface coverage at 100° C C_2H_4 slowly decomposes to CH_4 before C_2H_6 appears in the gas phase.

8. In the presence of excess H_2 (g), a C_2H_4-poisoned surface at 100° C evolves CH_4 very slowly--at a rate which increases with time (and with decreasing carbon surface coverage). Initially upon treatment of the C_2H_4 residue, C_2H_6 may also be evolved (depending upon experimental conditions) but it decomposes to CH_4.

FIGURES

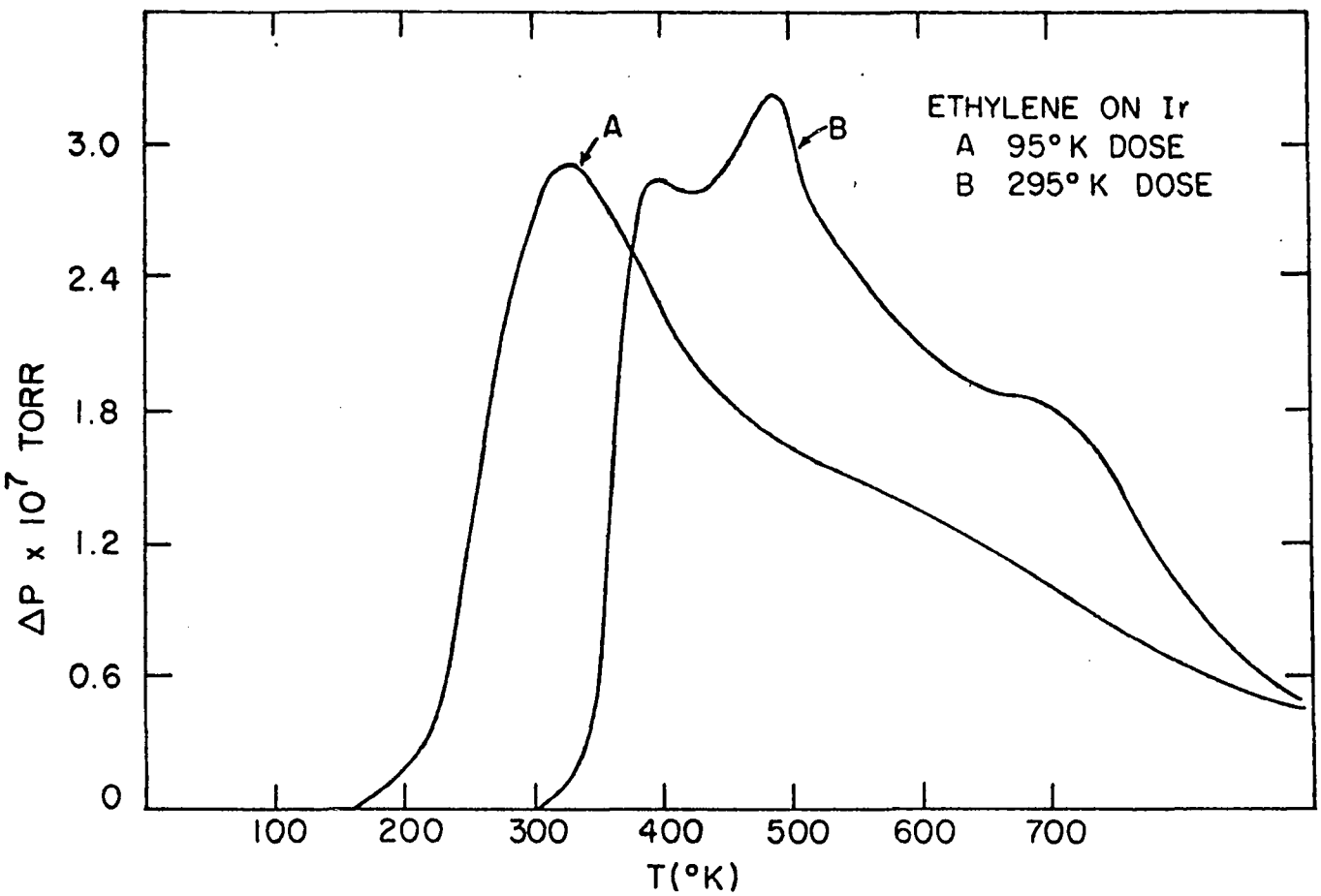

Figure 1. Flash filament desorption of hydrogen from C_2H_4 doses on Ir at 95 and 295° K, from Reference (5)

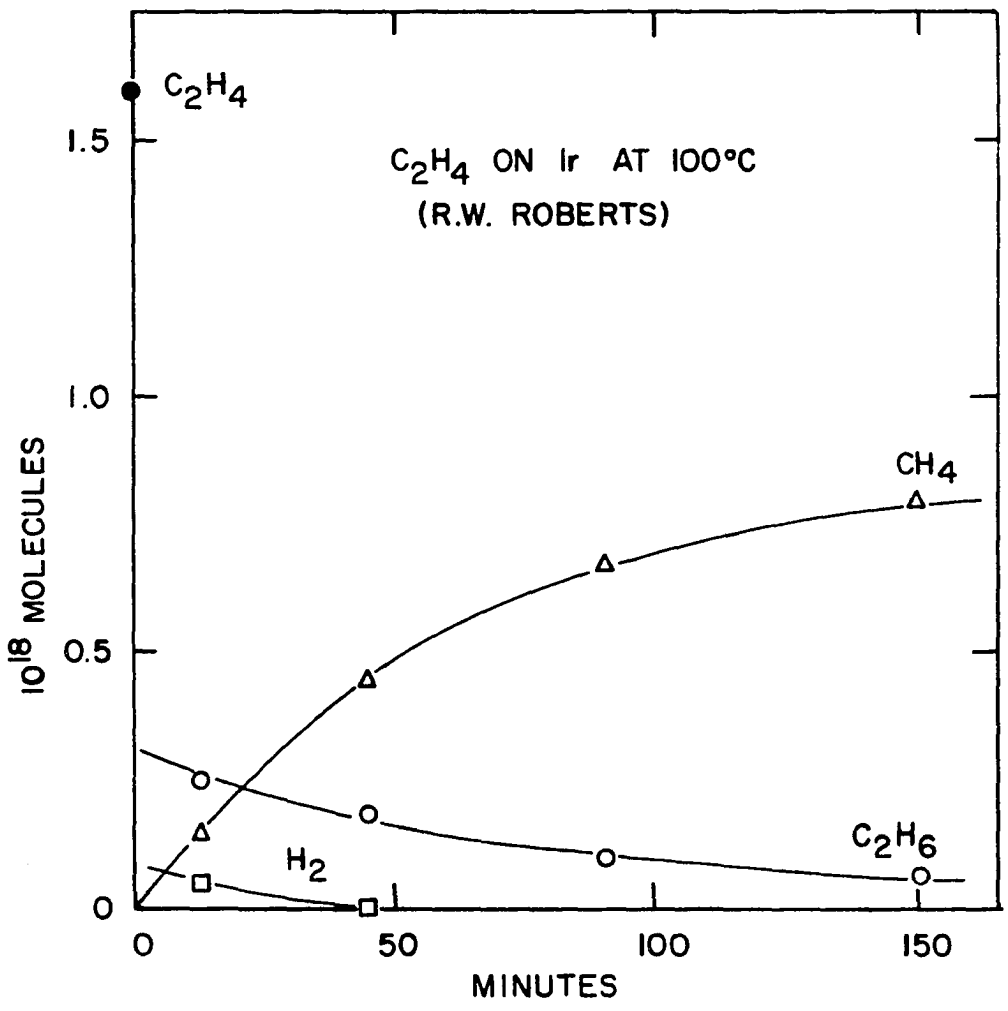

Figure 2. Decomposition of C_2H_4 on a 100° C Ir film, taken from Reference (7)

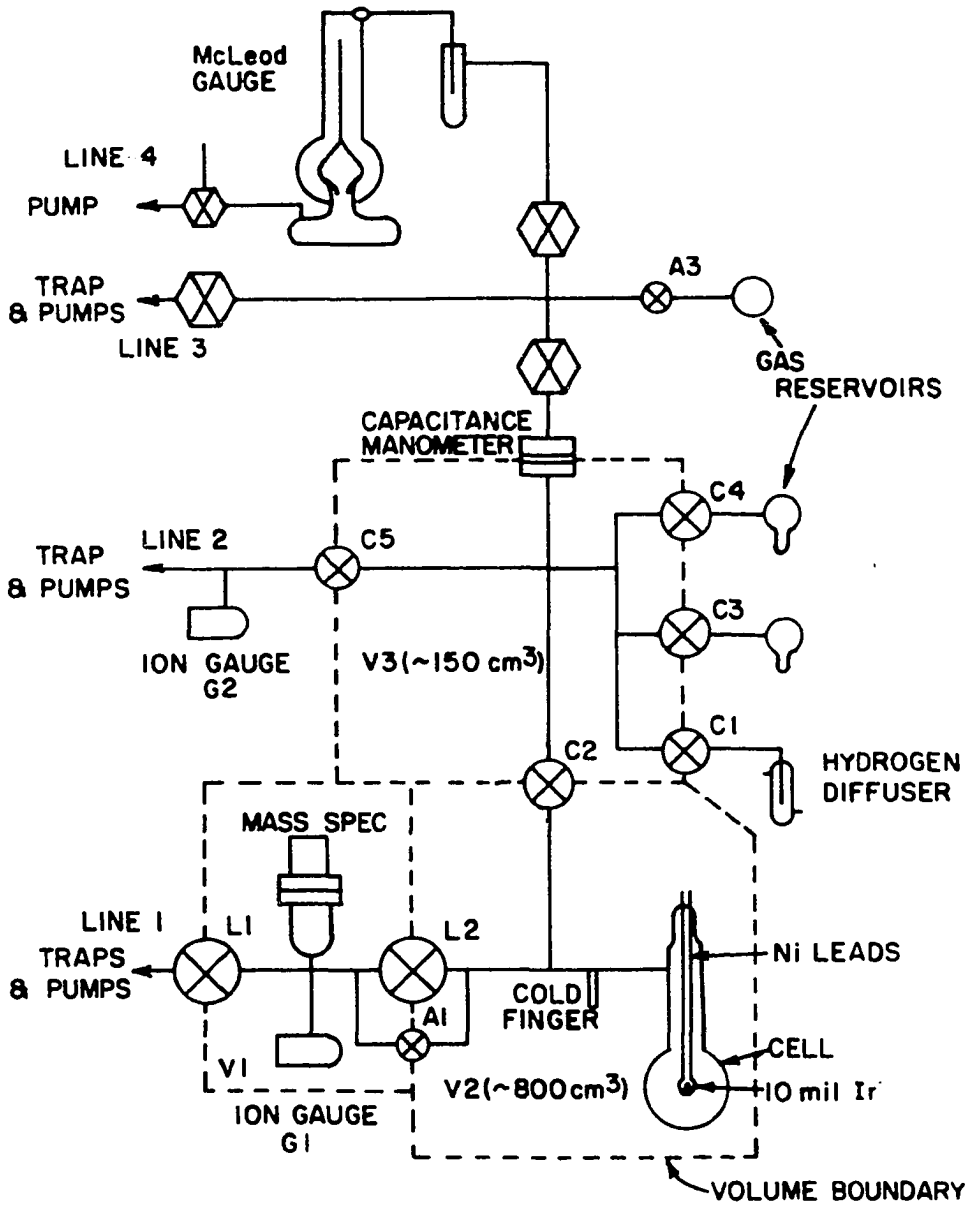

Figure 3. Schematic diagram of the vacuum system used for thin film studies showing the four separate vacuum lines. The dashed lines define the extent of three measured volumes, V1, V2, and V3. Circles and hexagons with inscribed X's represent metal valves and glass stopcocks, respectively

Figure 4. Photograph of the front of the vacuum rack showing the ultrahigh vacuum portion of the system. Principal features (starting at top center and moving clockwise around the panel) are the mass spectrometer head, ion gauge G1, the reaction cell, leak valve A1, liquid nitrogen trap, and (near the center) the two one-inch valves L1 and L2

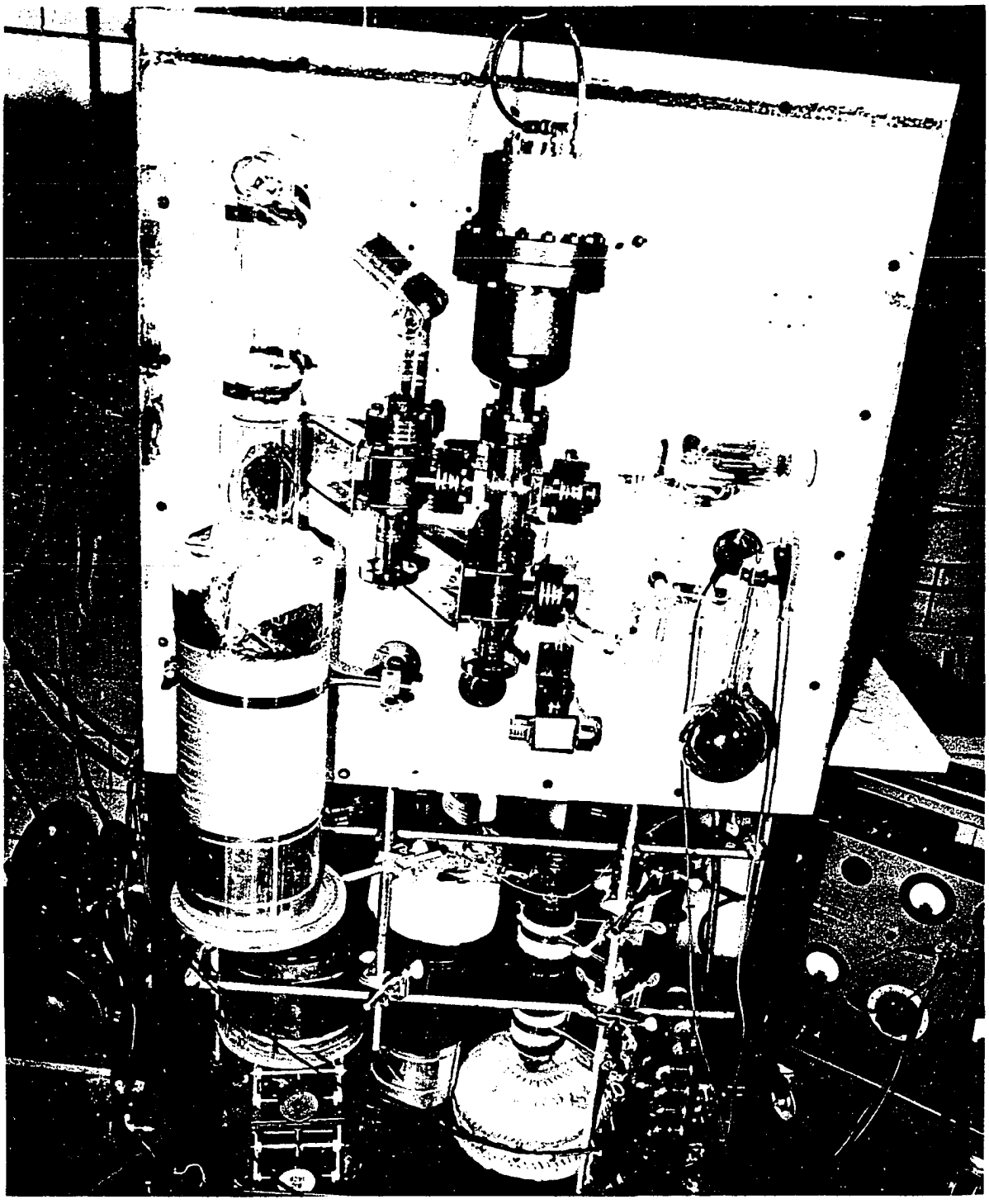

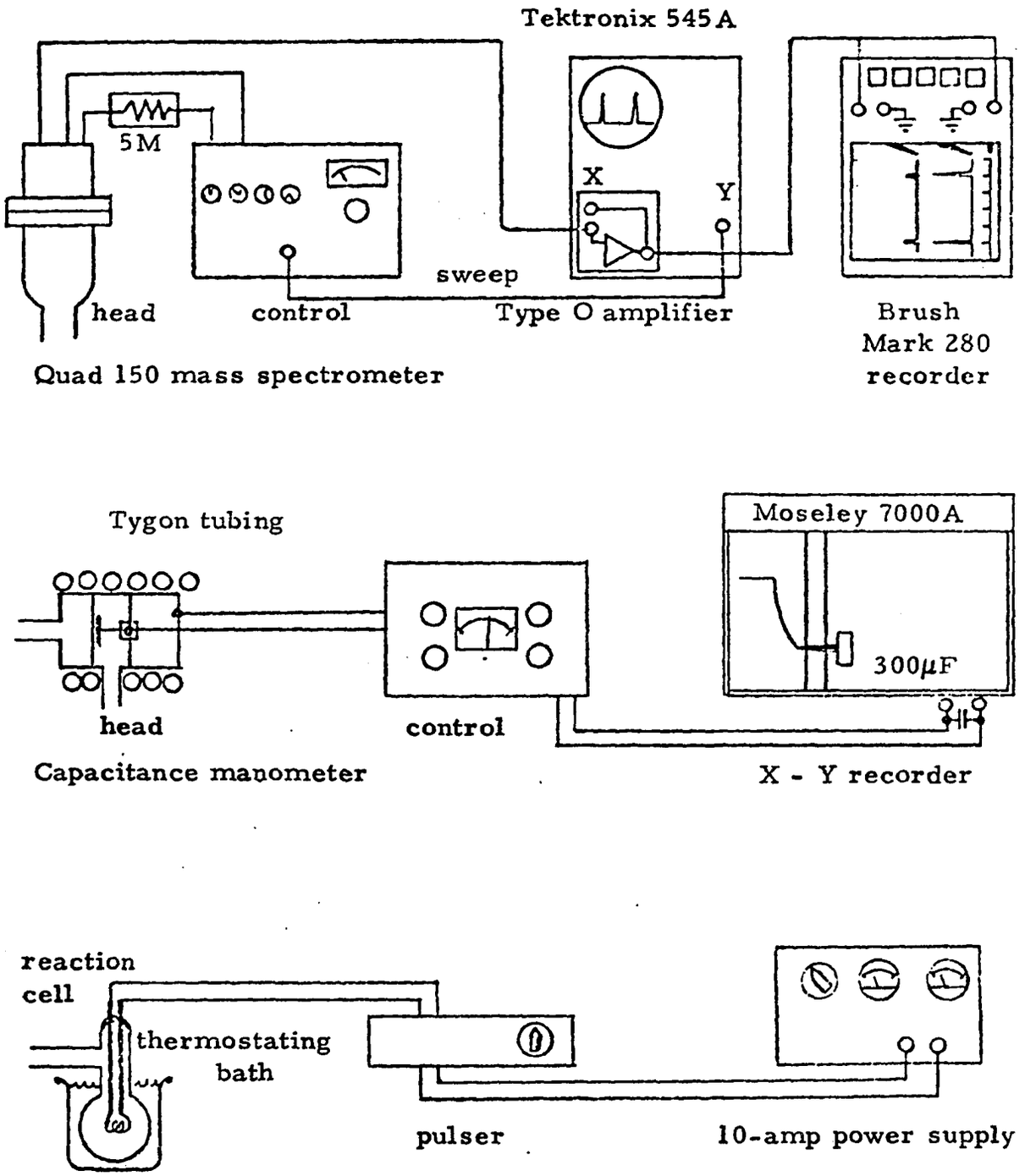

Figure 5. Mass spectrometer recording system, capacitance manometer recording system, and Ir filament heating circuit

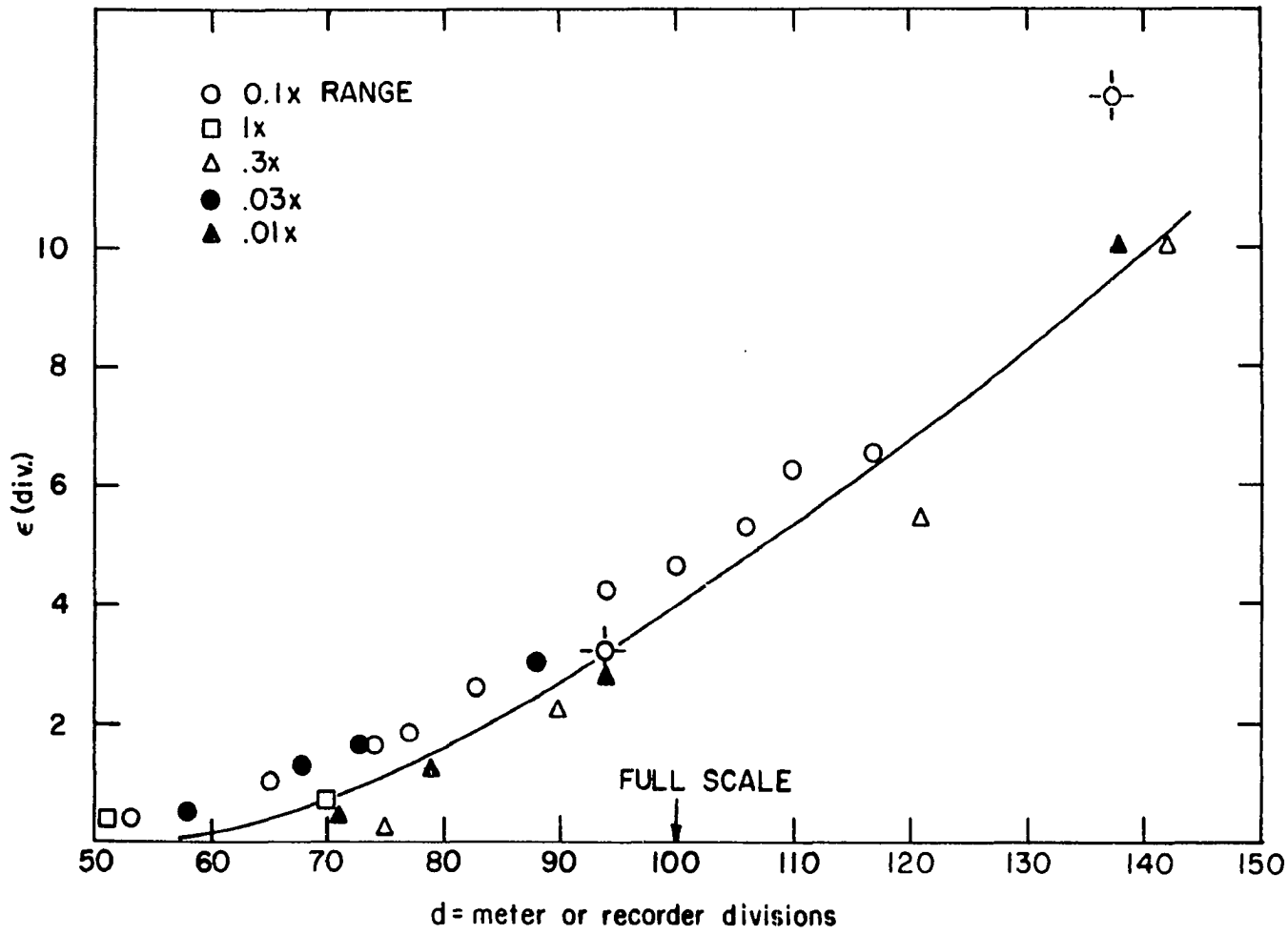

Figure 6. Capacitance manometer correction curve. The manometer output d (meter divisions) was corrected to give a "true reading" d' by the equation $d' = d + \epsilon$, where ϵ is the correction read on the ordinate. The curve was obtained with the "sensitivity" control set at 50 meter divisions

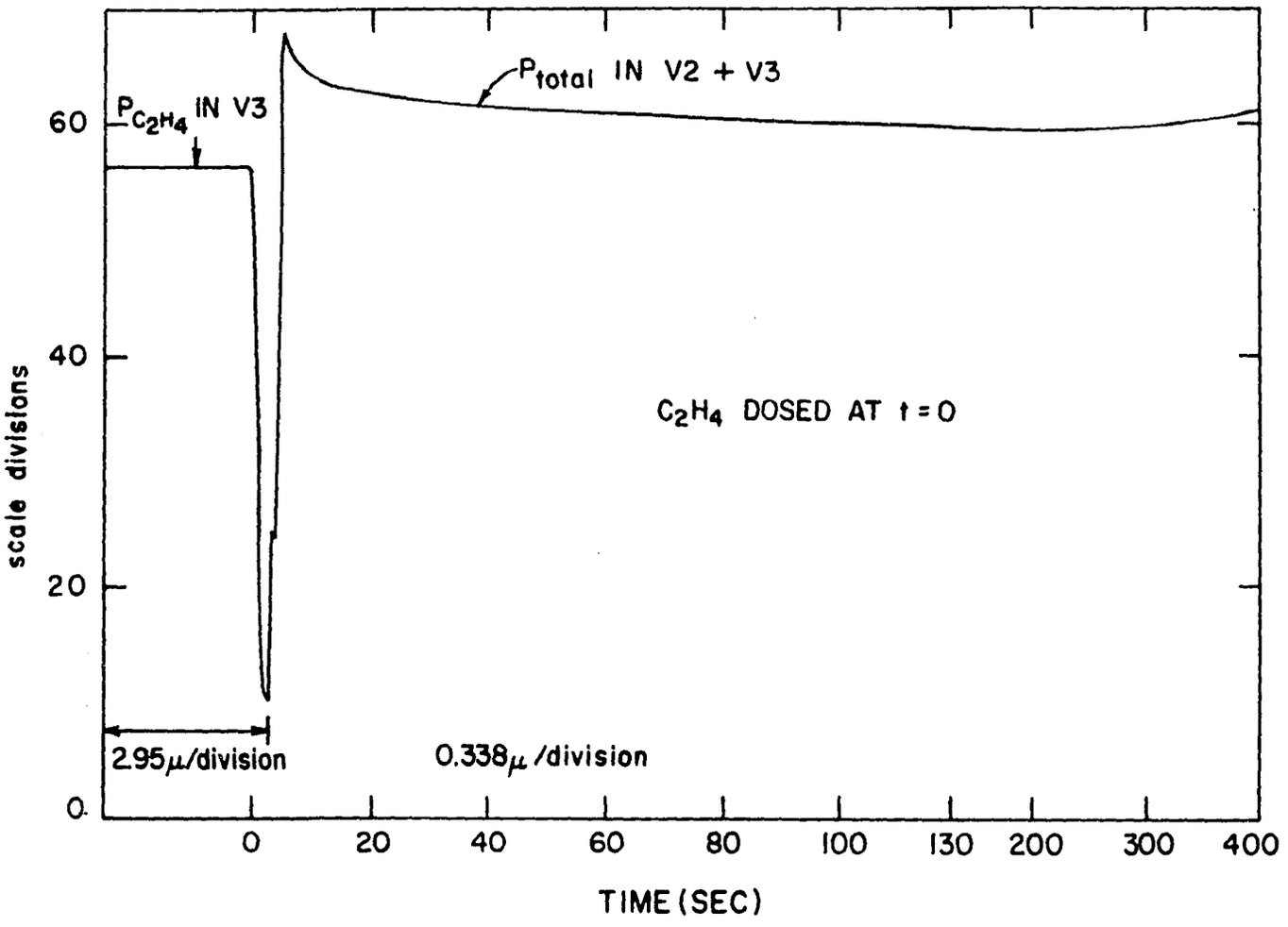

Figure 7. An example of the capacitance manometer pressure data as recorded on the Moseley X-Y recorder. The sharp drop at t = 0 is caused by the expansion of C_2H_4 from V3 into V2 as it was dosed to begin Experiment IV. The manometer was switched to a more sensitive range immediately following the drop. The recorder time sweep rate was decreased by a factor of 5 at t = 120 sec. The time scale is coincident with those of Figures 8 and 28

Figure 8. An example of the mass spectrometer output as recorded on the two-channel Brush recorder. The same signal was recorded on both channels but at different sensitivities, as indicated by the i_m scales. Individual seconds were marked by a third pen. (The m/e scale was added in the reproduction and does not appear on the original.) This shows the beginning of Experiment IV in which C_2H_4 was dosed on a D_2-predosed surface. See also Figures 7 and 28. Resolution of adjacent peaks was much better than this reproduction indicates. Background species evident (at $t < 0$) are H_2, HD, D_2 ($m = 2, 3, 4$), deuterated methane and water (major peak at $m = 18$), CO ($m = 28$), and CO_2 ($m = 44$)

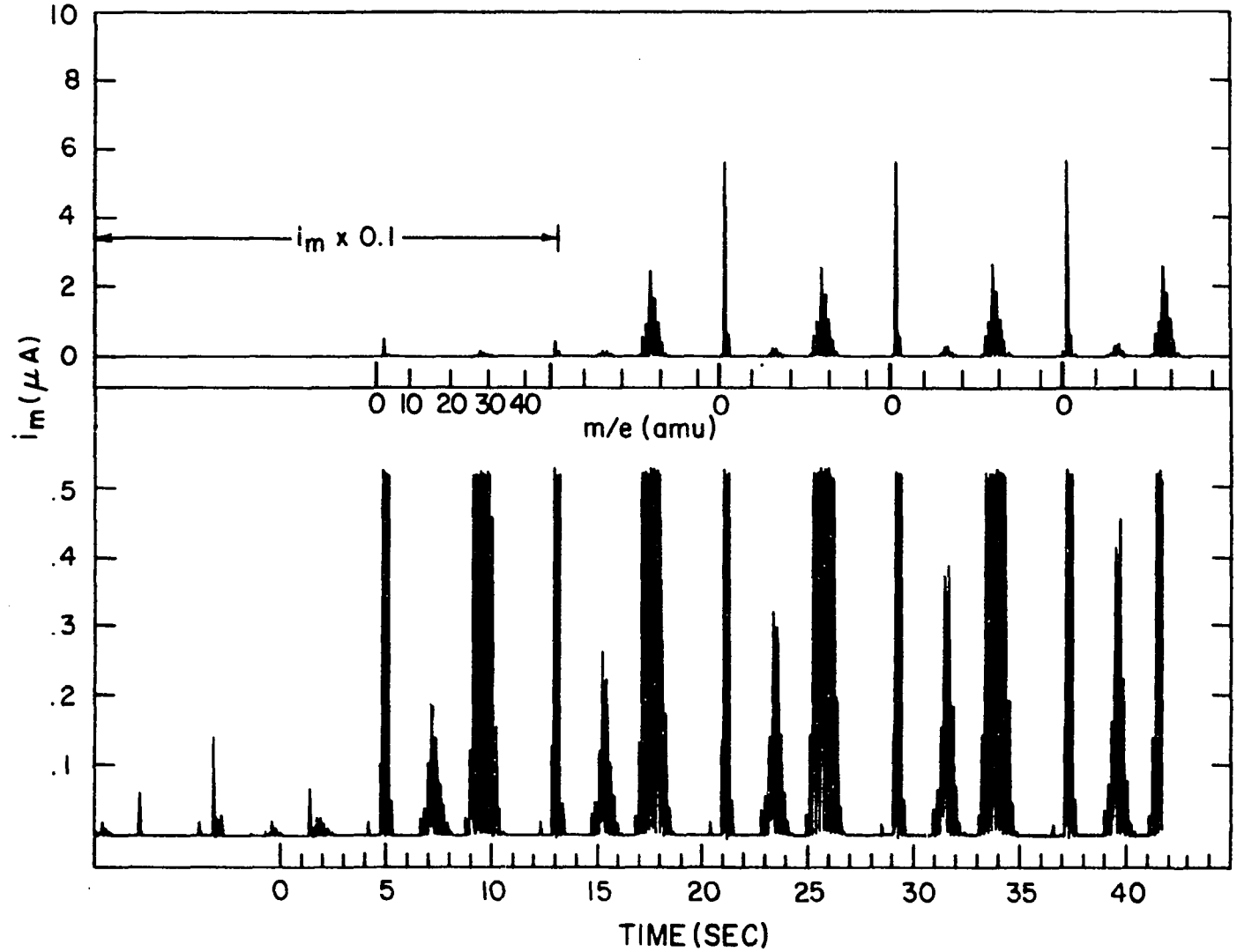
10
8
6
4
2
0
i_m x 0.1
i_m (μA)
0 10 20 30 40
m/e (amu)
.5
.4
.3
.2
.1
0
5
10
15
20
25
30
35
40
TIME (SEC)

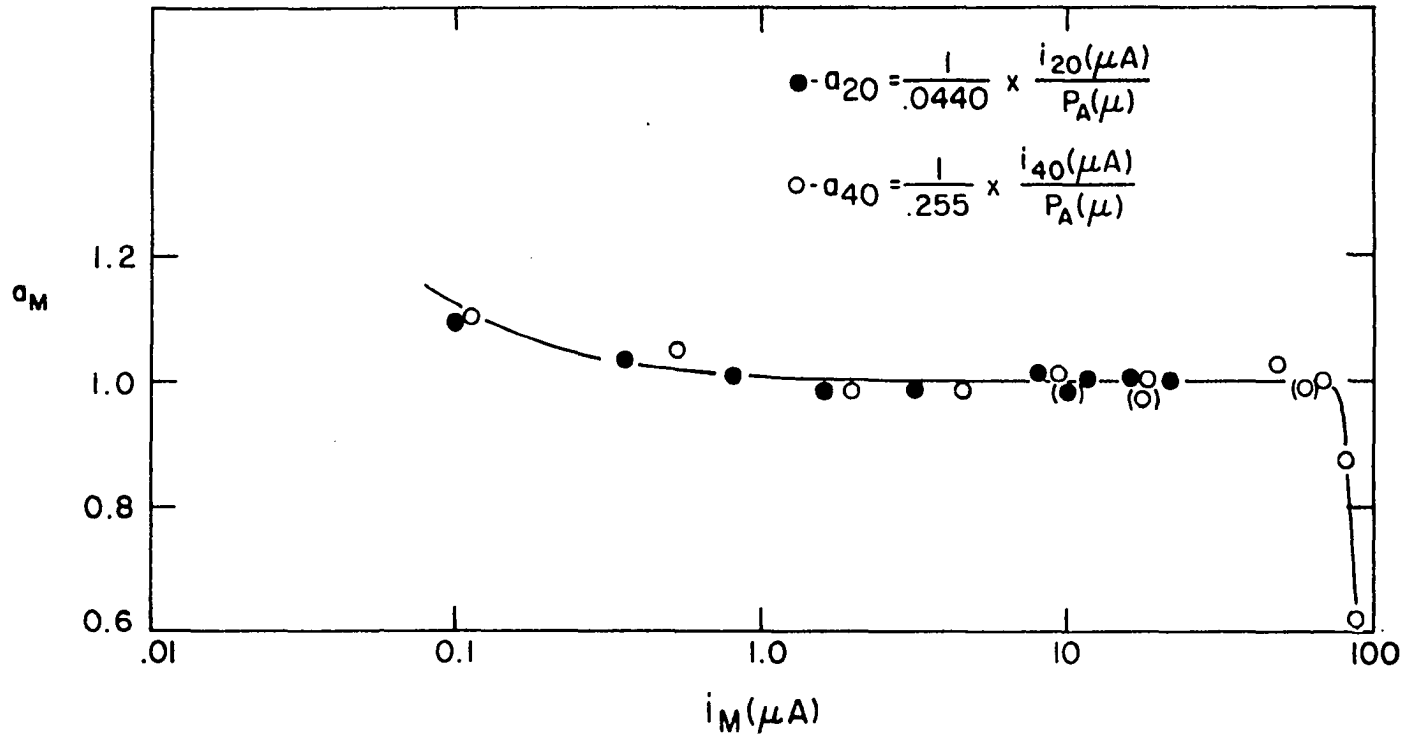

Figure 9. Variation in a_m with i_m for argon. This graph shows that the ion current obtained from argon leaking through valve A1 (at fixed setting) is proportional to argon pressure in the reaction cell, except at very low ion currents

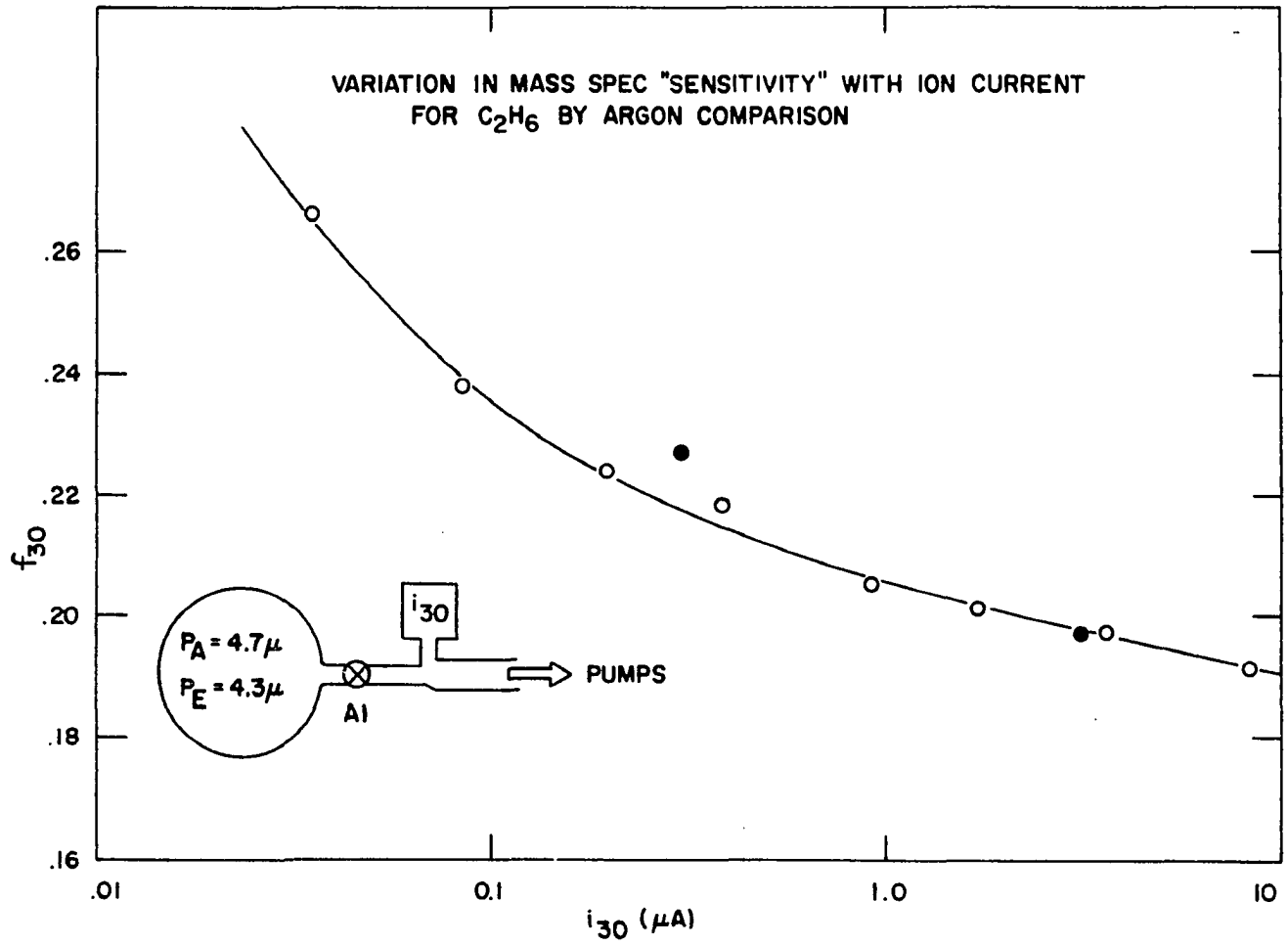

Figure 10. Variation in relative sensitivity f_{30} with i_{30} for ethane. Relative sensitivity f_m is defined by Equations 7 and 8 in text

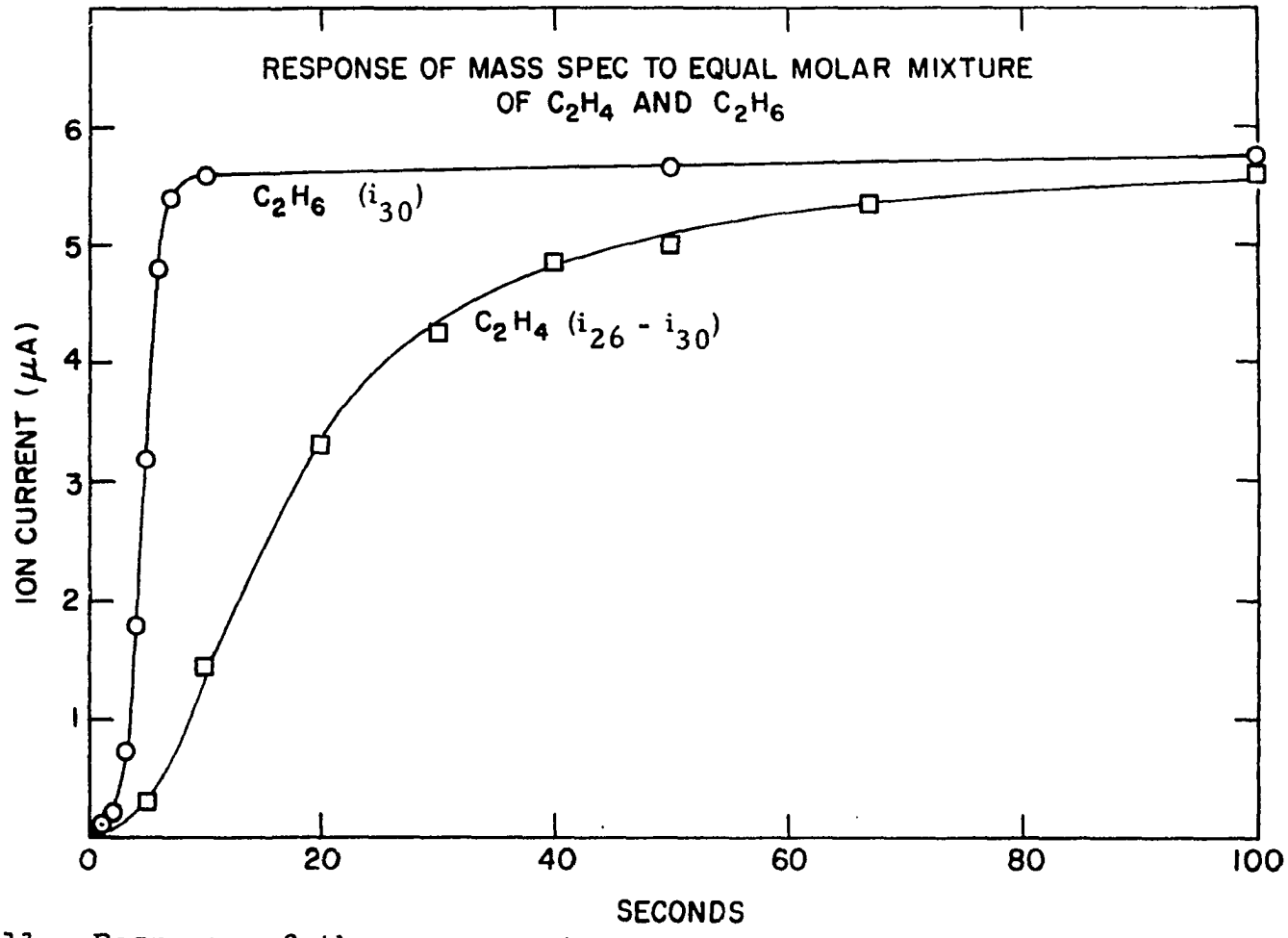

Figure 11. Response of the mass spectrometer to approximately equal pressures of C_2H_4 and C_2H_6 in the reaction cell. The leak valve A1 was opened beginning at t = 0, but was not finally adjusted until t = 2 or 3 seconds

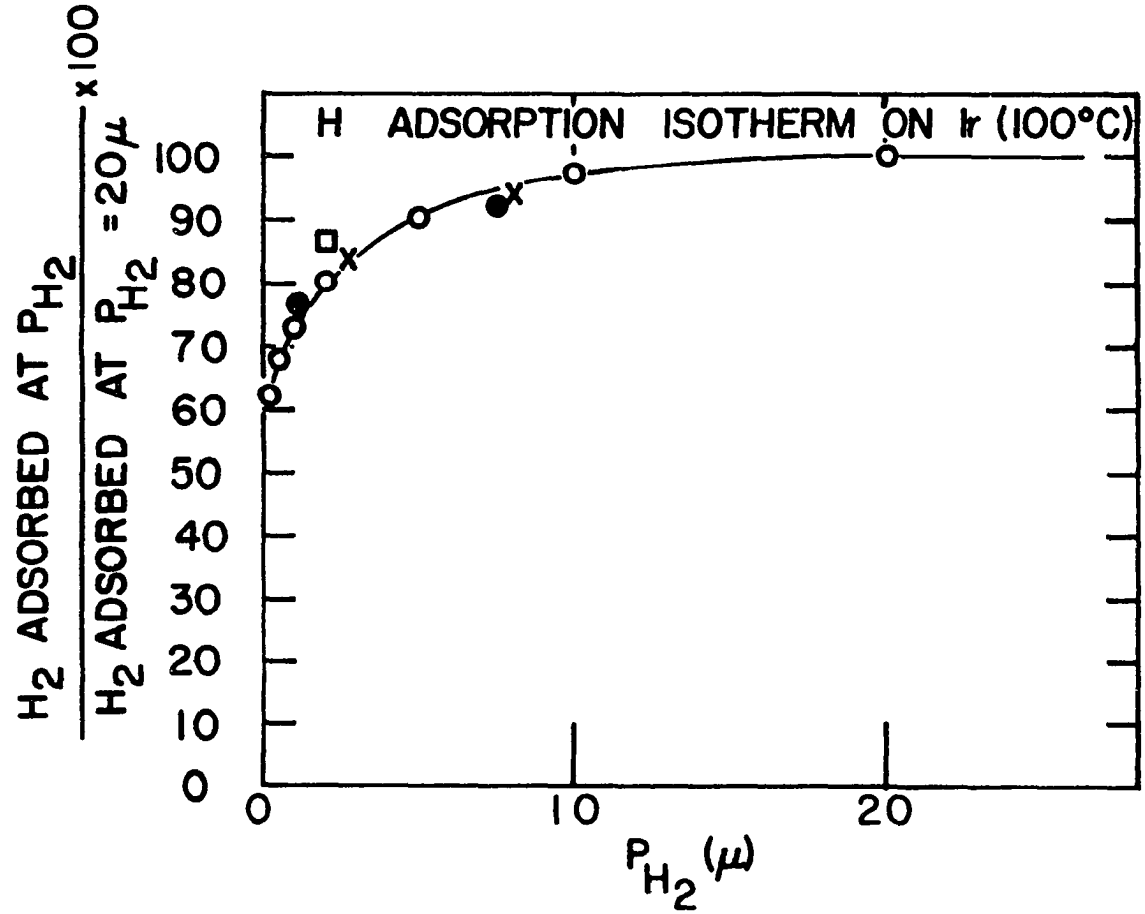

Figure 12. Hydrogen adsorption isotherm on Ir (100° C). The open circles and connecting line represent an average of two runs. Saturation adsorption was not determined directly for the runs designated by the symbols ● and X, but was calculated as the average of the 20μ adsorption predicted by the curve. Saturation adsorption of the run designated by the symbol □ was determined at 50μ

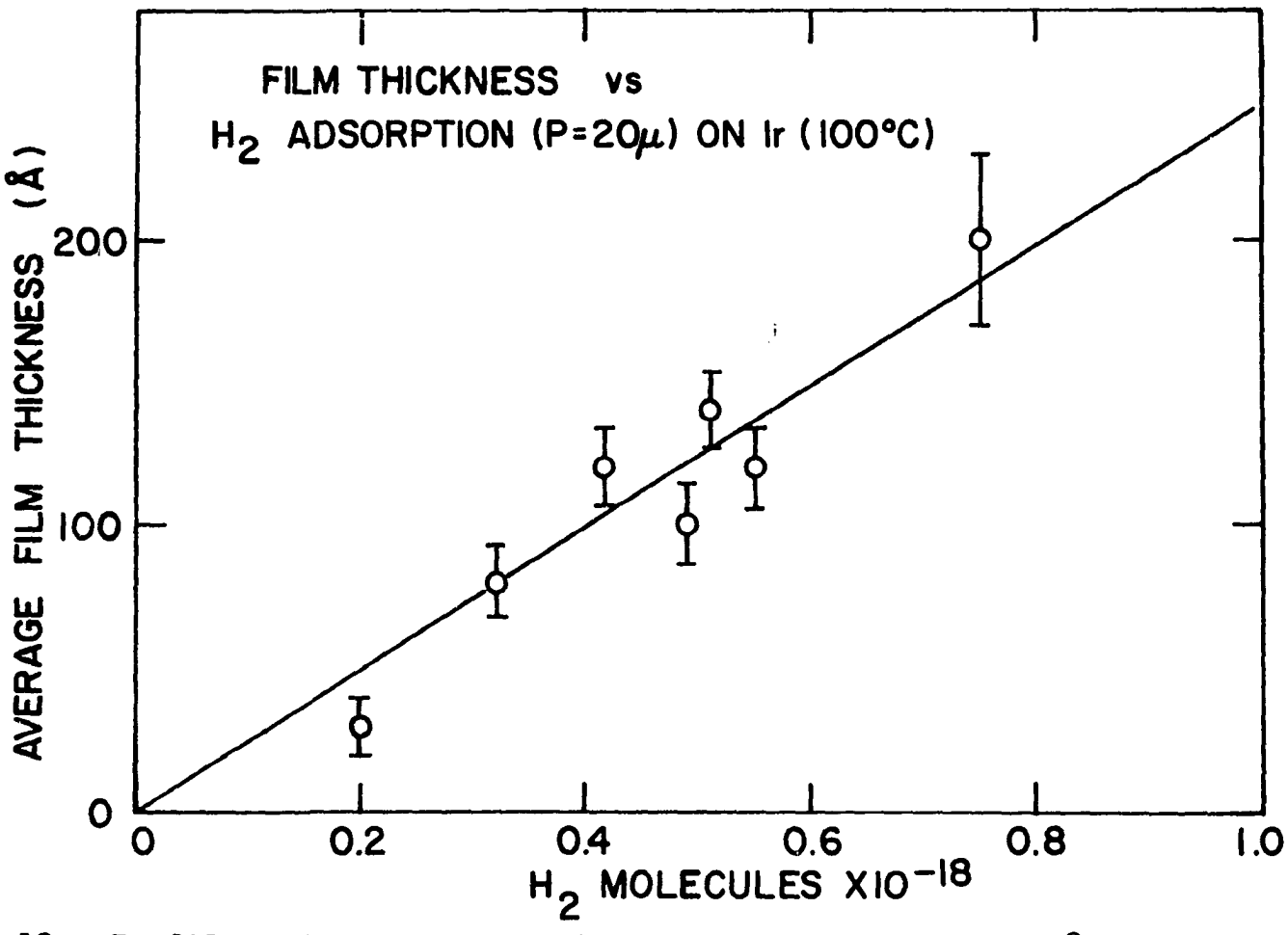

Figure 13. Ir film thickness versus hydrogen adsorption at 100° C. Adsorption was either measured at 20μ (or higher) or obtained by extrapolation of lower pressure values from the isotherm of Figure 12. The specific adsorption is 4.0×10^{15} molecules/Å^2

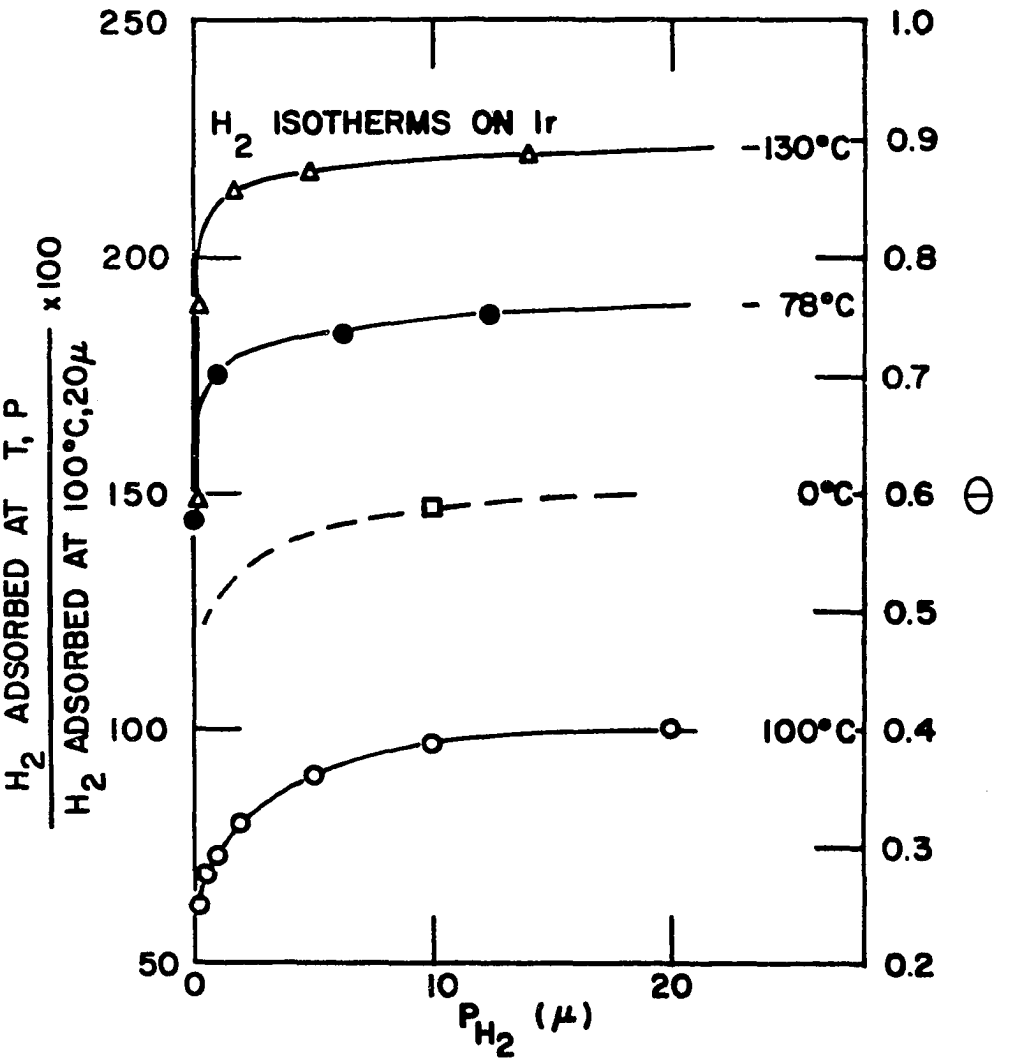

Figure 14. Hydrogen adsorption isotherms at various temperatures. Adsorption at 100° was first determined for the films used at each of the lower temperatures. Cooling the film and ambient gas resulted in the first point shown on each of the lower temperature curves

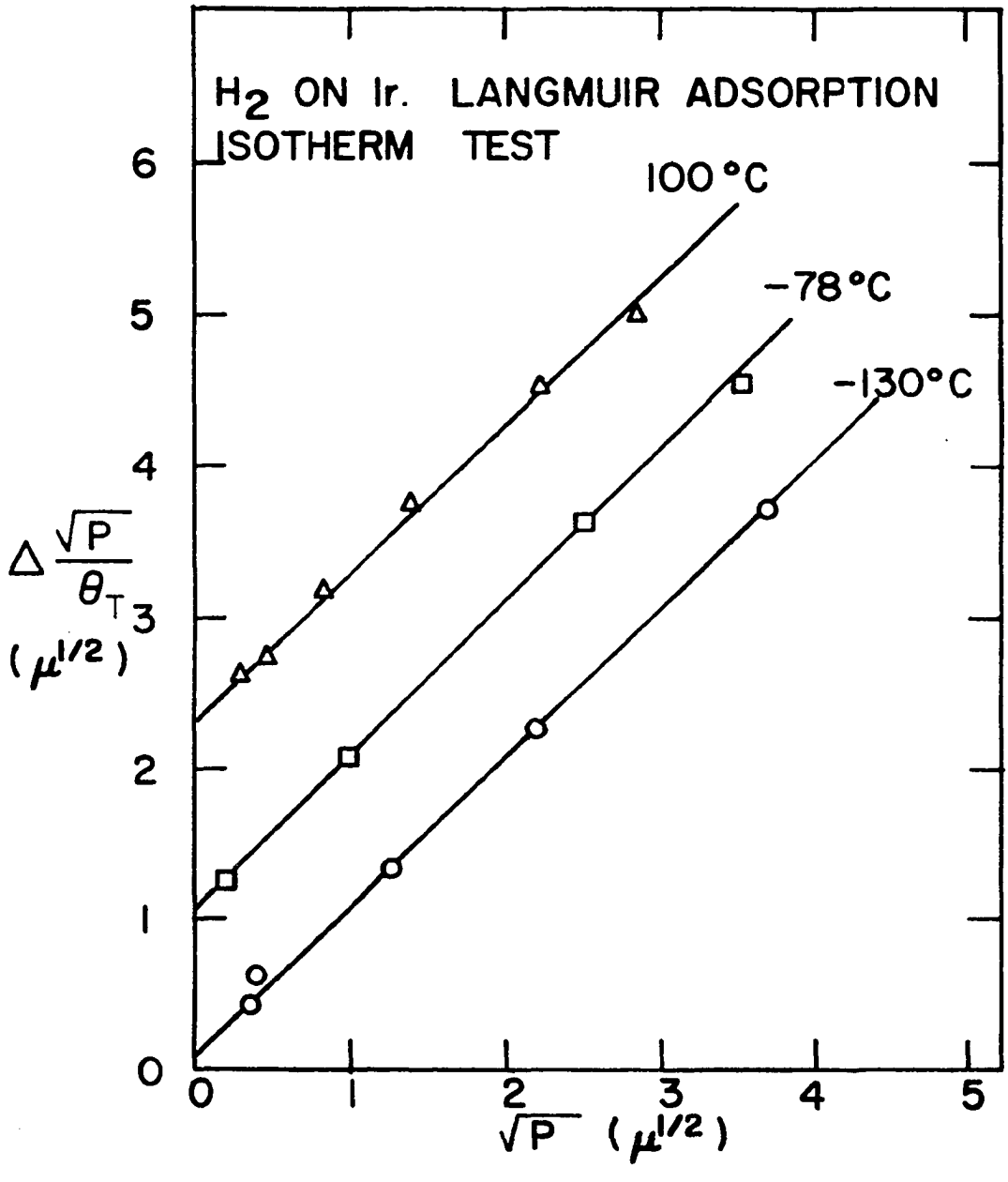

Figure 15. Langmuir adsorption isotherm test. The plots show that the data fit the modified form of the Langmuir isotherm (see Equations 12 and 13 in text) for atomic hydrogen adsorption. Adjacent plots have been displaced upward one unit each on the ordinate for clarity--hence the Δ symbol on the ordinate label

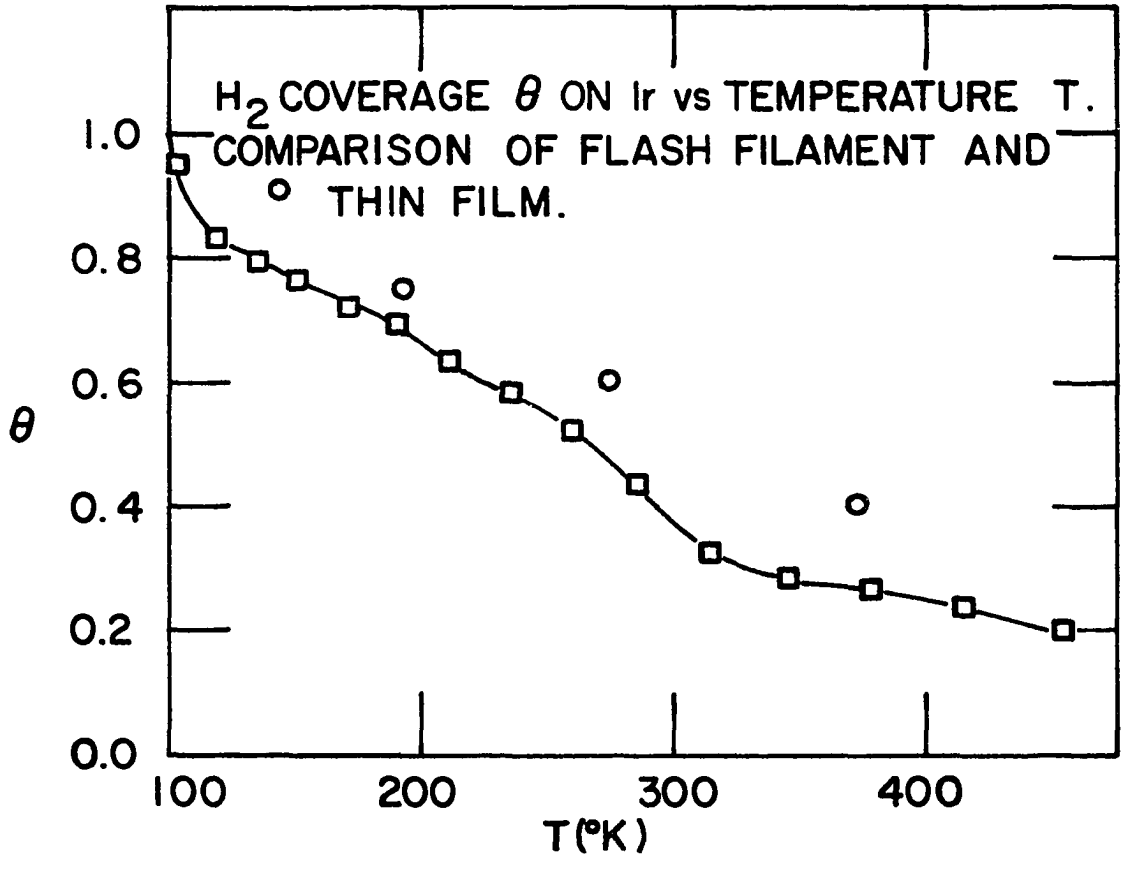

Figure 16. Hydrogen coverage as a function of temperature on an Ir filament during flash (line connecting square points) as compared to saturation coverage (at 20μ) on Ir thin films at various temperatures (circular points). The flash filament curve is based on data taken from Reference (5)

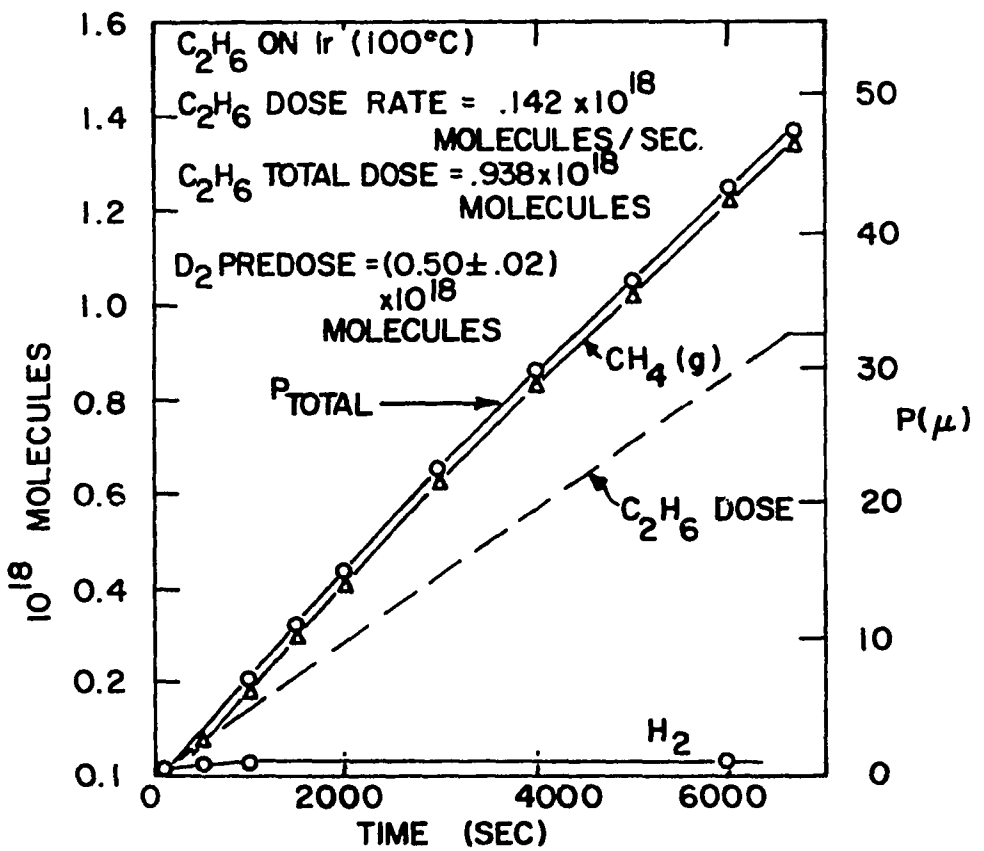

Figure 17. Experiment XII. C_2H_6 decomposition from a low pressure dose at 100° C on a D_2-predosed Ir film

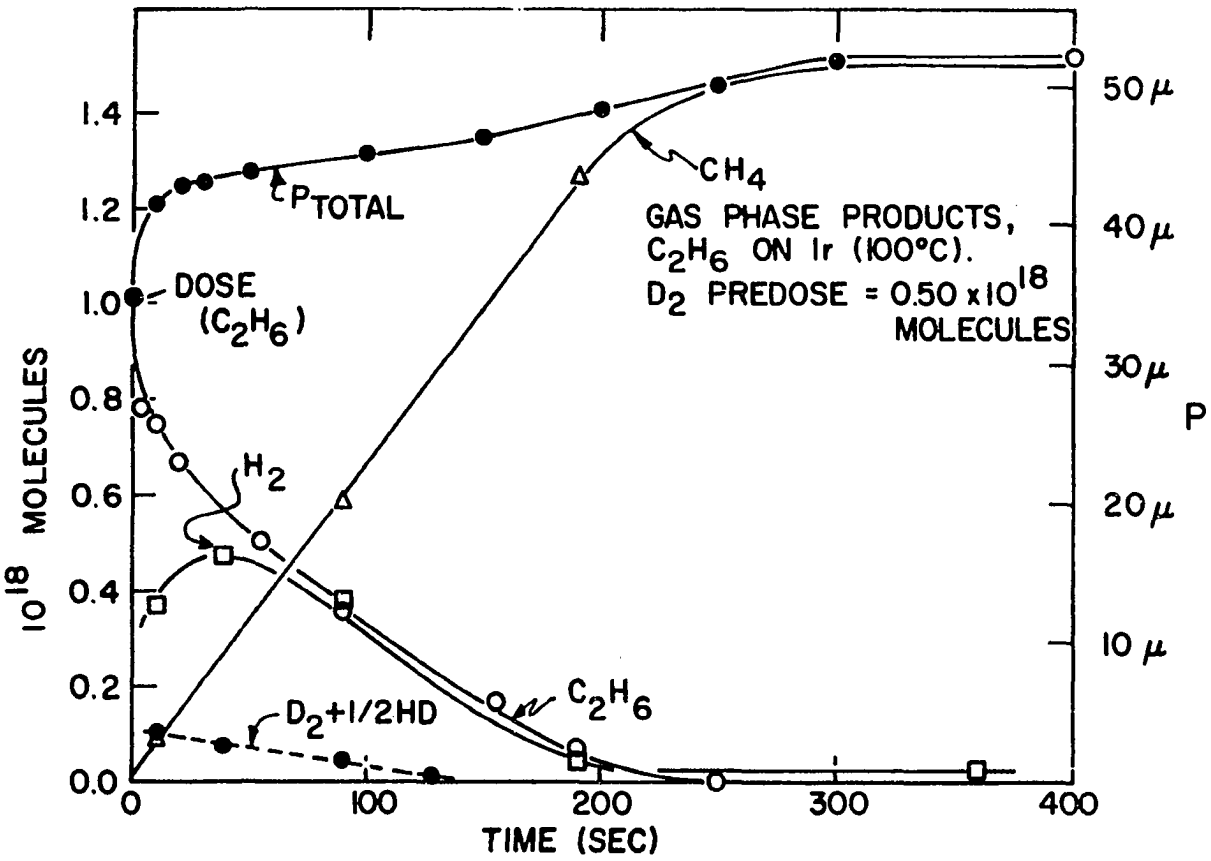

Figure 18. Experiment XIII. C_2H_6 decomposition at 100° C on a D_2-predosed Ir film. The curve labeled H_2 represents the sum of H_2, HD, and D_2 molecules in the gas phase

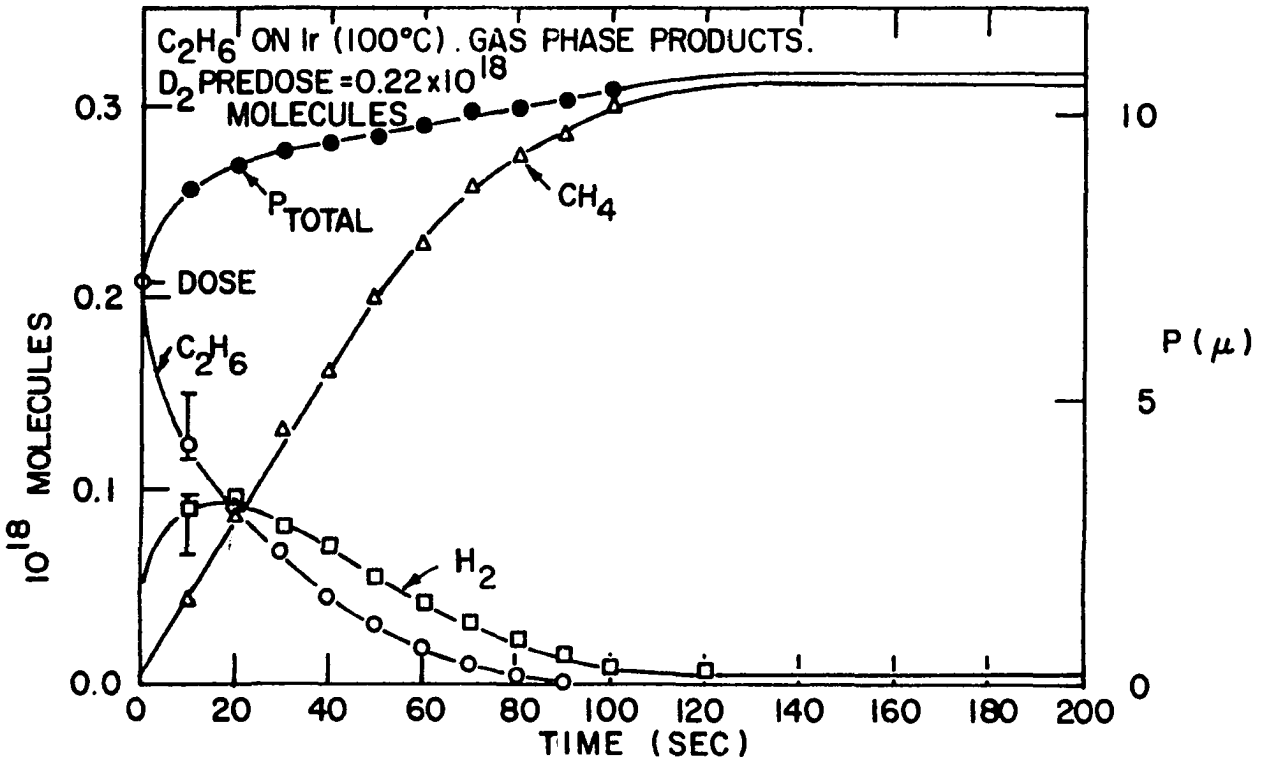

Figure 19. Experiment XIV. C_2H_6 decomposition at 100° C on a D_2-predosed Ir film

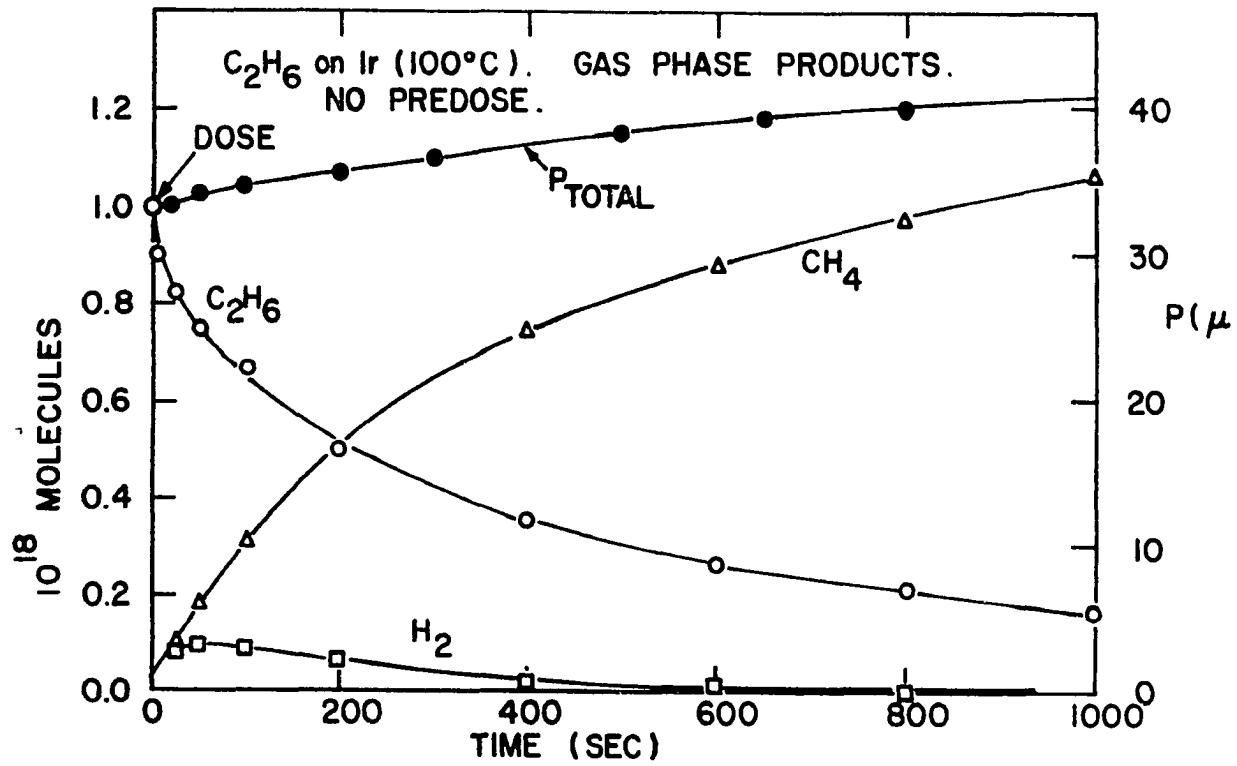

Figure 20. Experiment XV. C_2H_6 decomposition at 100° C on a bare Ir film

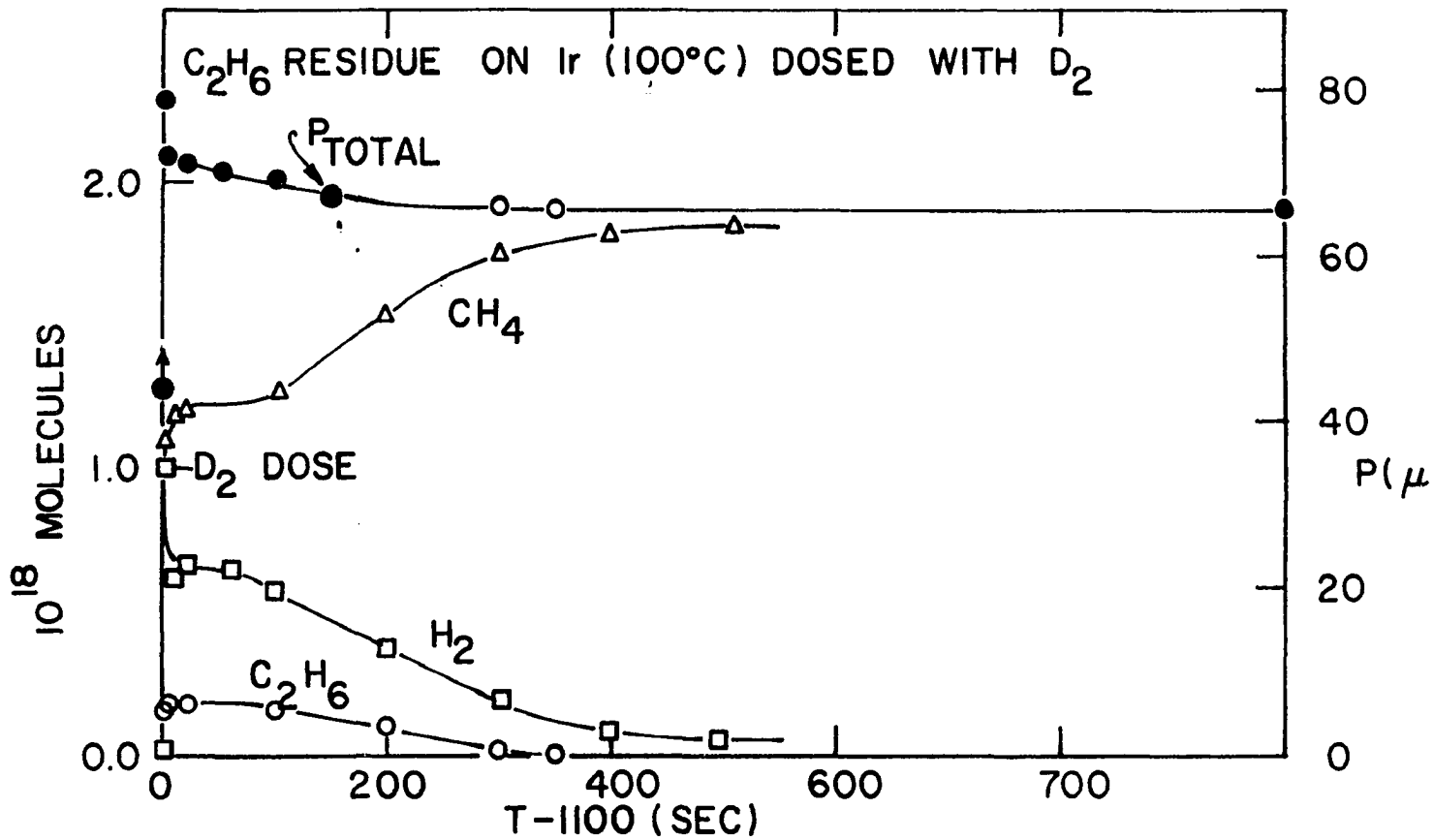

Figure 21. Results of adding hydrogen (D_2) to the reaction of Experiment XV (Figure 20) 1100 seconds after C_2H_6 was dosed

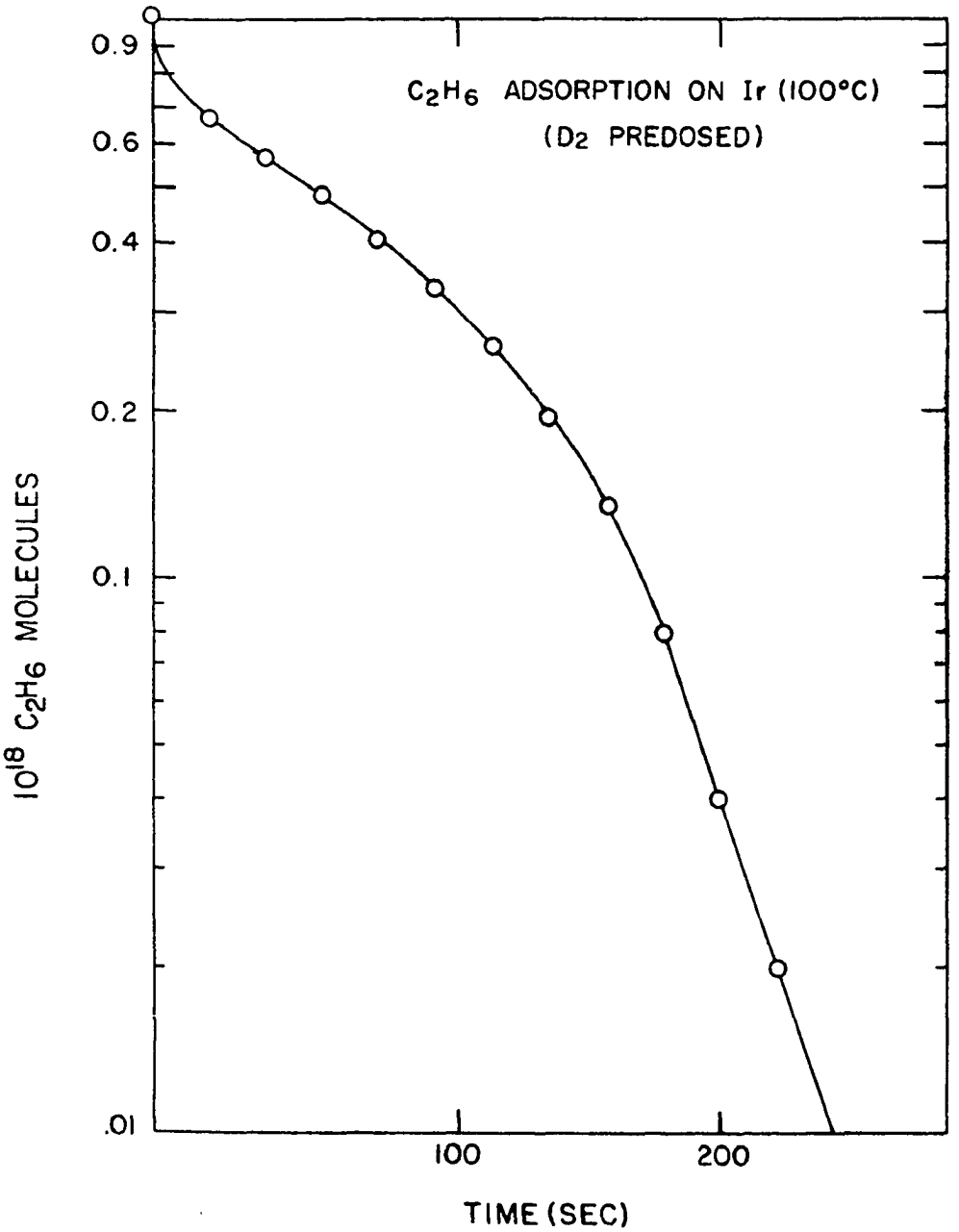

Figure 22. Semilog plot of C_2H_6 adsorption at 100° C on D_2-predosed Ir from Experiment XIII

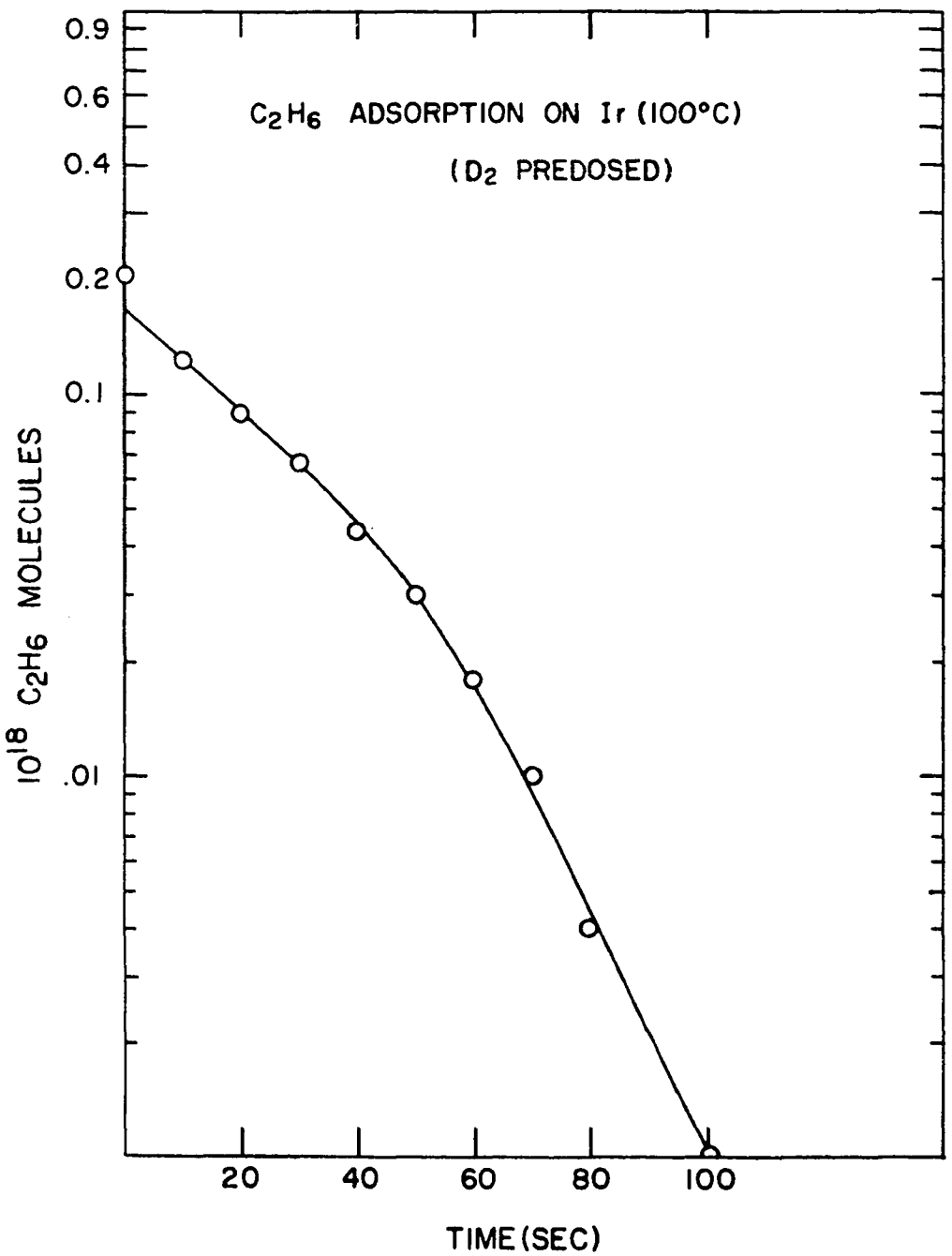

Figure 23. Semilog plot of C_2H_6 adsorption at 100° C on D_2-predosed Ir from Experiment XIV

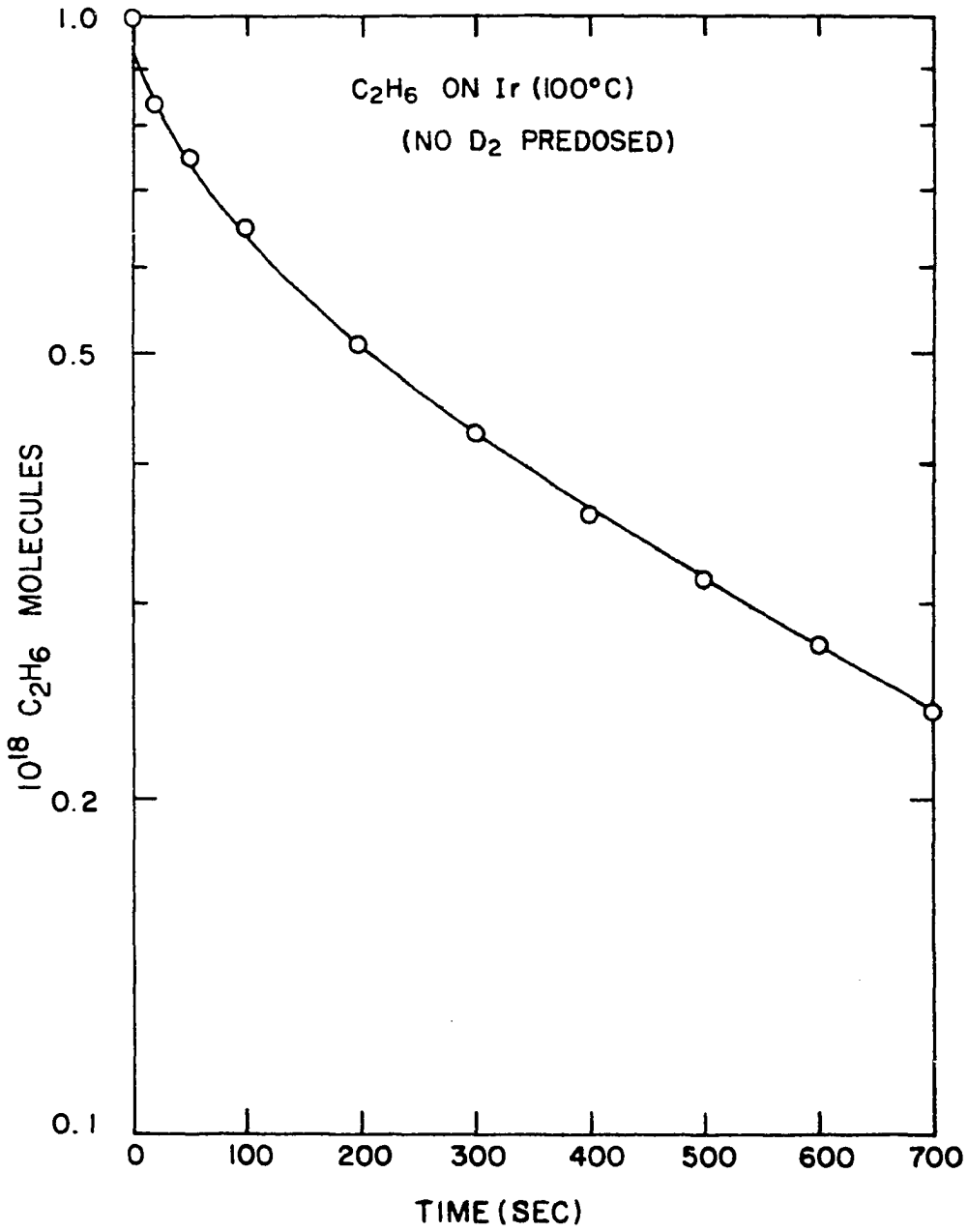

Figure 24. Semilog plot of C_2H_6 adsorption at 100° C on bare Ir from Experiment XV

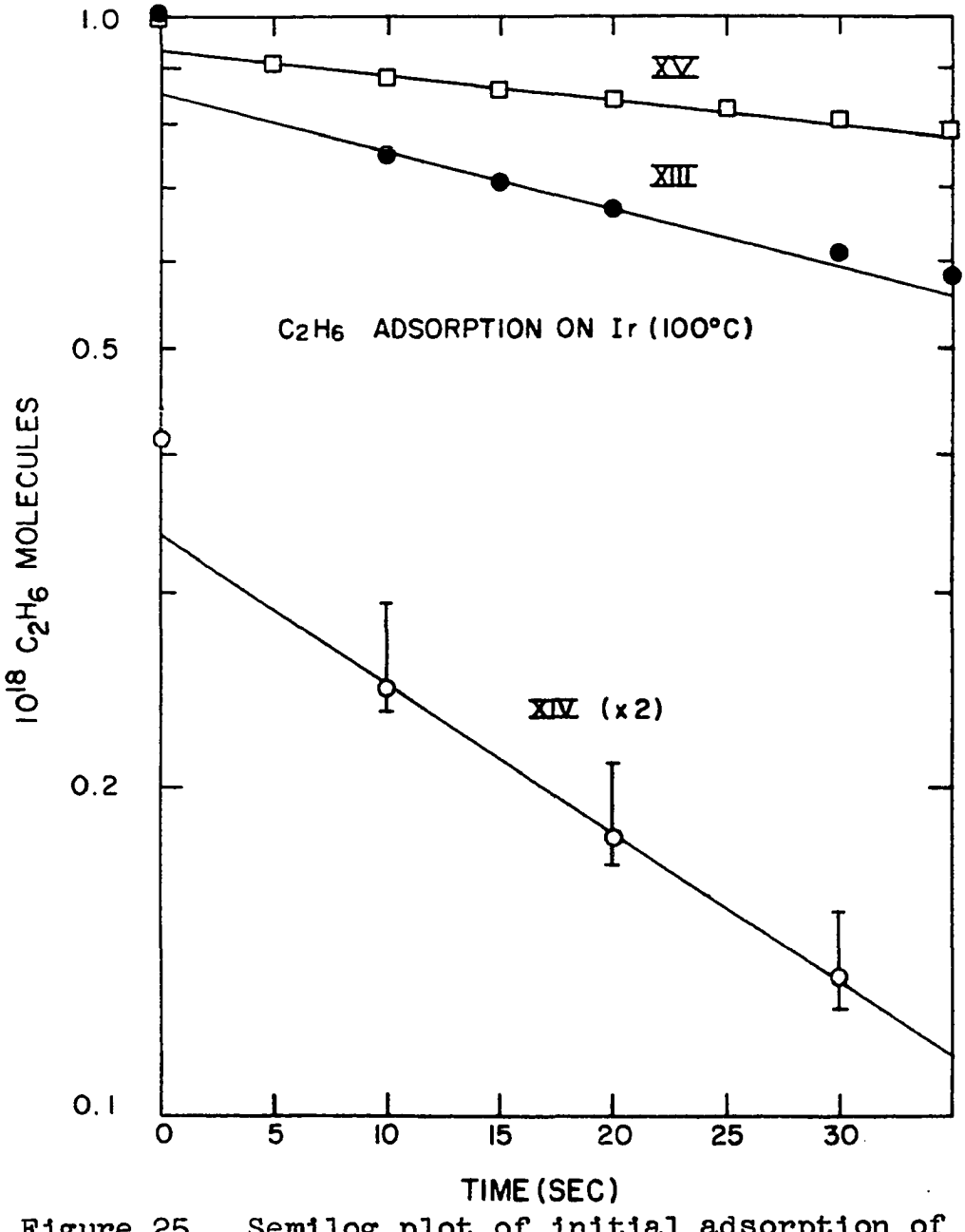

Figure 25. Semilog plot of initial adsorption of C_2H_6 from Experiments XIII, XIV, and XV. The amount of C_2H_6 from XIV has been multiplied by 2 for each point to facilitate scaling. (This does not affect the slope)

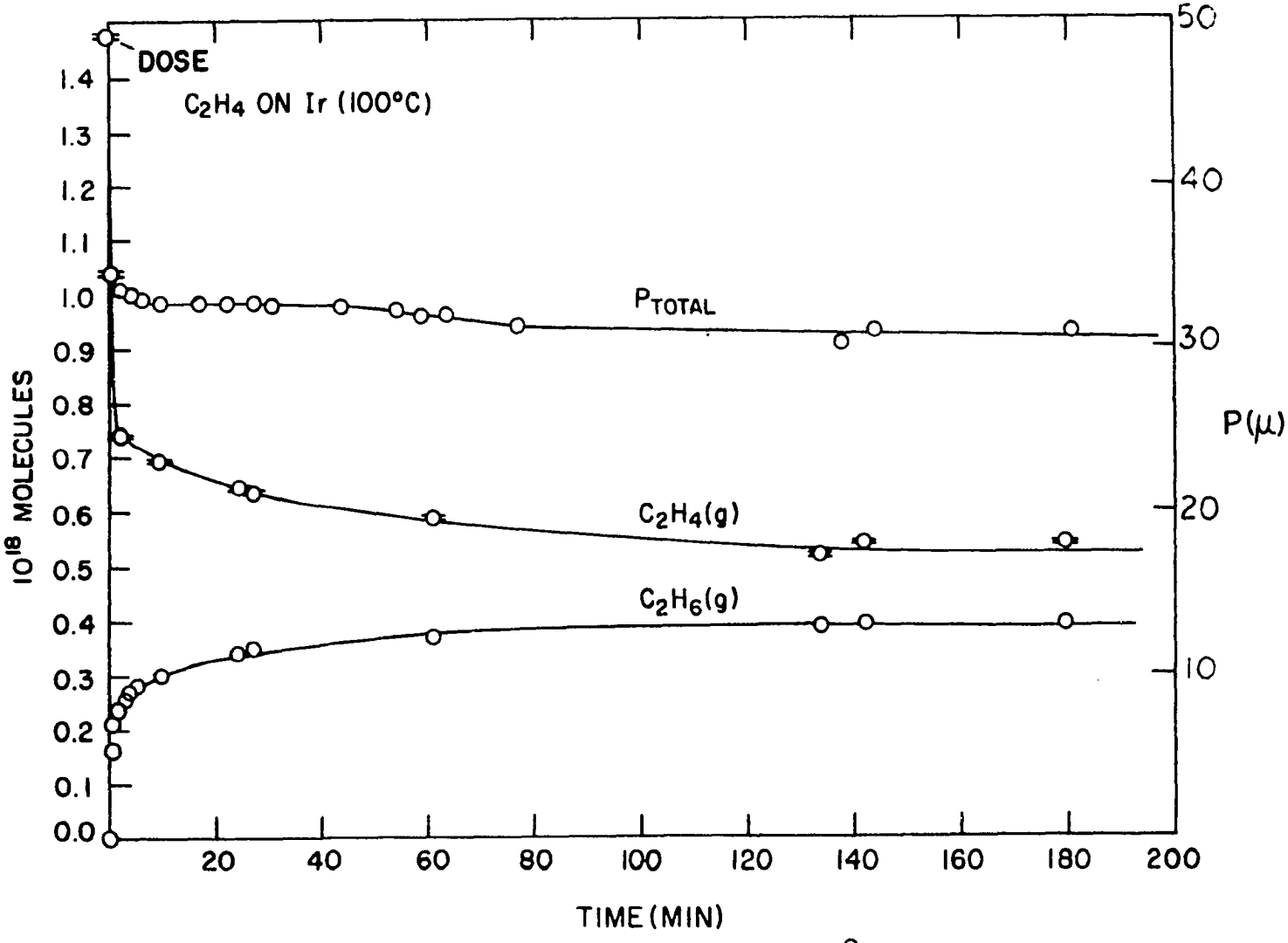

Figure 26. Experiment I. C_2H_4 dose on bare Ir at 100° C. The hydrogen pressure was not followed initially, but was no more than 0.1 μ in the latter part (t > 20 min). No CH_4 was produced

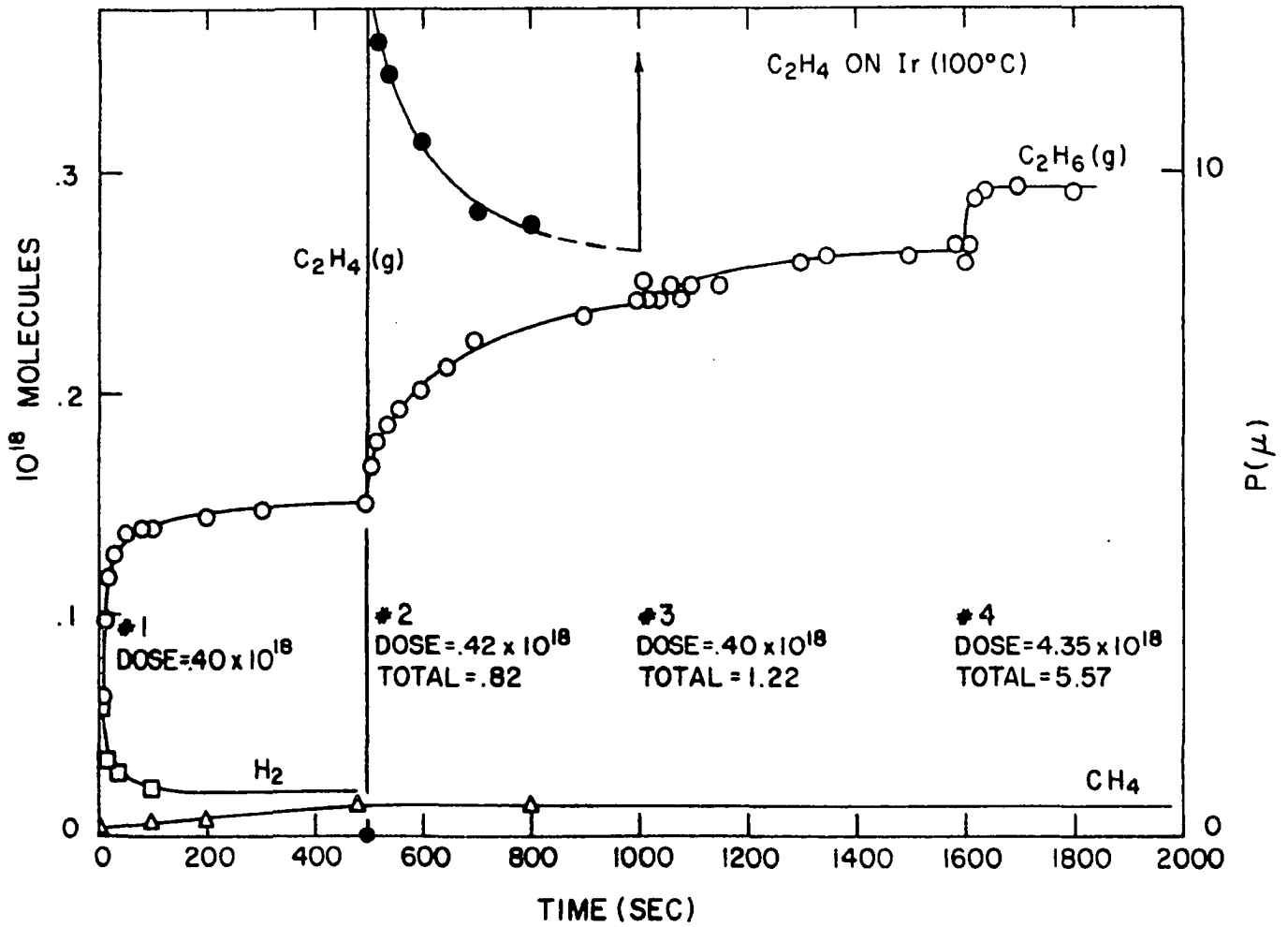

Figure 27. Experiment III. Successive doses of C_2H_4 on bare Ir at 100° C. C_2H_4 was added to the reaction at intervals as shown above

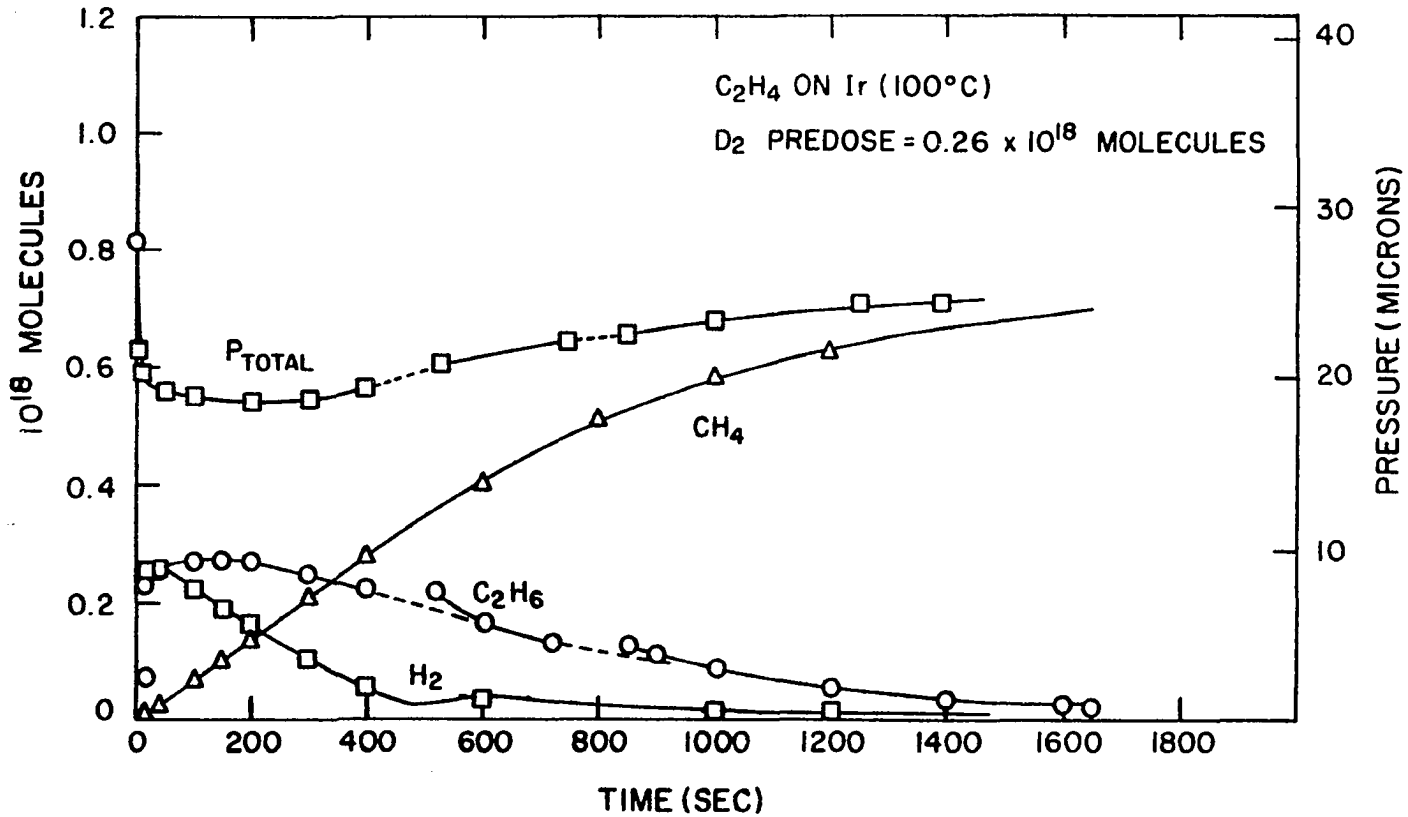

Figure 28. Experiment IV. C_2H_4 dosed on D_2-covered Ir at 100° C. Liquid nitrogen was on the cold finger (thereby reducing C_2H_6 pressure to about 0.1 μ) during the intervals indicated by the dashed line in the total pressure curve. The dashed portions of the C_2H_6 curve represent the assumed decay had no liquid nitrogen been used

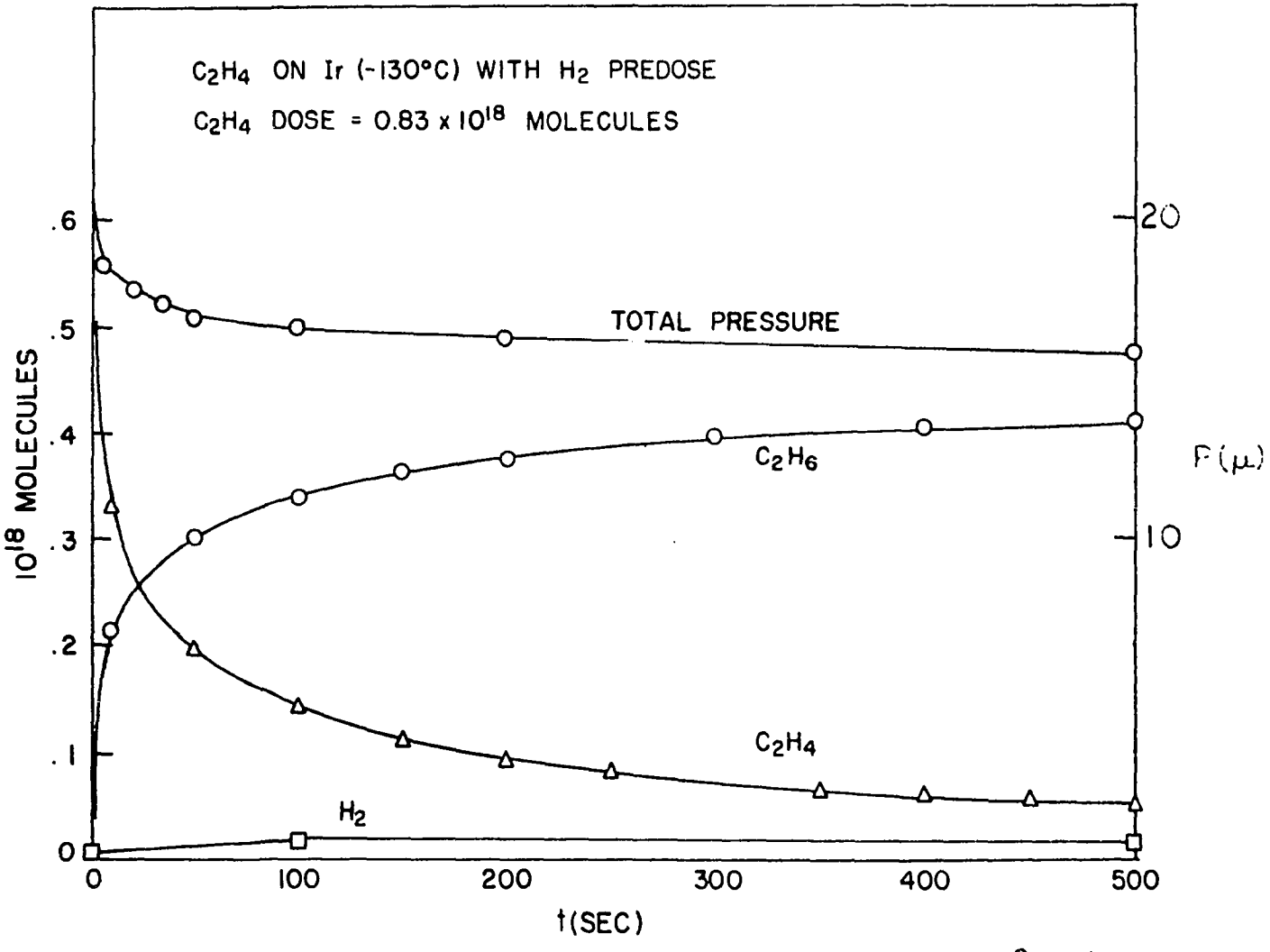

Figure 29. Experiment VII. C_2H_4 dosed on H_2-predosed Ir at -130° C (pentane-liquid nitrogen slush)

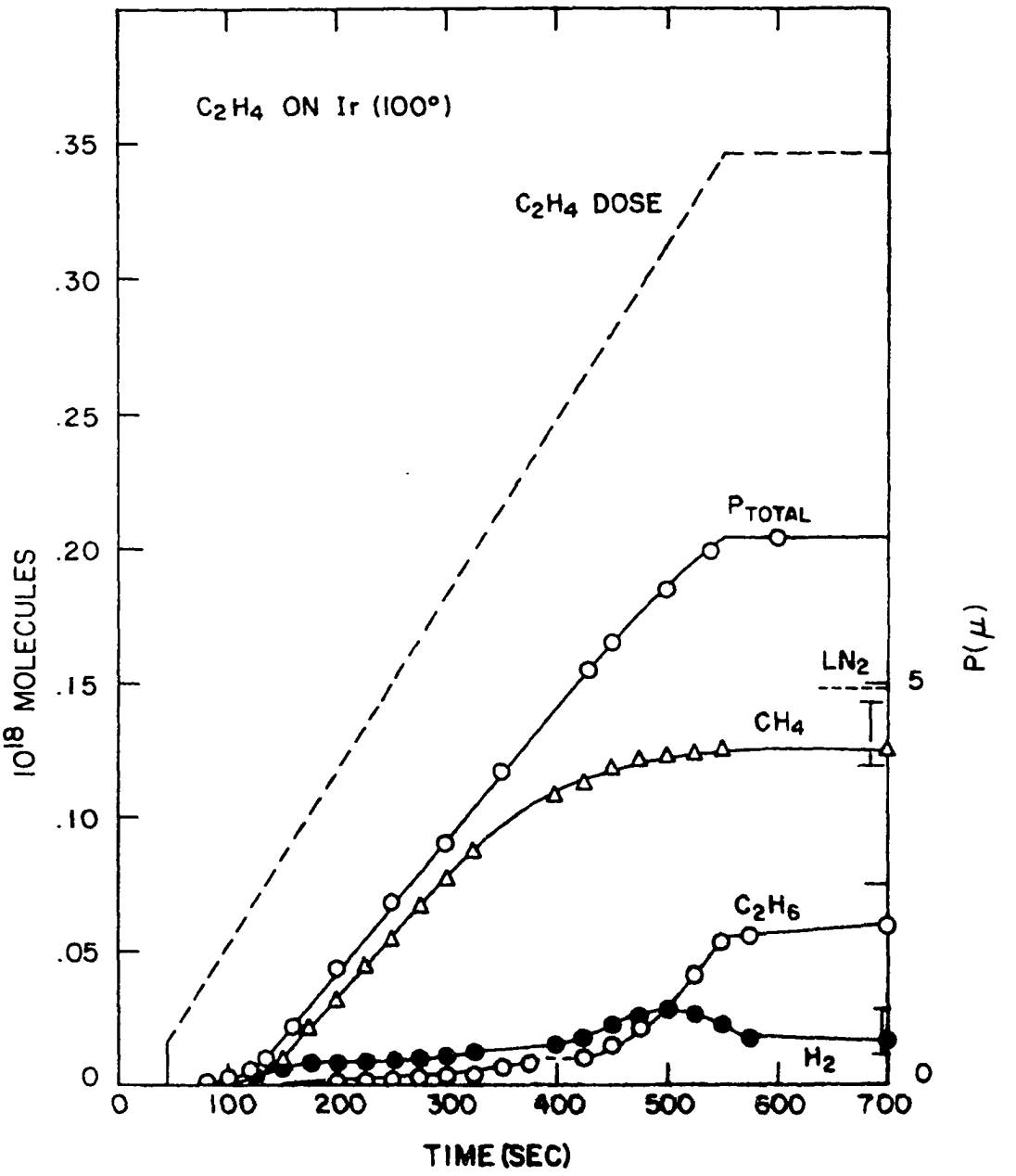

Figure 30. Experiment VIII. Low pressure dose of C_2H_4 on bare Ir at 100° C. The C_2H_4 dose leak began at t = 18 sec, but C_2H_4 was accumulated in volume V3 until t = 45 sec when it was introduced to the film. The dashed line labeled LN_2 is the total pressure (H_2 and CH_4) found with liquid nitrogen on the cold finger. It was also chilled at 400 sec as indicated by the dashed C_2H_6 curve

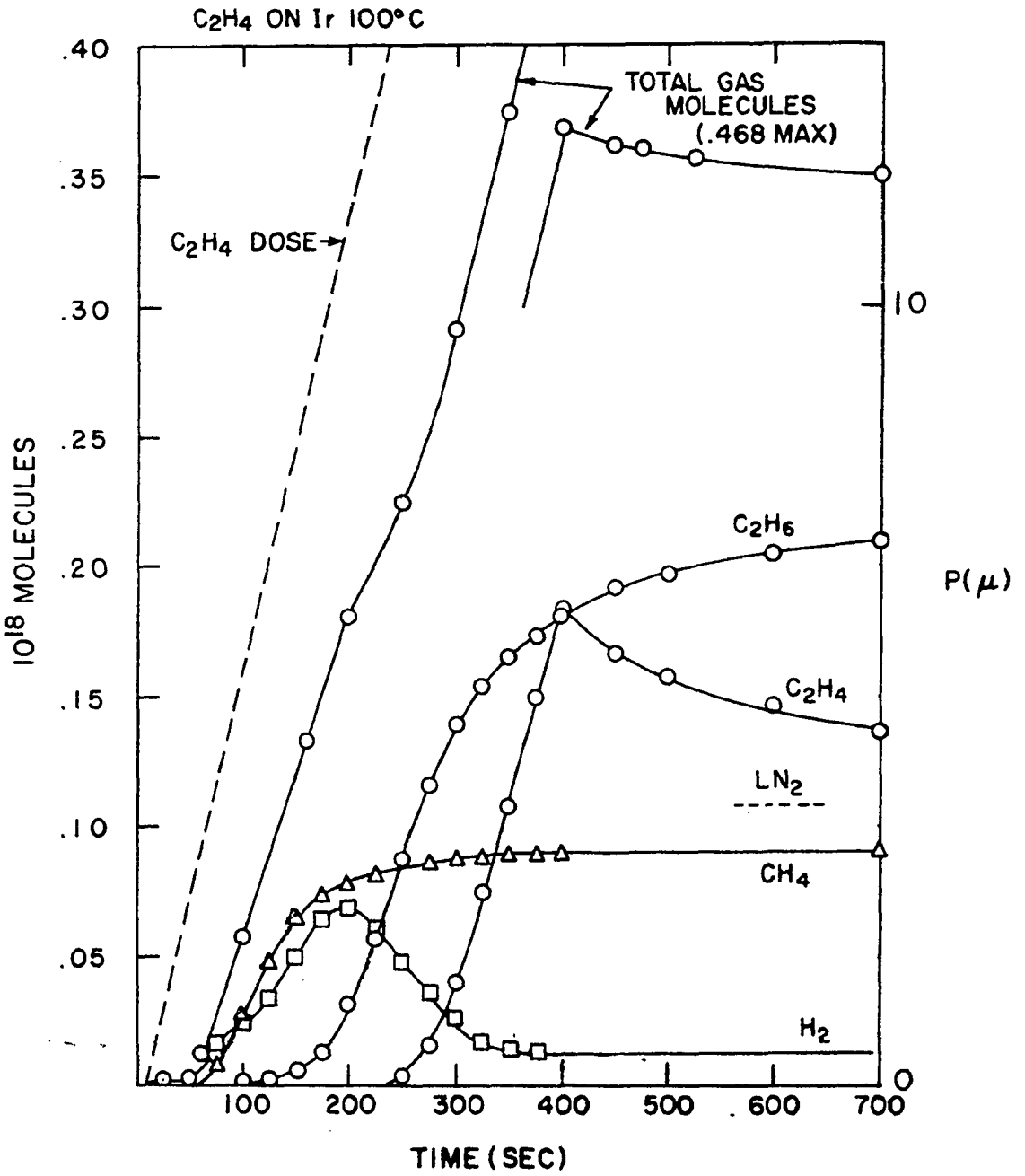

Figure 31. Experiment IX. Low pressure C_2H_4 doses on bare Ir at 100° C. The "total gas molecules" curve has been "folded" back to conserve space. Dosing was terminated at t = 400 sec

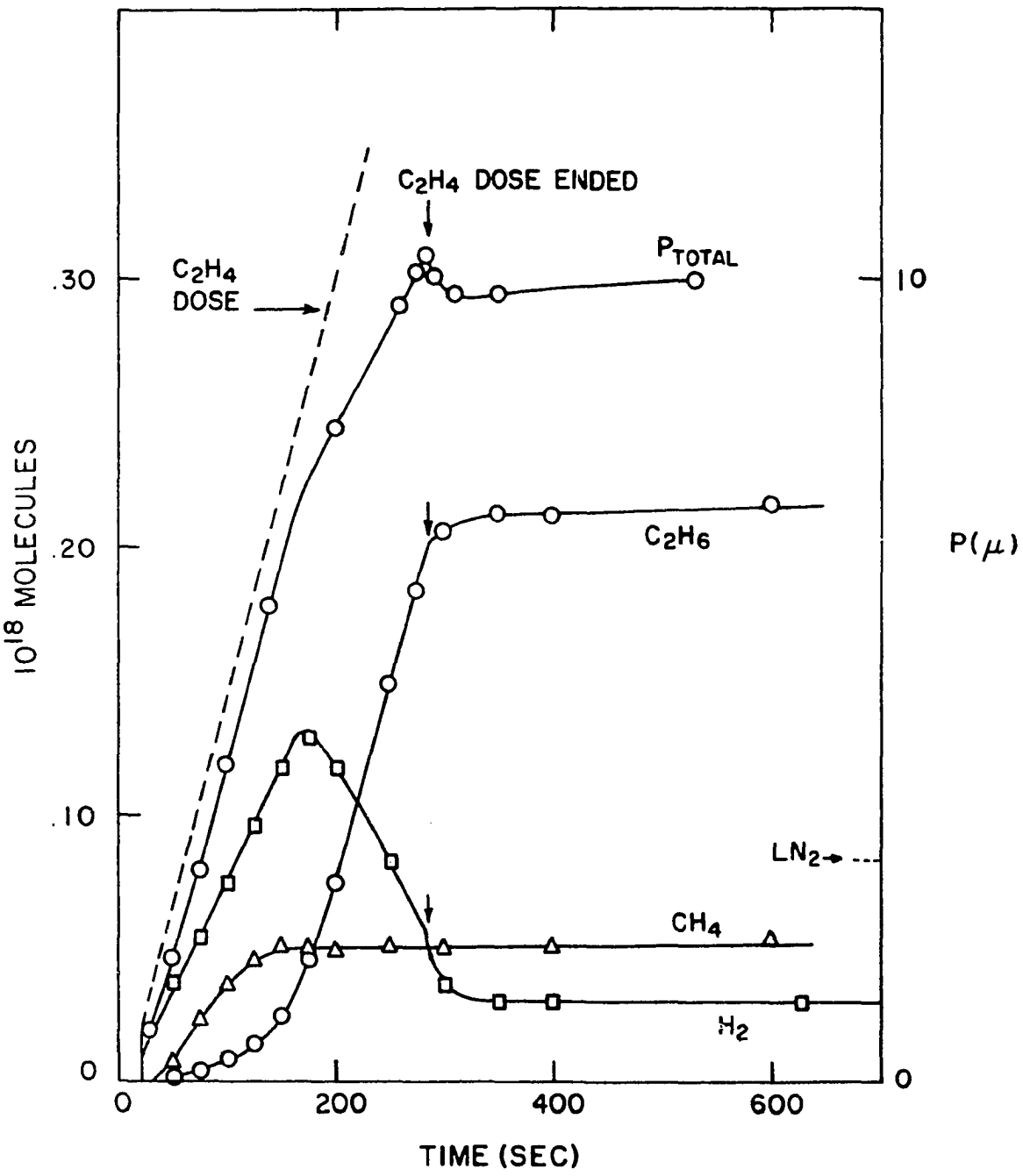

Figure 32. Experiment X. Low pressure C_2H_4 dose on a H_2-predosed Ir film at 100° C. The C_2H_4 leak dose was begun at t = 0 and ended at 277 sec, but it was accumulated in volume V3 for the first 25 sec. The dashed line marked LN_2 indicates the total pressure (H_2 and CH_4) at the end of the experiment when the cold finger was chilled with liquid nitrogen

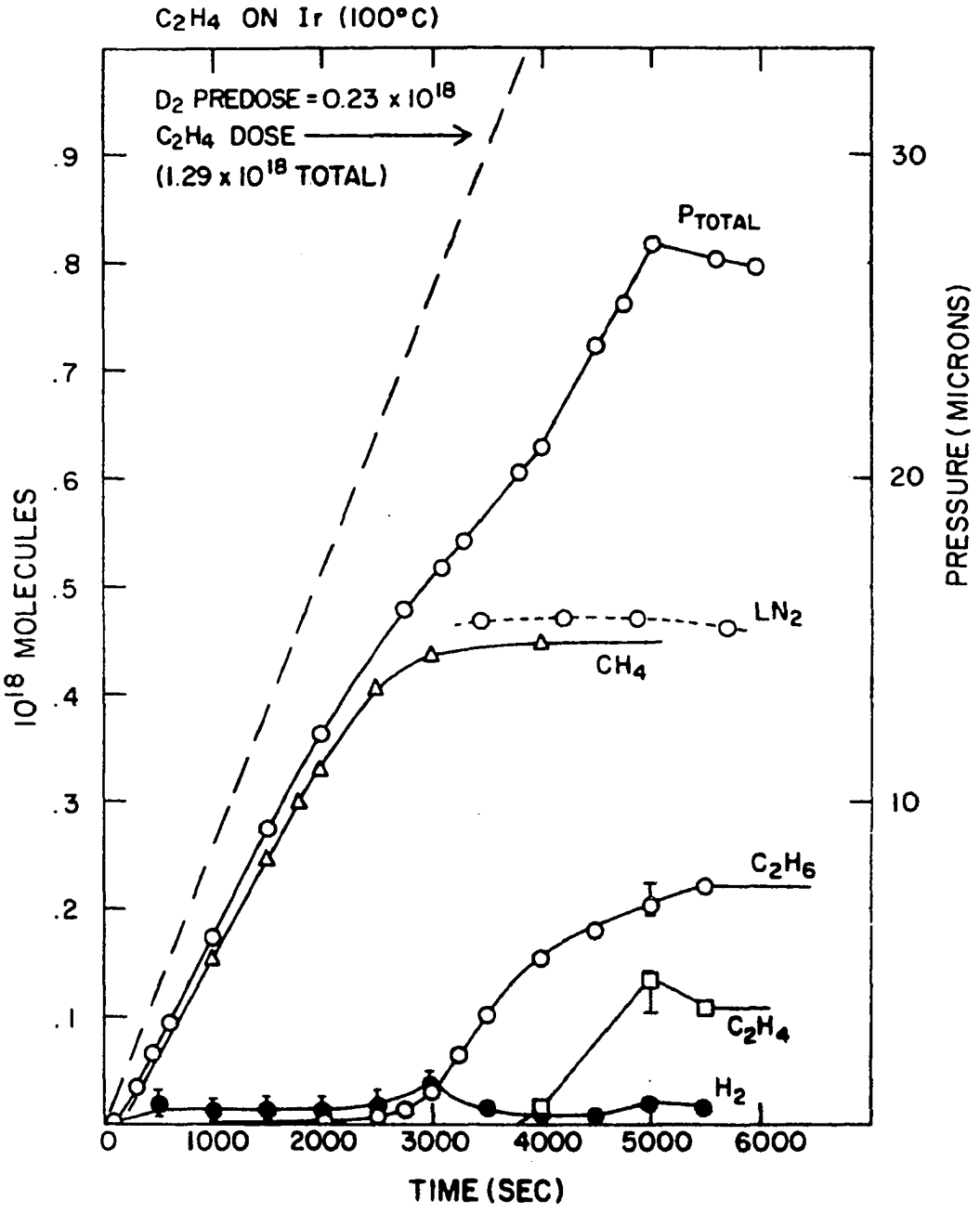

Figure 33. Experiment XI. Low pressure C_2H_4 dose on D_2-predosed Ir at 100° C. C_2H_4 was dosed at a constant rate from t = 0 to 5000 sec. The points on the dashed line marked LN_2 represent total pressure (hydrogen and methane) determined with the cold finger chilled by liquid nitrogen

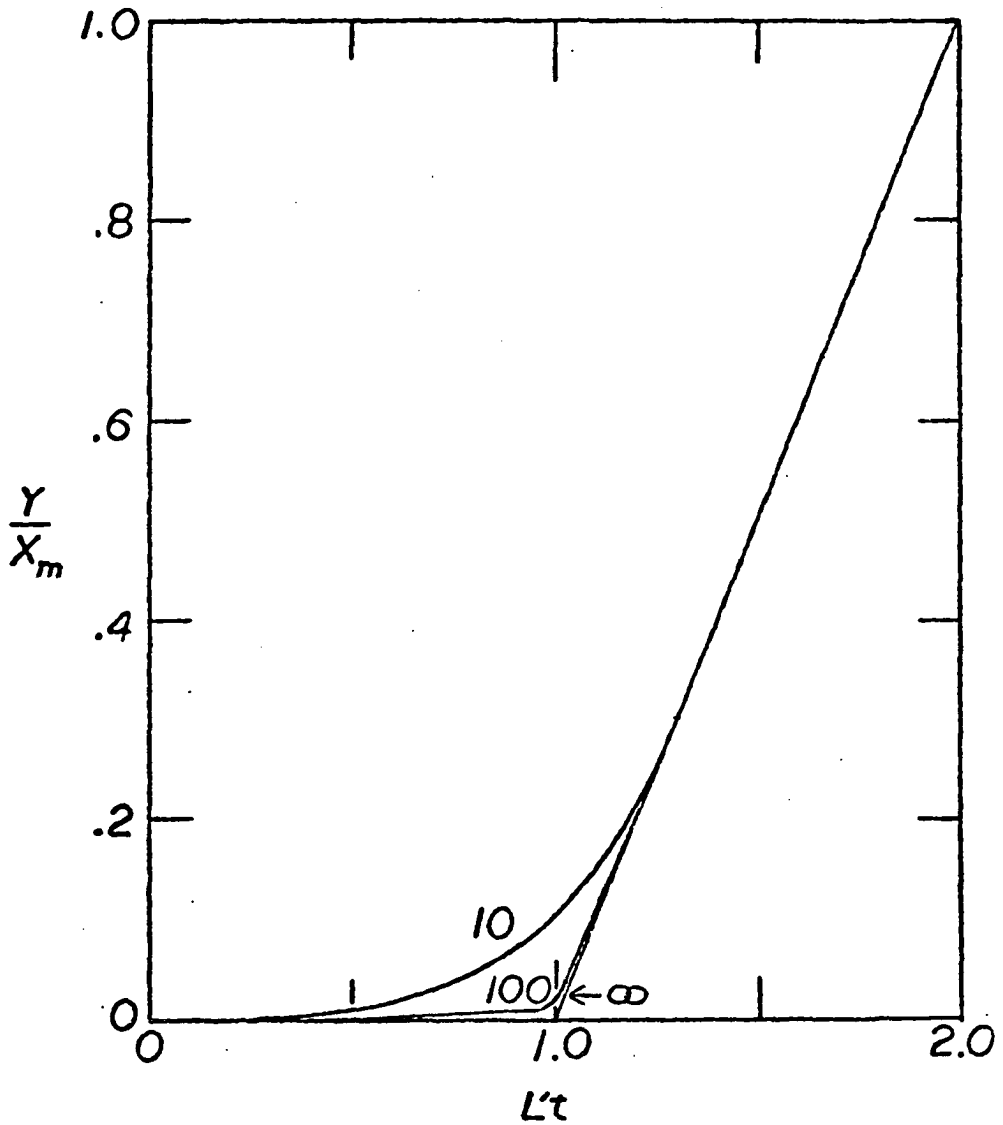

Figure 34. Theoretical curves for C_2H_6 production from self-hydrogenation of C_2H_4 as calculated by numerical integration of Equation 20. The ordinate gives the amount of C_2H_6 gas produced and the abscissa the amount of C_2H_4 dosed, both in units of monolayers. The dose rate L' is assumed low enough that the amount of C_2H_4 in the gas phase is negligible. The labels 10, 100, and ∞ are the assumed ratios of the rate constants, $a = k_1/k_2$, for adsorption and hydrogenation

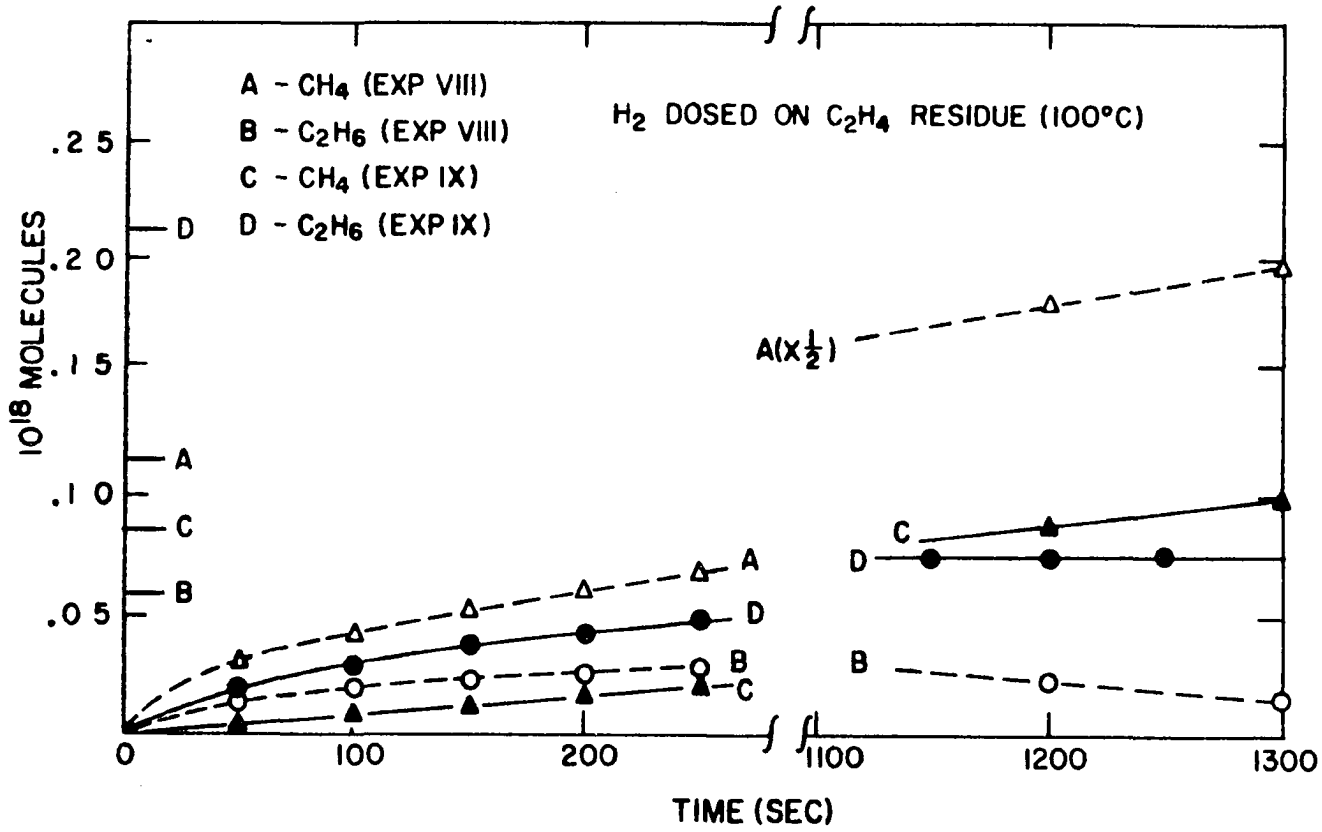

Figure 35. Desorption of hydrocarbons from C_2H_4 residue in excess hydrogen at 100° C. Curves A and B show CH_4 and C_2H_6 production upon dosing 25 μ of hydrogen on the residue from Experiment VIII after the ambient pressure had been reduced to about 0.1 μ. Curves C and D give the production from the residue of Experiment IX similarly treated with 40 μ of hydrogen. The hydrogen pressure at 1200 sec was about 5 μ and 25 μ over the respective residues. The lettered marks on the y-axis indicate the hydrocarbon levels (exclusive of C_2H_4) at the end of the C_2H_4-dosed experiments prior to pumping away the ambients (taken from Figures 30 and 31)

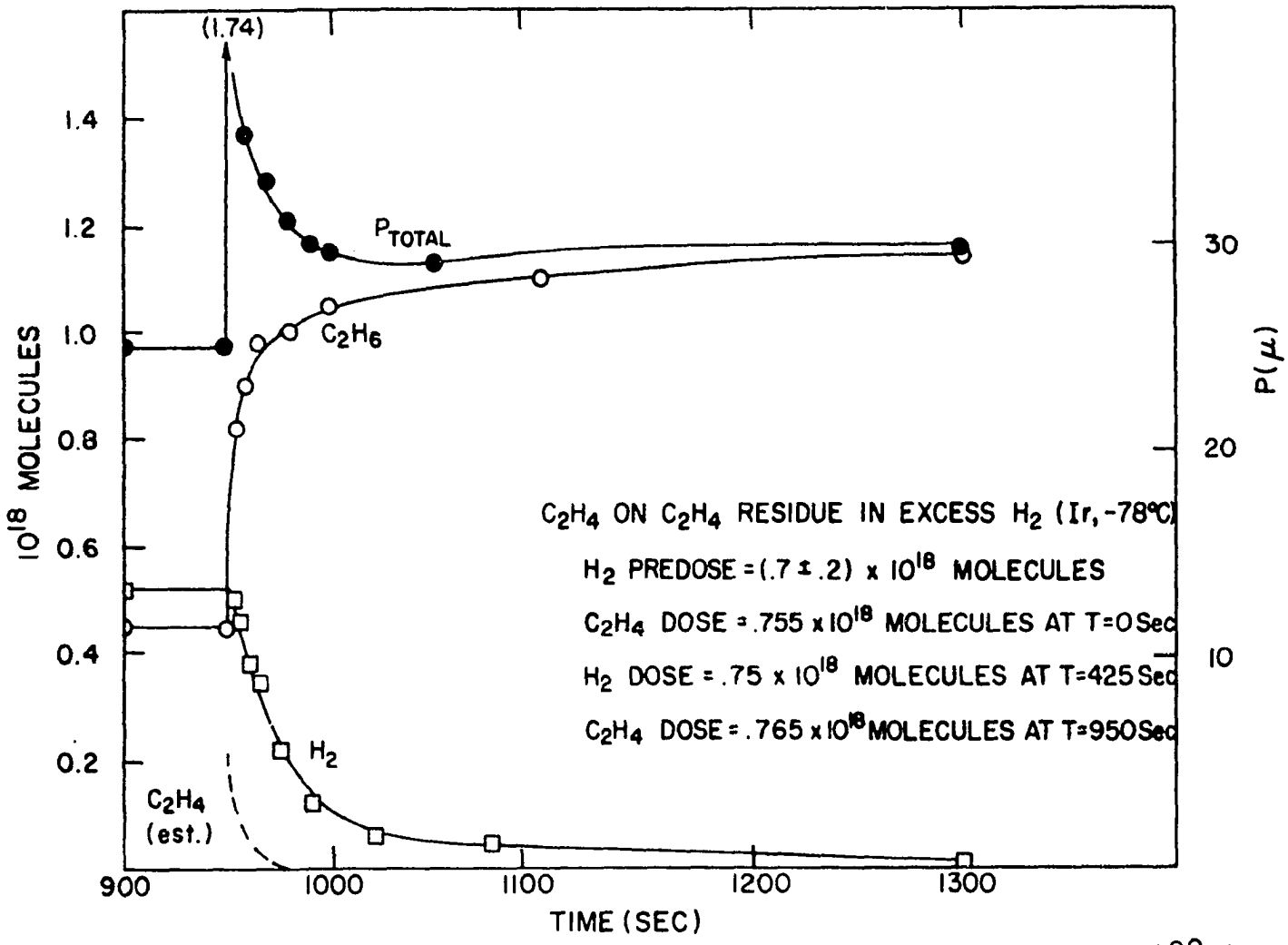

Figure 36. Hydrogenation of C_2H_4 over a carbon-covered Ir surface at -78° C. The surface was pretreated as shown above

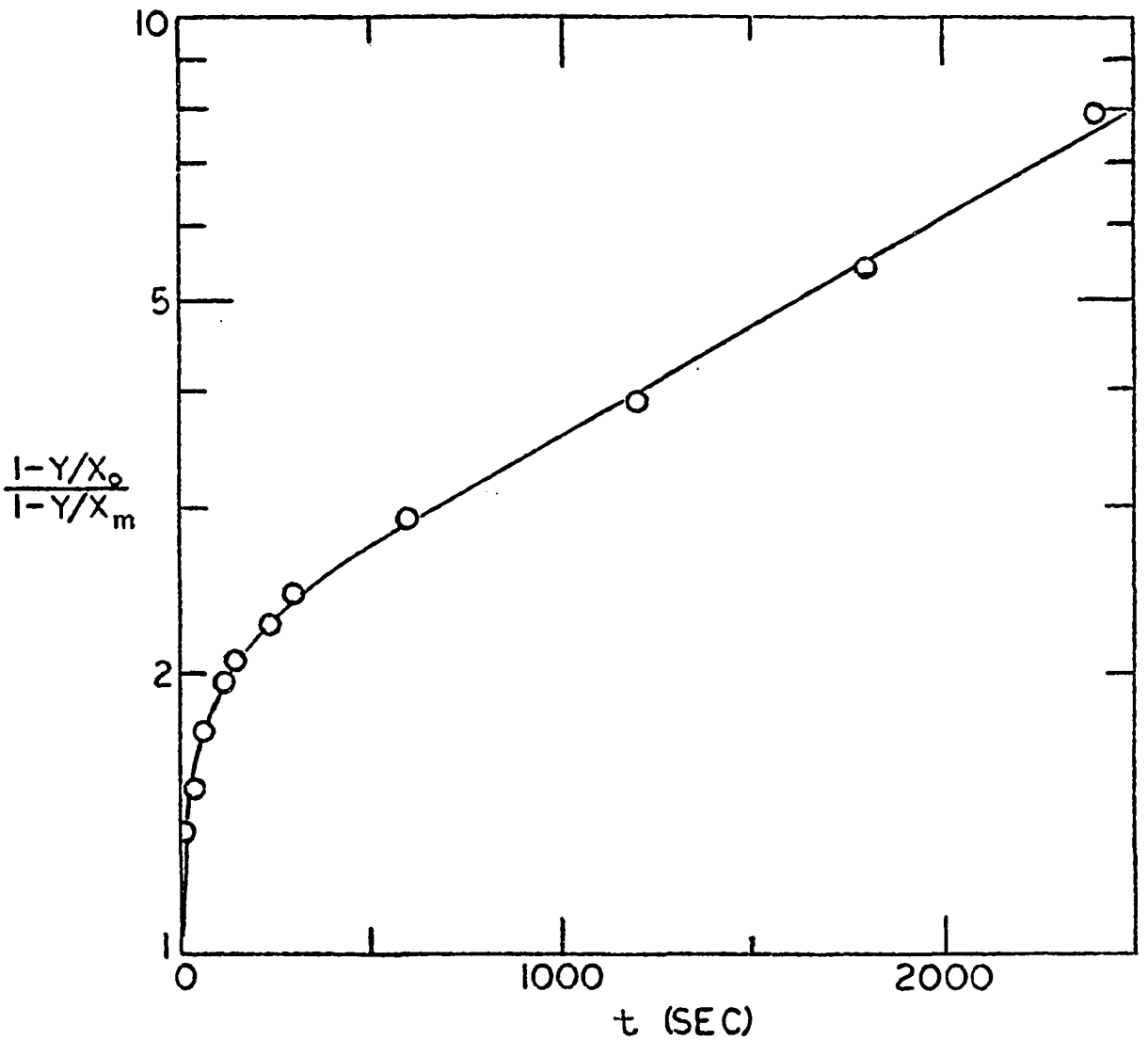

Figure 37. Kinetic plot of C_2H_6 data from Experiment I (Figure 26). The variable y is the number of C_2H_6 molecules at time t. The values of the constants are $x_o = 0.91 \times 10^{18}$ molecules and $x_m = 0.39 \times 10^{18}$ molecules

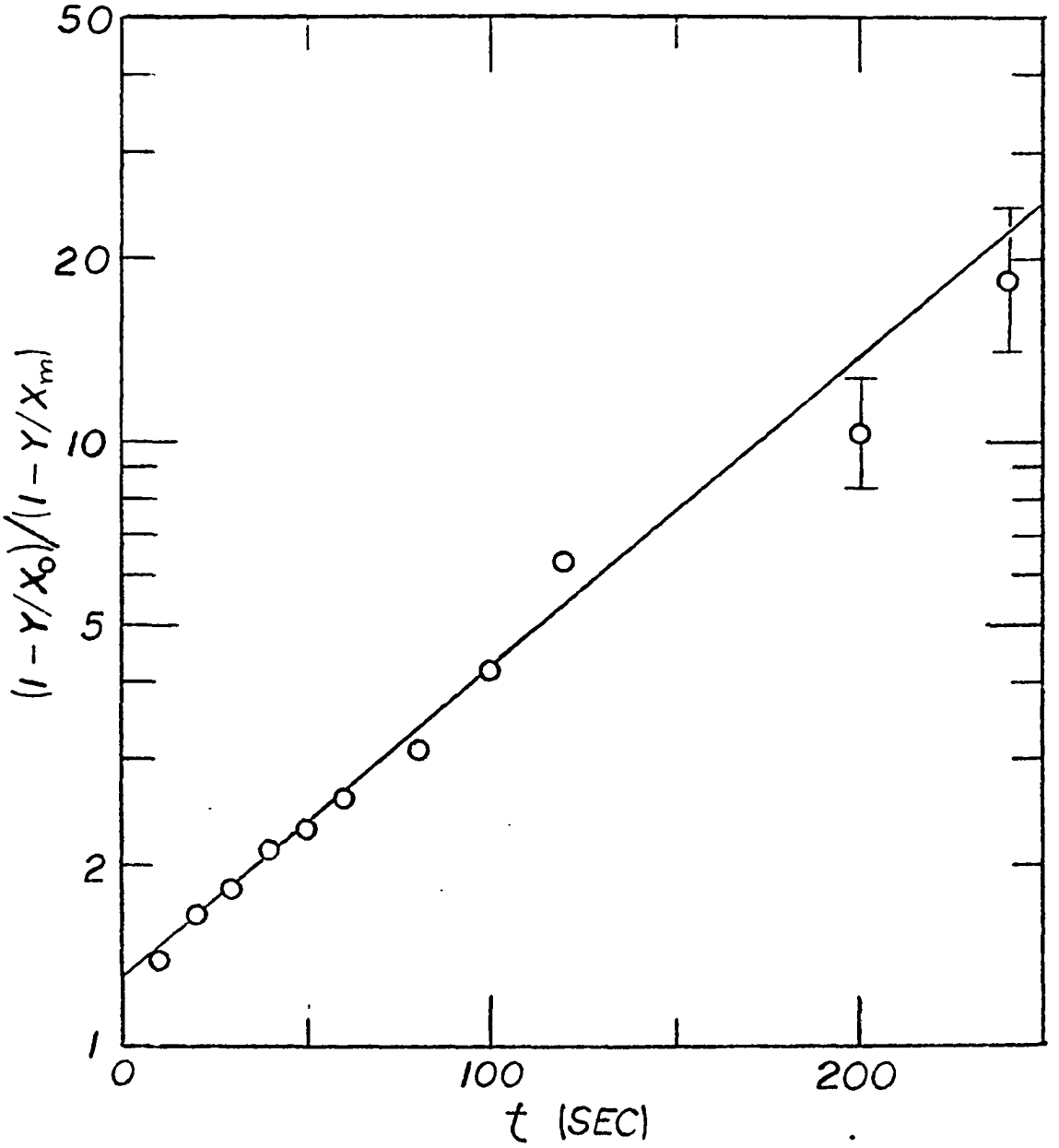

Figure 38. Kinetic plot of the "fast" reaction in Experiment I (Figure 26). The variable y is the number of C_2H_6 molecules at time t. The values of the constants are $x_0 = 0.91 \times 10^{18}$ and $x_m = 0.25 \times 10^{18}$ molecules

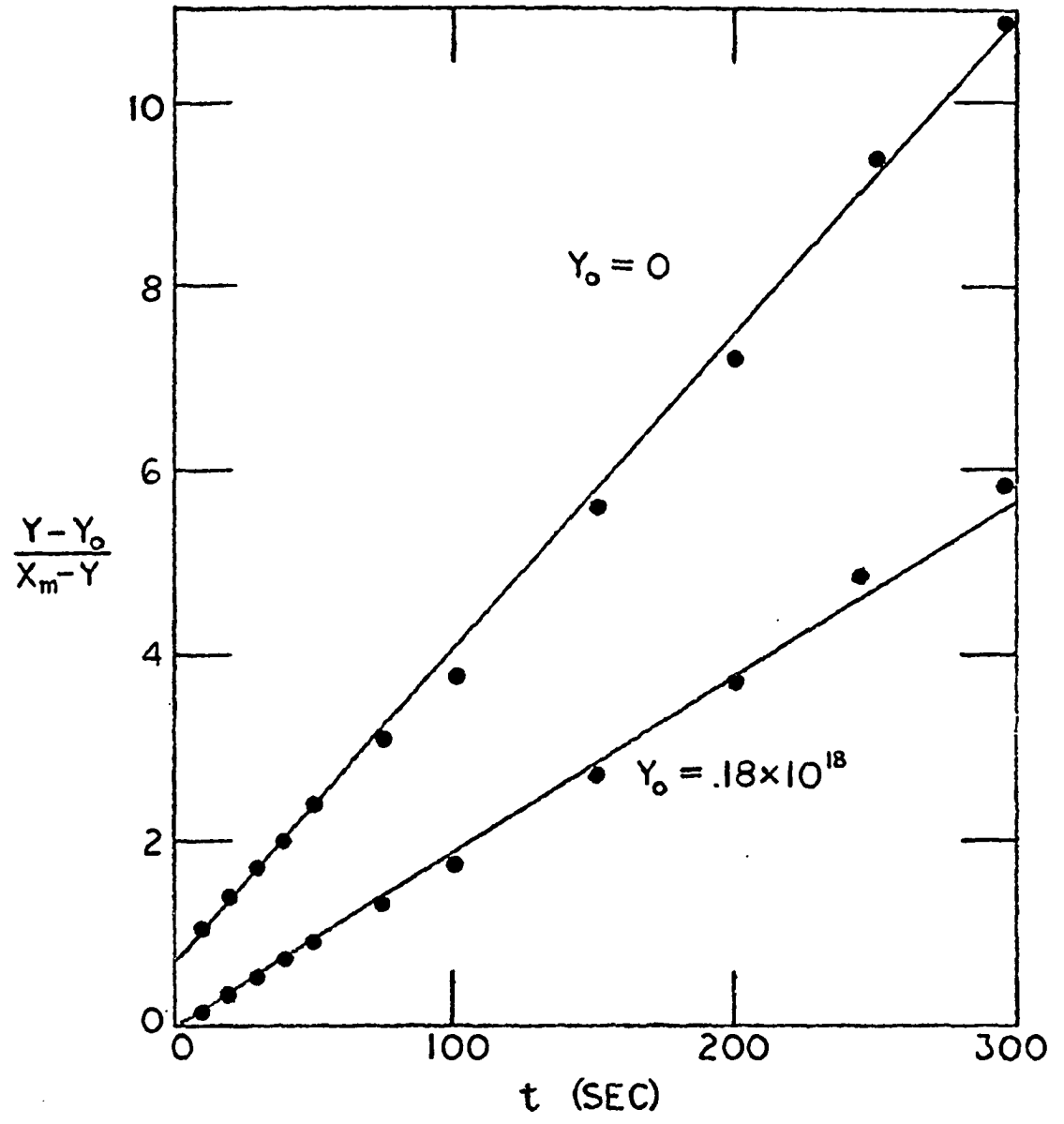

Figure 39. Kinetic plots for C_2H_6 production in Experiment VII (Figure 29). The variable y is the number of C_2H_6 molecules produced at time t; $x_m = 0.43 \times 10^{18}$ molecules

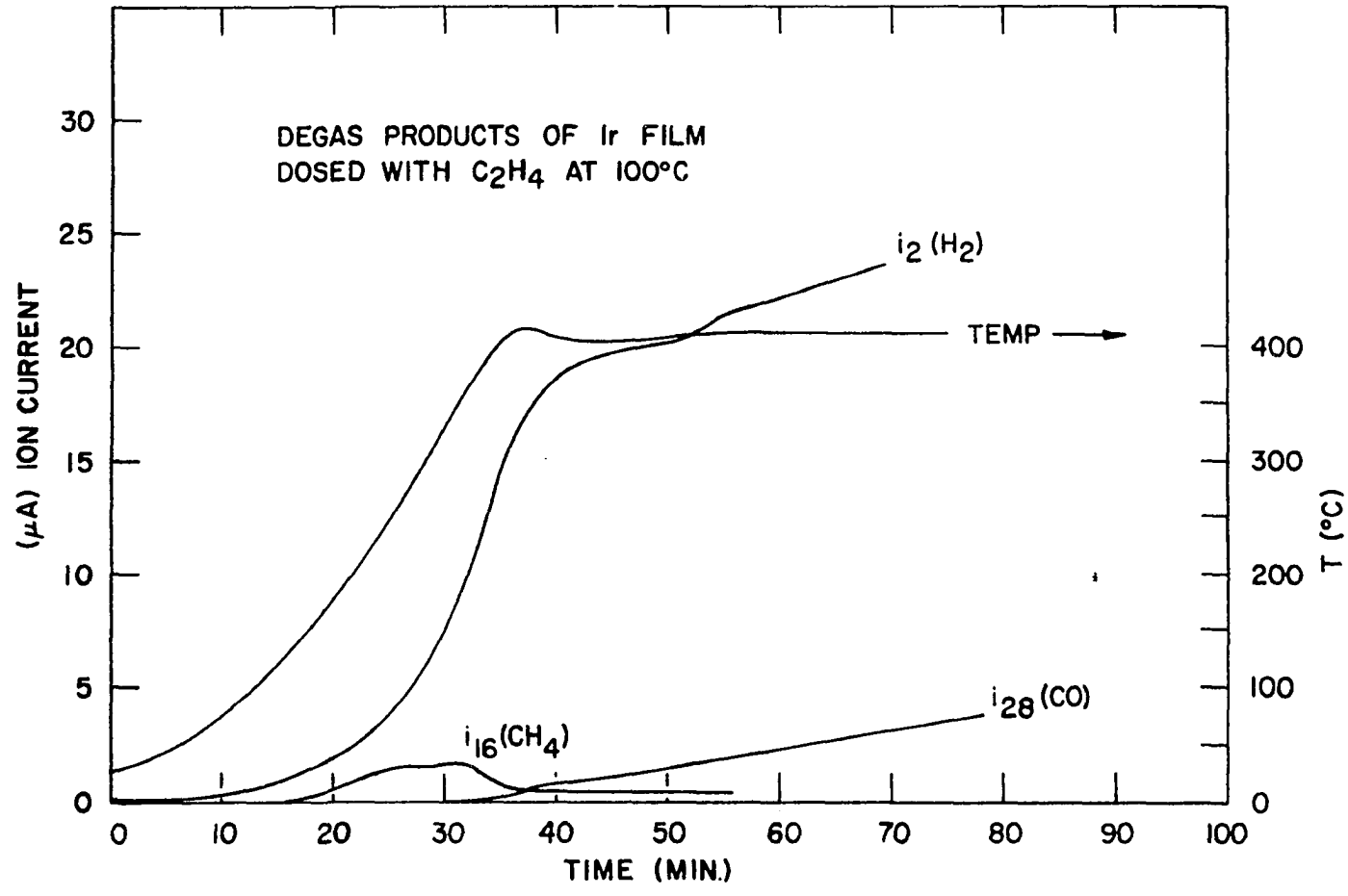

Figure 40. Desorption products upon heating the film and residue from Experiment II (C_2H_4 dosed on bare Ir at 100° C). The ambient pressure over the film was reduced to about 0.1 u before heating. The ion currents have been corrected for temperature effect on the pressure so that for each gas species i_m is proportional to the number of molecules present. At t = 45 sec the total pressure corrected to 100° C is 18.2 u, corresponding to 0.43 x 10^{18} molecules

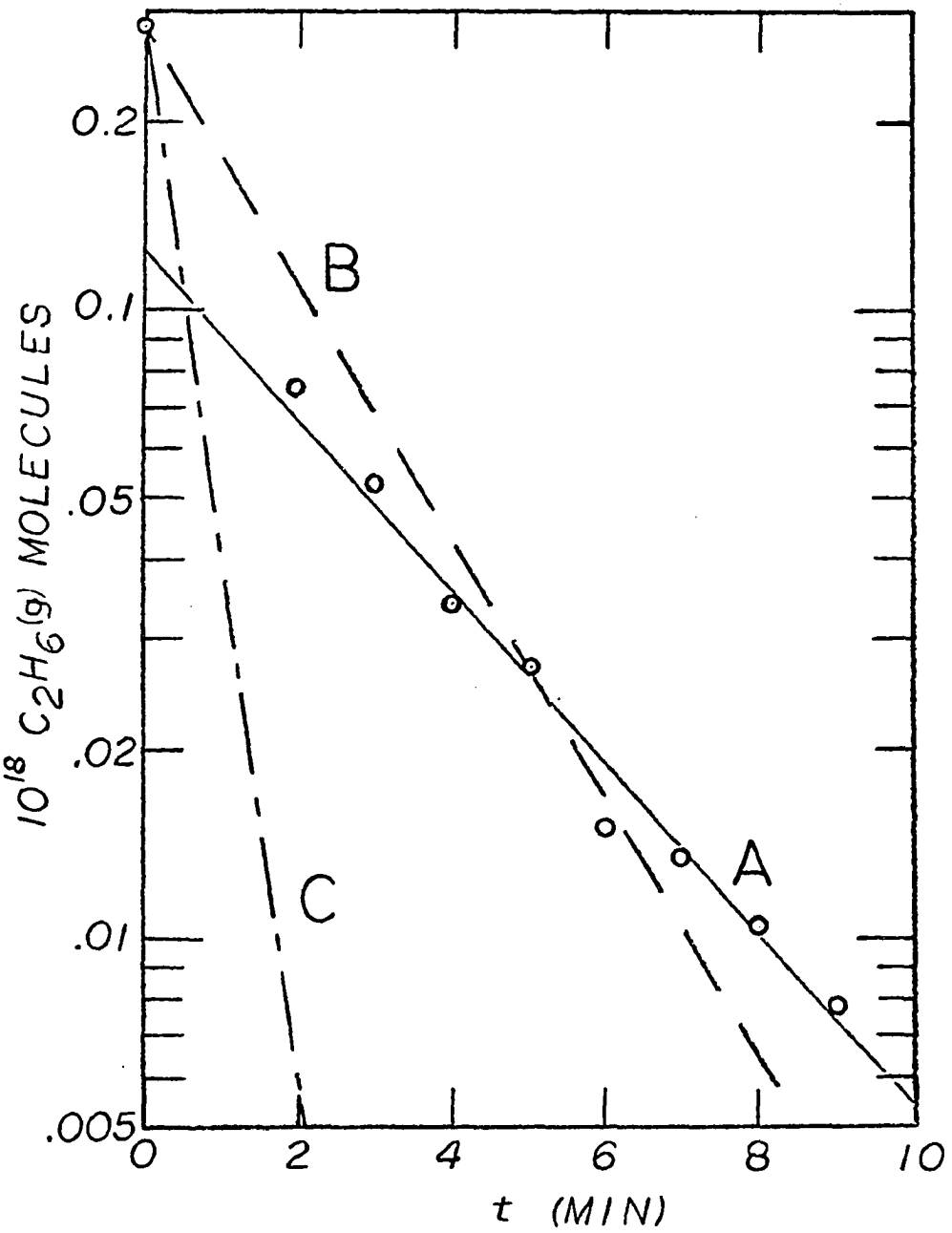

Figure 41. Log plot of C_2H_6 adsorption on Rh at 100° C. Data points were taken from Roberts' Figure 3, Reference (11). Curve A was drawn for best linear fit of all points exclusive of t = 0, and has slope of -0.30 min^{-1}. Curve B has slope of -0.56 corresponding to Roberts' value for the first-order rate constant. Curve C has slope of -2.50 min^{-1}

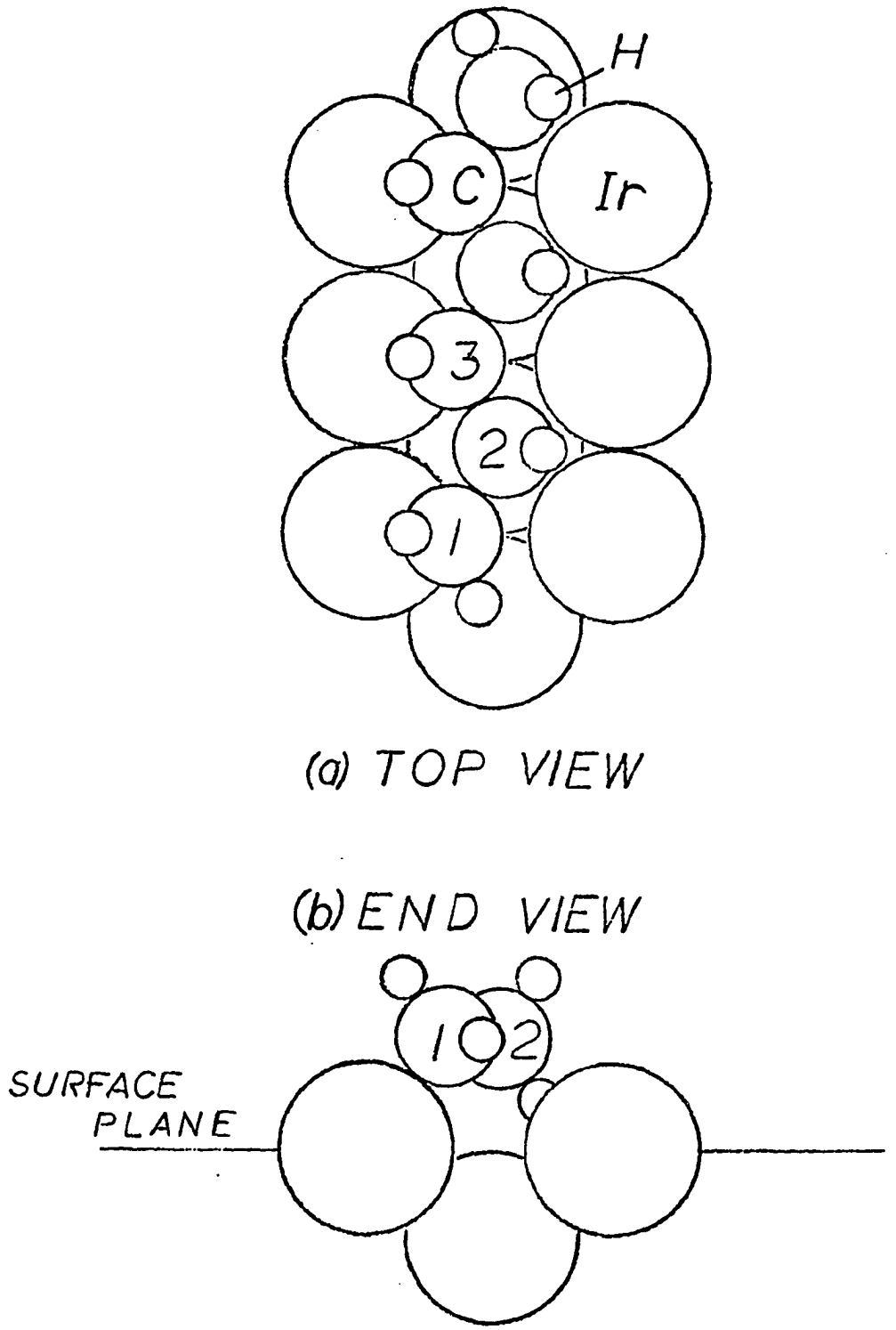

Figure 42. C_2H_4 trimer on the 110 face of Ir as seen (a) from directly above the surface and (b) parallel to the surface along the 110 "trough"

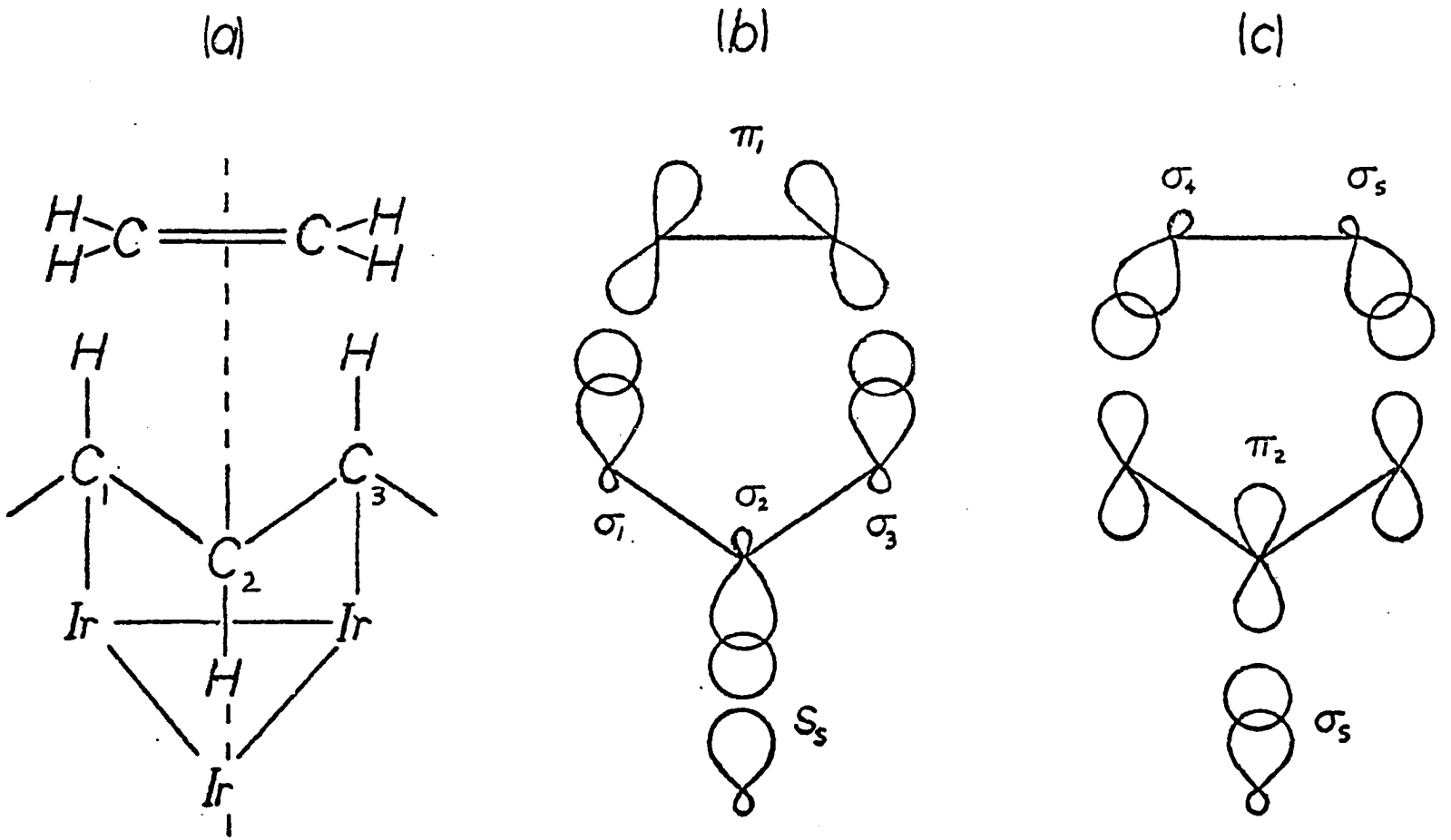

Figure 43. Concerted addition of hydrogen from a polymerized surface species to gaseous C_2H_4. The approach of C_2H_4 along the plane of symmetry (perpendicular to the page at the dashed line) is shown in (a). The surface species is similar to that represented in Figure 42. The orbitals involved in making and breaking bonds are shown in (b) just prior to reaction and in (c) just after reaction in which two hydrogens have been transferred from the surface to form C_2H_6, and one has been transferred from the polymer to an Ir atom just below the surface plane (see Figure 42)

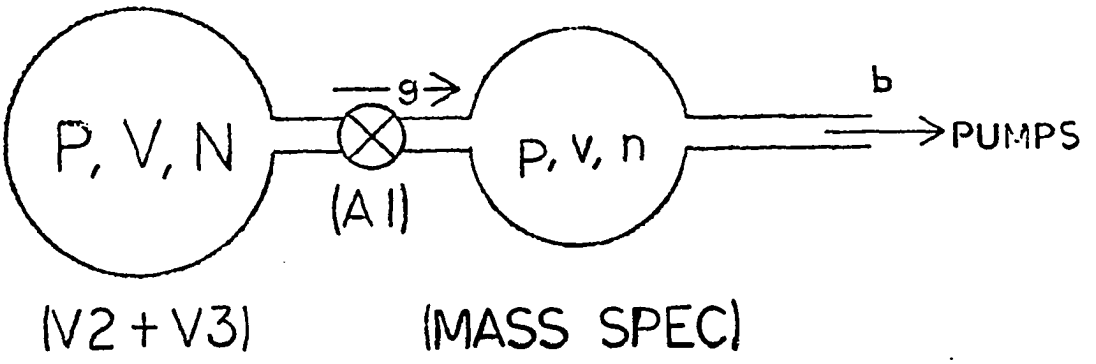

Figure 44. Idealized two-volume flow system. Real system counterparts are given in parentheses

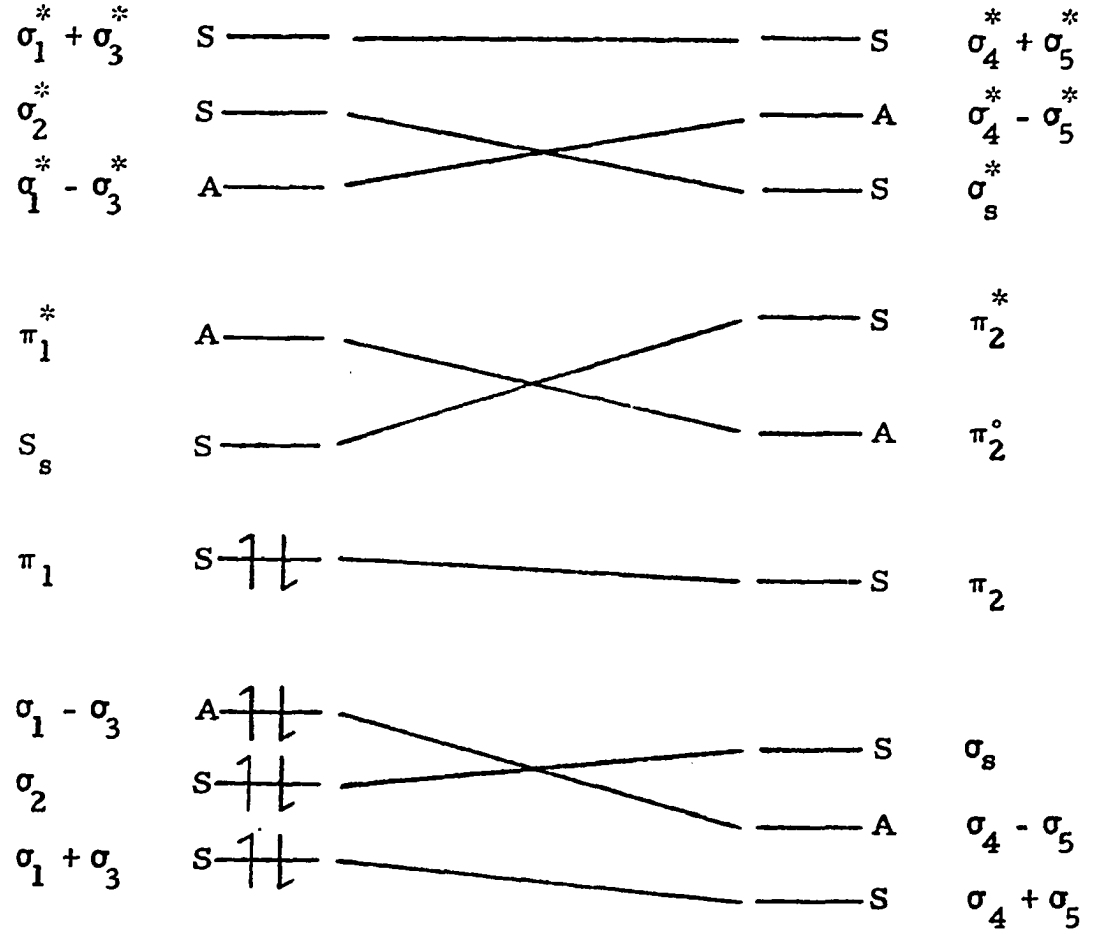

Figure 45. Correlation diagram for the concerted addition of hydrogen from a polymerized surface species to gaseous C_2H_4. On the left the approximate energy levels of the 9 reactant orbitals (with 8 electrons in the ground state) involved in the reaction are shown for C_2H_4 far from the surface. At right are the levels of the product orbitals for C_2H_6 far from the surface. The orbitals shown in Figure 43 have been combined where necessary to obtain resultant orbitals which are either symmetric (S) or antisymmetric (A) with respect to the plane of symmetry

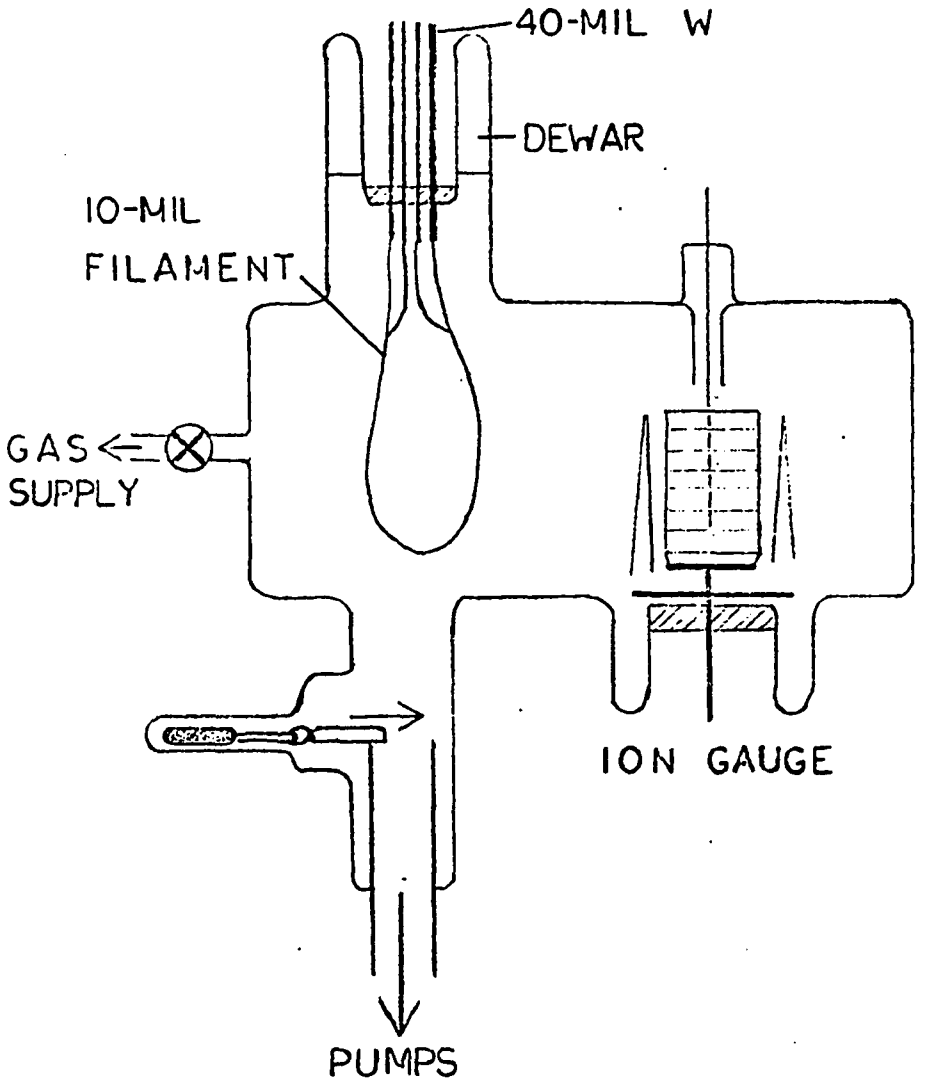

Figure 46. Isothermal flash filament cell

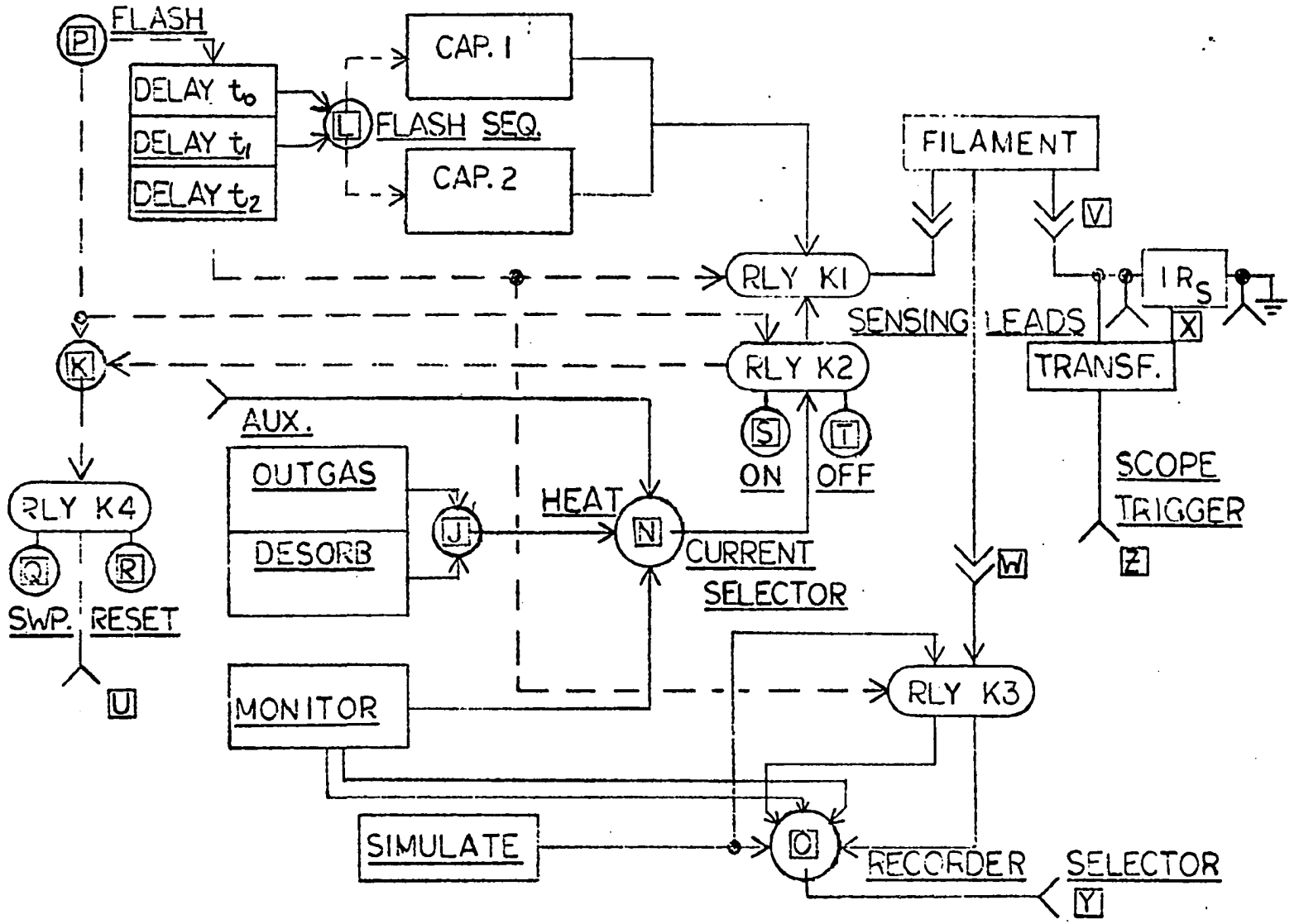

Figure 47. Block diagram of MF-305 flash unit circuitry

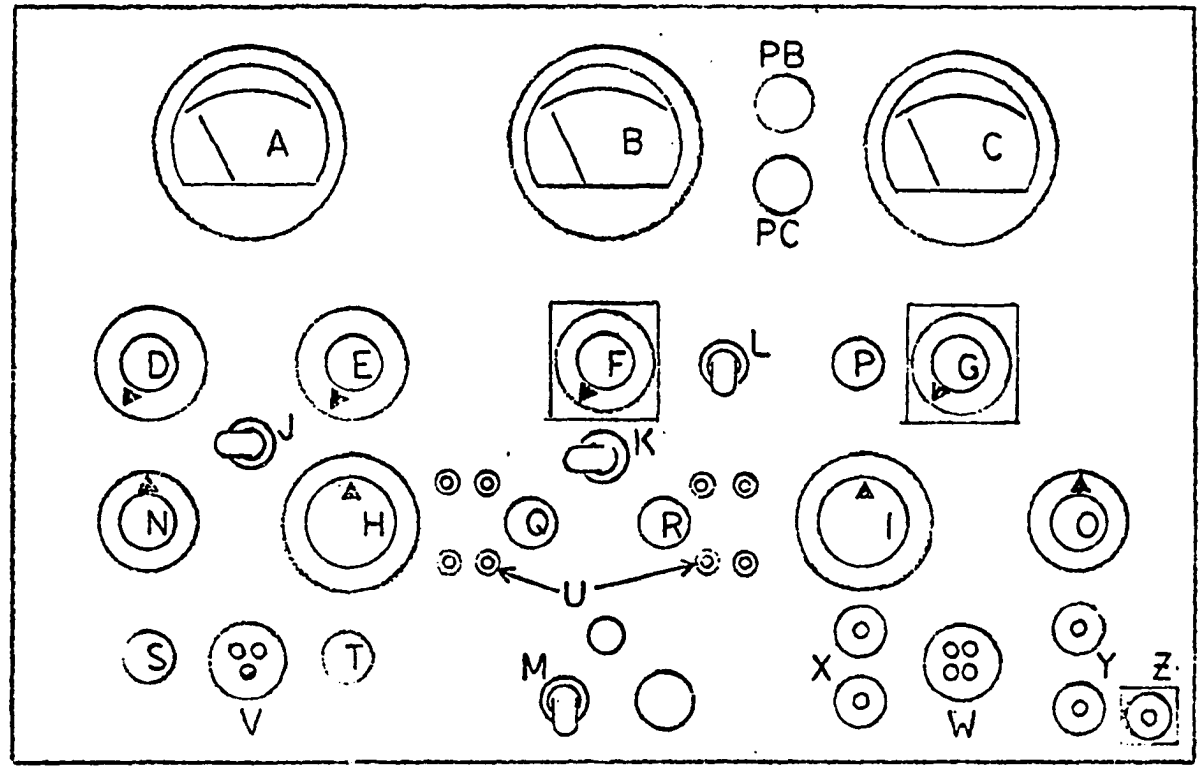

Figure 48. Front panel layout of the MF-305 flash unit showing meters A to C, pots D to I, PB, and PC, toggle switches J to M, rotary switches N and O, push-button switches P to T, and input/output jacks U to Z

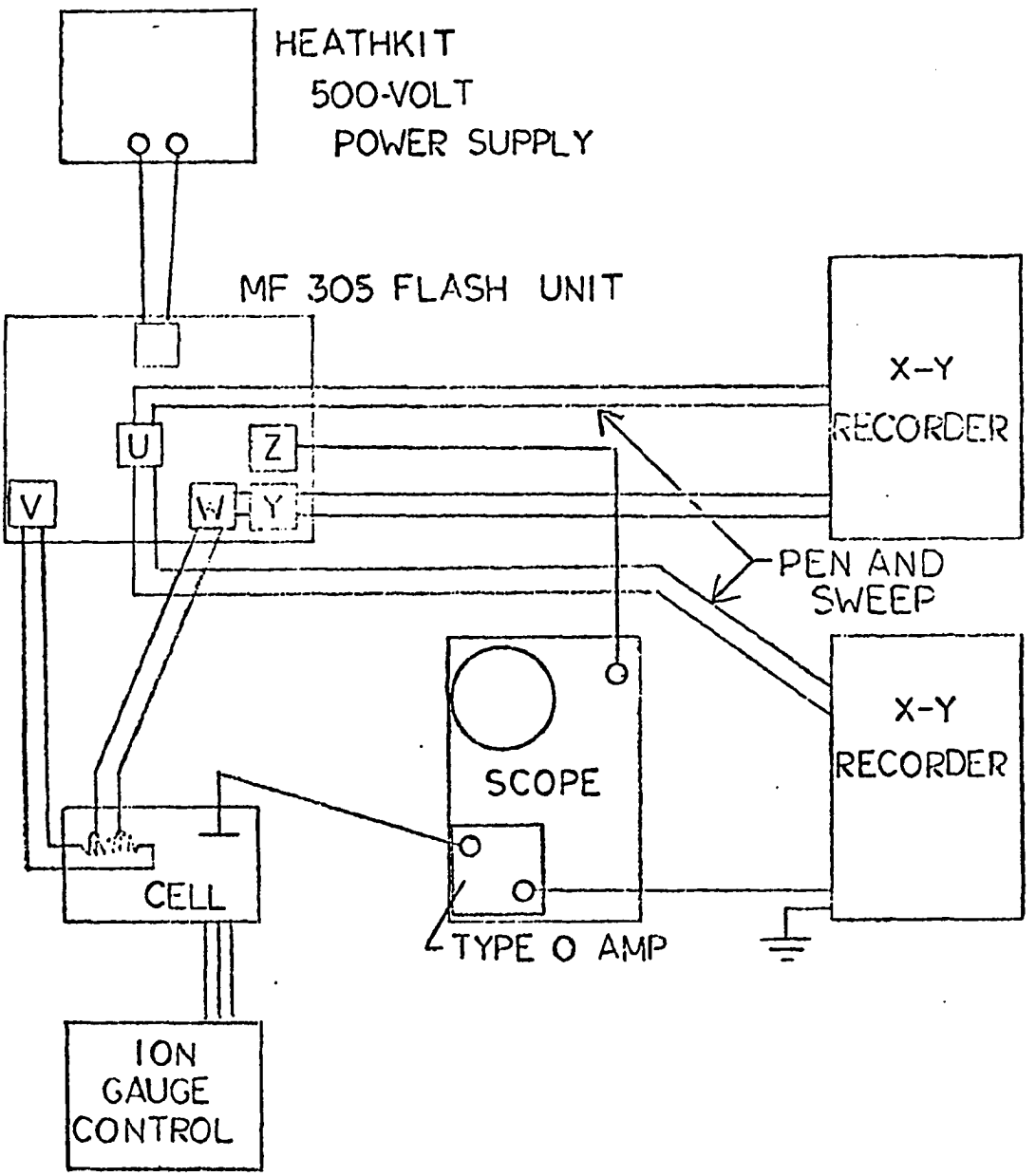

Figure 49. Isothermal flash filament data-recording system

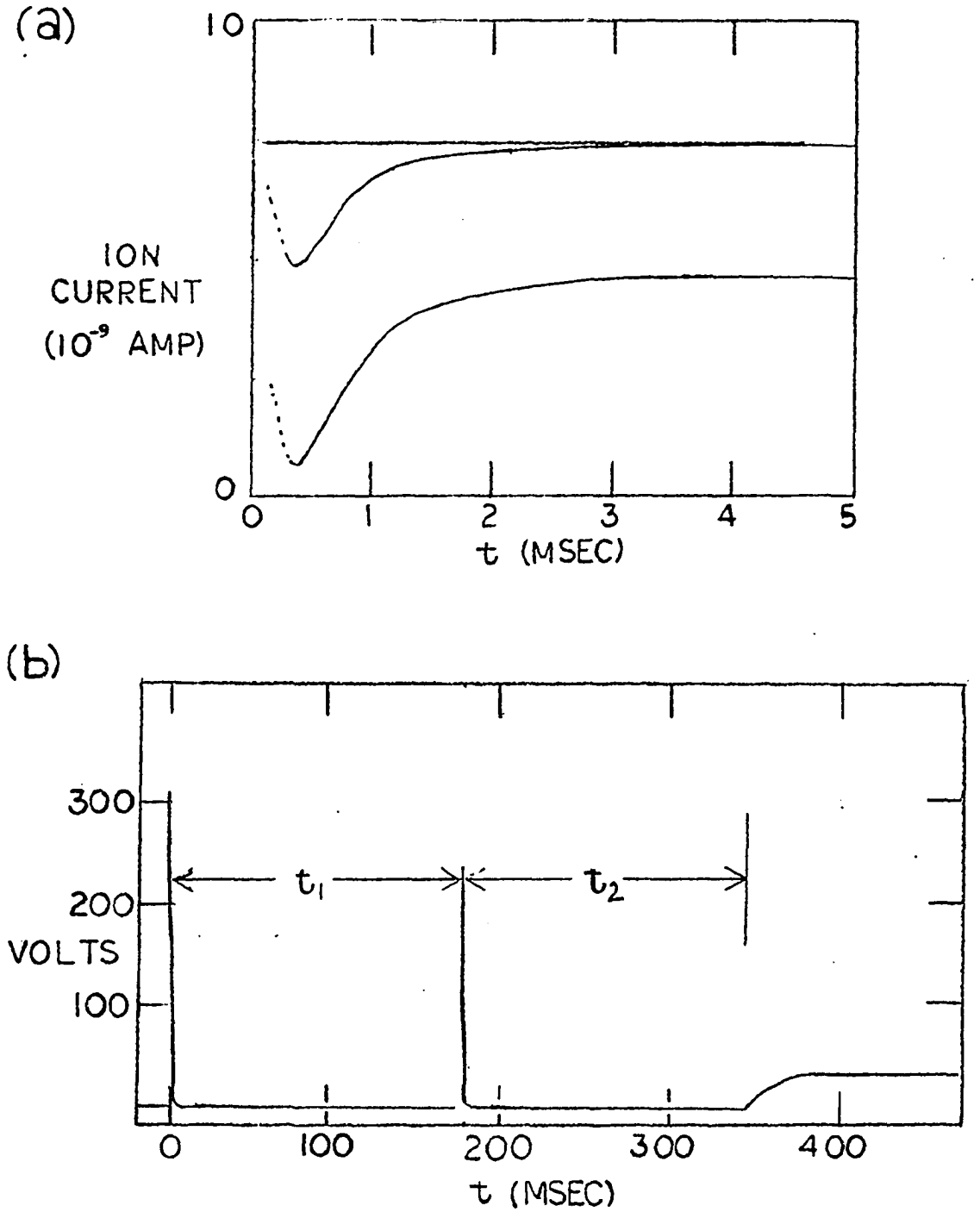

Figure 50. Oscilloscope trace (a) showing the pressure (ion current) increases resulting from heating the filament with a voltage function similar to that in (b), generated from two successive capacitor discharges followed by a constant-voltage heating current

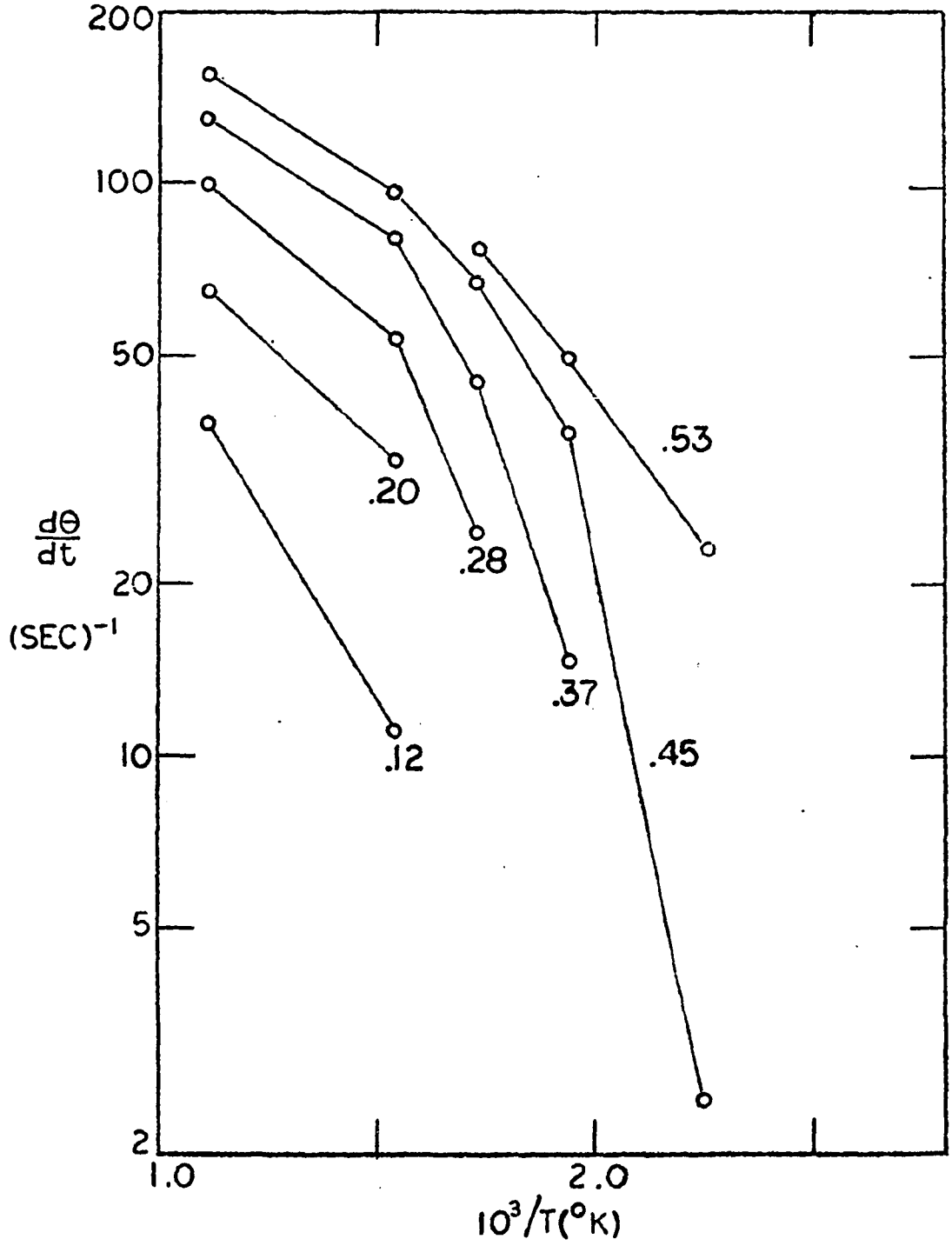

Figure 51. Rate of desorption of hydrogen from tungsten plotted for constant coverages (θ) against the reciprocal desorption temperature

TABLES

Table 1. Typical f_m values for various gases of interest

Gas	m	f_m
Argon	40	1.00
C_2H_6	30	0.26
C_2H_4	26	0.38
CH_4	16	1.48
H_2	2	1.78
HD	3	0.89
D_2	4	0.65
$\sum_{n=0}^{6} C_2H_{6-n}D_n$	E	1.85
$\sum_{n=0}^{4} CH_{4-n}D_n$	M	3.14

Table 2. Slope and intercept data from hydrogen isotherm test (Figure 15)

T (°C)	Slope	b ($\mu^{-1/2}$)
-130	0.99	12 ± 1
- 78	1.18	11 ± 1
0	-	7 (est.)
100	0.98	3.0 ± .3

Table 3. Calculation of the D_2-predose loss from hydrogen isotopic distribution before and after C_2H_4 dose (Experiment IV)

Hydrogen (10^{18} atoms)	^1H	D	Total
Predose at 20 μ	.02	.98	1.00
C_2H_4 dose	3.26	-	3.26
Gas phase at equil. (as CH_4)	2.44	.40	2.84
On surface at equil.	.84[a]	.14[b]	.98
Total at equil.	3.28	.54	3.82

$$\% \ D_2 \text{ predose lost} = \frac{.98 - .54}{.98} \times 100 = 45\%$$

[a]Calculated assuming that none of the predosed ^1H atoms were lost.

[b]Calculated assuming that the surface H-D composition was equal to gas phase composition. The experimentally determined percentages of deuterated methanes (in order from d_0 to d_4) with the calculated (binomial theorem) distribution in parentheses were 54.2 (55.0), 36.1 (35.1), 8.6 (8.95), 1.01 (0.98), and 0.08 (0.04).

Table 4. C_2H_6 decomposition on Ir films at 100° C

	Experiment	XII	XIII	XIV	XV
1	Film thickness[a] (Å)	187	187	80	80
2	s (no. of H sites) x 10^{-18}	3.75	3.75	1.6	1.6
3	D_2 predose/s (atom/site)	.27	.27	.28	-
4	C_2H_6 dose (10^{18} molecules)	.938	1.015	.208	1.00
5	C_2H_6 dose/s (molecule/site)	.25	.27	.16	.62
	Final Gas Composition				(1000 sec)
6	CH_4 (10^{18} molecules)	1.34	1.52	.31	1.22
7	H_2 " "	.03	< .03	< .01	.01
8	C_2H_6 " "	-	-	-	.16

[a]Calculated from 100° C saturation coverage when hydrogen predose was used, otherwise measured as described in Experimental.

Table 4. (Continued)

	Experiment	XII	XIII	XIV	XV
	Surface Composition (atom/site)				
9	n_C/s (max)	.142	.186	.092	.38
10	n_C/s (final)	.142	.133	.062	.38
11	n_H/s "	.34	.27	.28	.29
12	$\frac{\text{No. of } CH_4 \text{ molecules produced}}{\text{No. of } C_2H_6 \text{ molecules adsorbed}}$	1.43	1.50	1.49	1.22
13	$r_M \times 10^{-15}$ (molecules/sec)	.22	6.5	3.9	2.8
14	$(r_M/s) \times 10^3$ (molecules/sec/site)	.060	1.7	2.4	1.8
15	Initial C_2H_6 ads. (10^{18} molecules)	-	.17	.04	.07
16	Initial C ads. (atom/site)	-	.090	.050	.088
17	d ln $N_E/dt \times 10^3$ (sec^{-1})	-	11	31	5.0
18	$\frac{d \ln N_E}{sdt} \times 10^{21}$ (sec-site)$^{-1}$	-	2.9	19	3.1

Table 5. C_2H_4 high pressure doses

	Experiment	I		
1	Temperature (° C)	100		
2	Film thickness[a] (Å)	102		
3	s x 10^{-18} (sites)	2.04		
4	Hydrogen predose (10^{18} molecules)	-		
5	x_d(C_2H_4 dose) x 10^{-18} (molecules)	1.5		
6	x_d/s (molecule/site)	.74		
7	Contact time (sec)	500	1000	9000
8	N(C_2H_6) x 10^{-18} (molec.)	.29	.32	.39
9	$\Delta N(C_2H_4)$ x 10^{-18} "	.80	.83	.98
10	n_C^* x 10^{-18} (atoms)	.44	.38	.40
11	n_C^*/s (atom/site)	.22	.19	.20
12	n_C x 10^{-18} (atoms)			1.18
13	n_C/s (atom/site)	.49	.49	.58
14	r_M/r_M^o	-	-	-

[a]Calculated from 100° C saturation coverage when hydrogen predose was used, otherwise measured as described in Experimental.

[b]Value calculated from the measured saturation coverage (20 μ) at T and the coverage (Θ_T) given by Equation 12, assuming an equilibrium hydrogen pressure of 0.2 μ following removal of the saturation ambient.

II	IIIa	IIIb	IV	V	VI	VII
100	100	100	100	0	- 78	-130
110	50	50	124	138	128	104
2.20	1.0	1.0	2.45	2.75	2.55	2.08
-	-	-	.27	.65[b]	.84[b]	.79[b]
.74	.40	.42	.815	.805	.755	.83
.33	.40	.42	.33	.29	.30	.40
500	500	1000	100	500	500	500
.305	.15	.24	.27	.39	.44	.41
.74	.40	.55	.815	.805	.755	.78
.26	.20	.15	.55	.05	- .25	- .08
.12	.20	.15	.23	.02	- .10	- .04
.86	.49	.62	1.02	.83	.63	.71
.39	.49	.62	.42	.30	.25	.34
.001	.01	-	.16	-	-	-

Table 6. C_2H_4 low pressure doses (100° C)

	Experiment	VIII	IX	X	XI
1	Film thickness[a] (Å)	50	60	50	100
2	s x 10^{-18} (sites)	1.0	1.2	1.0	2.05
3	Hydrogen predose (10^{18} molec.)	-	-	.11	.23
4	Total C_2H_4 dose "	.35	.685	.432	1.29
5	r_d x 10^{-15} (molecules/sec)	.65	1.73	1.56	.257
6	(r_d/s) x 10^{-3} (sec^{-1})	.65	1.45	1.56	.125
7	t_1-t_0 (sec)	107	65	30	150
8	n_C/s (atom/site)	.132	.165	.086	.04
9	n_H/s "	.248	.31	.34	.29
10	$(n_H-n_C)/s$ "	.116	.145	.25	.25
11	t_2-t_0 (sec)	425	175	140	2780
12	n_C/s (atom/site)	.415	.404	.345	.482

[a]Calculated from 100° C saturation coverage when hydrogen predose was used, otherwise measured as described in Experimental.

Table 6. (Continued)

	Experiment	VIII	IX	X	XI
13	n_H/s (atom/site)	.53	.56	.53	.73
14	$(n_H-n_C)/s$ "	.115	.16	.185	.25
15	n_H/n_C	1.28	1.39	1.54	1.52
16	$[n_C + 2N(C_2H_6)]/s$ (atom/site)	.44	.425	.39	.495
17	$[n_C - n_C(t_1) + 2N(C_2H_6)]/s$ (atom/site)	.31	.36	.30	.455
	Final composition				
18	$N(H_2) \times 10^{-18}$ (molecules)	.02	.01	.03	.03
19	$N(CH_4) \times 10^{-18}$ "	.125	.09	.051	.45
20	$N(C_2H_6) \times 10^{-18}$ "	.06	.20	.215	.22
21	$N(C_2H_4) \times 10^{-18}$ "	-	.14	-	.11
22	n_C/s (atom/site)	.45	.48	.38	.70
23	n_H/s "	.48	.48	.39	.95
24	n_H/n_C	1.07	1.0	1.03	1.36

Table 6. (Continued)

	Experiment	VIII	IX	X	XI
25	r_M/r_d	.69	.46	.41	.70
26	r_E/r_d	.80	.69	.96	.56
27	$r_M/(r_M)_{max}$	.38	.78	.49	.11

Table 7. Experimental evaluation of $a = k_1/k_2$

Experiment	IX		XI	
t (sec)	151	175 = t_2	2450	2800 = t_2
$n_C \times 10^{-18}$ (molecules)	.423	.484	.86	.99
$2N(C_2H_6) \times 10^{-18}$ (molecules)	.012	.026	.010	.030
θ	.83	.95	.84	.97
y/x_m	.024	.051	.010	.030
$-\ln(1-\theta) - \theta$	.94	2.05	.99	2.5
$a = k_1/k_2$	40 ± 10	40 ± 10	99 ± 25	83 ± 25

Table 8. C_2H_6 decomposition on Ir at 27° C as determined by Roberts

Source	Table I (6)		Figure 1 (7)
Film thickness (Å)	80	244	306
Dose (10^{18} molecules)	1.28	1.28	1.54
Contact time (min)	1101	1475	1500
Products (10^{18} molecules)			
C_2H_6 (g)	.189	.147	.14
CH_4 (g)	.110	.154	.75
H_2 (g)	.072	.110	.01
C (ads)	2.07	2.11	2.05
H (ads)	5.96	5.96	5.38

Table 9. Correlation of Roberts' Rn film thickness with rate of C_2H_6 disappearance at 100° C (11)

Experiment	Film thickness (Å)	k (min^{-1})	.0143 x film thickness (min^{-1})
D1	30	.44	.43
D2	49	.68	.70
D3	175	.56	2.50
D4	14	.1	.20

BIBLIOGRAPHY

1. Bond, G. C. Catalysis by metals. New York, N.Y., Academic Press. 1962.

2. Arthur, J. R., Jr. and Hansen, R. S. Ann. N.Y. Acad. Sci., 101, 756 (1963).

3. Hansen, R. S., Arthur, J. R., Jr., Mimeault, V. J., and Rye, R. R. J. Phys. Chem., 70, 2787 (1966).

4. Tomcsik, T. L. Flash decomposition studies of simple hydrocarbons on iridium. Unpublished M.S. thesis. Ames, Iowa, Library, Iowa State University of Science and Technology. 1969.

5. Burns, R. A. Surface studies of simple hydrocarbons on iridium by flash decomposition. Unpublished Ph.D. thesis. Ames, Iowa, Library, Iowa State University of Science and Technology. 1970.

6. Roberts, R. W. J. Phys. Chem., 67, 2035 (1963).

7. Roberts, R. W. J. Phys. Chem., 68, 2718 (1964).

8. Dushman, S. Scientific foundations of vacuum techniques. 2nd ed. New York, N.Y., John Wiley and Sons, Inc. 1962.

9. Gabbe, D. R. and Hume, D. N. Anal. Chim. Acta, 30, 308 (1964).

10. Sandell, E. B. Colorimetric determinations of traces of metals. 3rd ed. New York, N.Y., Interscience Publishers, Inc. 1959.

11. Roberts, R. W. Trans. Faraday Soc., 58, 1159 (1962).

12. Beeck, O., Smith, A. E., and Wheeler, A. Proc. Roy. Soc. (London), A177, 62 (1941).

13. Trapnell, B. M. W. Trans. Faraday Soc., 51, 368 (1955).

14. Gardner, N. C. and Hansen, R. S. J. Phys. Chem., 74, 3298 (1970).

15. Beeck, O. Discuss. Faraday Soc., 8, 118 (1950).

16. Block, J., Thimm, H., and Zühlke, K. J. Vac. Sci. Technol., 7, No. 1 (1970).

17. Rye, R. R. and Hansen, R. S. J. Phys. Chem., 73, 1667 (1969).

18. Woodward, R. B. and Hoffmann, R. The conservation of orbital symmetry. Weinheim, West Germany, Verlag Chemie, GmbH. 1970.

ACKNOWLEDGMENTS

The author would like to express his appreciation for the substantial work done by personnel of the Ames Lab glass shop, electronics shop, and machine shops in support of the research reported herein.

Many fellow students through the years have provided helpful advice and discussions, of both a practical and academic nature.

Particular thanks are extended to Melvin Tschetter, who was responsible for the weight analyses of the iridium films; to Dr. Orville Chapman for helpful discussions on the conservation of orbital symmetry; and most of all, to Dr. Robert S. Hansen for his continuing counsel, support, and encouragement.

APPENDIX A

Correction for Mass Spectrometer Sensitivity Variation

Consider a pumped flow system as shown in Figure 44 of two parts, the first of volume V at pressure P with N molecules of a single species, and the second of volume v at pressure p containing n molecules of the same species. There is a constriction of small conductance between the two parts such that p is very small compared to P.

The leak rate out of V is

$$-\frac{dN}{dt} = -\frac{V}{kT}\frac{dP}{dt} = \frac{V}{kT}gP \ , \qquad (29)$$

where g is a time constant (reciprocal time units) with its value assumed dependent solely on the conductance of the constriction and on the mass of the species present. (In practice, the value of g is controlled by the setting of valve A1, which is variable at will.) Similarly, the pumping rate out of v may be characterized by a time constant b, such that

$$-\frac{dn}{dt} = -\frac{v}{kT}\frac{dp}{dt} = \frac{v}{kT}bp \qquad (30)$$

When steady state conditions prevail in volume v, the leak rate in and the pumping rate out are equal, and consequently

$$p = \frac{gV}{bv}P \ . \qquad (31)$$

If ion current i_m of mass m is measured at pressure p (for a fixed emission current), we will assume a pressure dependence of the form

$$i_m = a_m \sigma_m P \ , \tag{32}$$

where σ_m is a sensitivity constant (current pressure^{-1} units) and a_m is a dimensionless coefficient which corrects for deviations from linearity in the current-pressure relationship. Then ion current is related to pressure P by

$$i_m = \left(\frac{\sigma_m V}{bv}\right) a_m g P \ , \tag{33}$$

where the term in parentheses is a constant. (Since a_m is to be determined experimentally from values of i_m and P, it may also incorporate deviations in b (nonlinear pumping), but in practice it is not necessary to separate this effect from the nonlinear ion current-pressure effect.)

To determine a_m as a function of i_m, arbitrarily select a standard state corresponding to a fixed ion current (say 1.0 μA), where $i_m = i_m^0$ and set $a_m^0 = 1.0$. (This defines σ_m if p is known.) For a fixed value of g, we then have

$$\frac{i_m}{i_m^0} = a_m \frac{P}{P^0} \ . \tag{34}$$

By varying P in known fashion and measuring i_m under steady

state conditions, we may obtain a plot of $i_m P^o (i_m^o P)^{-1}$ against i_m, which gives a_m as a function of i_m. This function is assumed valid for any practical combination of values of g and P.

Consider now two gaseous species in volume V with partial pressures P_1 and P_2. Their respective ion currents i_{m1} and i_{n2} will be related by

$$\frac{i_{m1}}{i_{n2}} = \frac{c a_{m1} g_1 P_1}{a_{n2} g_2 P_2} \tag{35}$$

which follows from Equation 33. The constant $c = \sigma_{m1} b_2 (\sigma_{n2} b_1)^{-1}$, where the subscripts 1 and 2 denote gas species. It is assumed in Equation 35 that the two species are perfectly independent of each other as to leak rate through A1, ionization in the mass spectrometer, and pumping.

Assume that a_{n2} has been determined as described above for an inert gas such as argon which will be used as a calibration gas at known pressure P_2 in an experiment. The problem then is to determine P_1 from i_{m1} by comparison with argon, by the relationship

$$P_1 = \frac{a_{n2}}{f_{m1}} \frac{P_2}{i_{n2}} i_{m1} , \tag{36}$$

which is just a rearrangement of Equation 35, where f_{m1} is a function of i_{m1} only, defined by

$$f_{m1} = \frac{c g_1}{g_2} a_{m1} . \tag{37}$$

To use Equation 36 for determining the pressure P_1 of any species of interest (e.g., H_2, C_2H_6, C_2H_4), we must determine the function f_{m1}. To do this, establish known partial pressures $P_1 = P_1'$ and $P_2 = P_2'$. Vary the conductance of A1 (which changes g_1 and g_2, but presumably not g_1/g_2) and measure i_{m1}, i_{m2}. Plot

$$f_{m1} = \frac{i_{m1}}{i_{m2}} \frac{P_2'}{P_1'} a_{n2} \tag{38}$$

as a function of i_{m1}.

It may be of interest also to determine a_{m1}, although this is not necessary for the application of Equation 36. As above, define $i_{m1} = i_{m1}^0$ at $a_{m1} = a_{m1}^0 = 1.0$ and $f_{m1} = f_{m1}^0$. Then

$$a_{m1} = \frac{f_{m1}}{f_{m1}^0} . \tag{39}$$

APPENDIX B

Conservation of Orbital Symmetry in Concerted Hydrogenation

In Figure 42 is shown a C_2H_4 polymer adsorbed on the 110 face of Ir. The reaction to be considered is the concerted abstraction of hydrogen from carbons 1 and 3 by a gaseous C_2H_4 molecule as shown in Figure 43a. This reaction has a nontrivial element of symmetry (mirror plane) and hence is subject to the conservation of orbital symmetry (18). The numbering of the carbon atoms in Figure 43a corresponds to that of Figure 42; the reaction, however, is assumed to be general for any section of the polymer chain, and may be written

$$\underset{*}{RCHCH_2}\underset{*}{CHR} + C_2H_4\,(g) \rightarrow C_2H_6\,(g) + \underset{*}{H}^{-} + [\underset{*}{RC}=\overset{\oplus}{\underset{*}{C}}\underset{*}{HCR} \longleftrightarrow \underset{*}{RC}\overset{\oplus}{\underset{*}{C}}H=\underset{*}{CR}] \qquad (x)$$

where the stars (*) represent adsorption sites (Ir atoms in this case). The R groups (not shown in Figure 43) may be hydrogen atoms or hydrocarbon groups; it is not necessary that they be identical, as the electronic effect for either is the same as far as the symmetry arguments are concerned. The adsorbed complex resulting from the reaction is an allyl radical (shown as a resonance hybrid in the above reaction) with a formal positive charge, and a hydrogen atom adsorbed to a subsurface Ir atom (see Figure 42 for

its location), with a formal negative charge. The origin of the charge separation is discussed below. Presumably the charges will be delocalized through the metal. For the approach of C_2H_4 as indicated in Figure 43a, the reaction has a plane of symmetry perpendicular to the page, in the position indicated by the dashed line.

To determine whether or not the reaction is symmetry allowed, it is necessary that all orbitals involved in bond breaking and bond forming be symmetric (S) or antisymmetric (A) with respect to the mirror plane. If any individual orbital does not possess one of these symmetry properties, it and one or more other orbitals must be combined to give orbitals which do.

The four molecular orbitals (σ_1, σ_2, σ_3, and π_1) and one atomic orbital (S_s) of the reactants are shown in Figure 43b just prior to reaction, in the configuration identical to that of Figure 43a. The approximate energy levels of these orbitals and their antibonding counterparts (σ_1^*, σ_2^*, σ_3^*, and π_1^*)--properly mixed so that symmetric or antisymmetric combinations are obtained--are shown at the left side of Figure 45 for C_2H_4 far from the surface. The product orbitals involved are shown in Figure 43c just after C_2H_6 has been formed and a hydrogen atom has been transferred from carbon 2 to the subsurface Ir atom. The approximate energy levels of the properly mixed product

orbitals are shown at the right side of Figure 45 for C_2H_6 far from the surface. Note that there are three allyl π orbitals: π_2 (bonding), π_2^o (nonbonding), and π_2^* (antibonding).

A reactant orbital may correlate only with a product orbital of like symmetry property--symmetric (S) or antisymmetric (A)--as shown in the correlation diagram (Figure 45). A central tenet of orbital symmetry conservation is that a concerted reaction is symmetry forbidden if an electron must be promoted in energy by an amount large compared to kT (e.g., as in a transition from a bonding orbital to an antibonding orbital) to satisfy the symmetry correlations. The reaction is symmetry allowed if no promotion of this magnitude is required.

As the correlation diagram is drawn the reaction is symmetry allowed, but it incorporates three assumptions concerning the subsurface Ir orbital S_s; if any of these assumptions is false, the concerted reaction as written is symmetry forbidden. It is assumed that the metal orbital S_s is: 1) symmetric with respect to the mirror plane; 2) vacant (contains no electrons), because it correlates with an antibonding orbital (π_2^*); 3) higher in energy than the ethylene π orbital (π_1), because otherwise π_1 will be forced to correlate with an antibonding orbital.

Of these restrictions, the second is probably the

most severe; because of it both electrons in the σ_s bond must be donated from the adsorbed complex, and this is the origin of the formal charge separation shown in reaction (x). But until more is known of the nature of the orbitals at the metal surface, no meaningful judgement based on symmetry arguments can be made as to the feasibility of this concerted mechanism.

APPENDIX C

Isothermal Flash Filament

In the conventional flash filament technique of studying adsorption, desorption, and thermal decomposition of gases on metals, one of the drawbacks is that upon heating (flashing) the filament the temperature along its length is not uniform. The nonuniformity arises principally from heat losses to the cooler supporting leads at the filament ends, and consequently is more pronounced the slower the heating rate. It was pointed out by Dr. Hansen that it should be possible to heat the filament very rapidly so that the conduction losses would become insignificant, and at the same time a simplification of the analysis of the desorption kinetics would result. That is, if heating to a given temperature were accomplished before a substantial fraction of the adsorbed gas desorbed, the subsequent desorption should be "isothermal".

The general kinetic equation for desorption is known as the Polanyi-Wigner equation, and may be written

$$- d\Theta/dt = \Theta^{x}\nu_{x}e^{-\Delta H/RT} .$$

The desorption coverage Θ is equal to n/n_0, the number of adsorbed molecules at time t divided by the number in a monolayer, and is experimentally determined from $\Theta = 1 - P/P_{max}$, where $P = (n_0 - n)kT/V$ (assuming n_0 molecules were

adsorbed before the flash began) and $P_{max} = n_0 kT/V$--if the ideal gas law is valid. ΔH is the heat of desorption, R the gas constant, T the absolute temperature, ν_x the frequency factor, and x the kinetic order--1 or 2 for most gases of interest.

Obviously, the rate of desorption is temperature dependent; hence kinetic analysis from conventional flash desorption must deal with T as a function of t. Generally this is done by approximating the temperature during flash with a function of the form $1/T = a + bt$ (a and b are experimentally determined constants). For isothermal desorption, however, the Polanyi-Wigner equation reduces to the simple kinetic equation

$$- d\theta/dt = k_x \theta^x$$

if ΔH is independent of θ.

Since isothermal desorption was necessarily rapid, the filament and ion gauge were mounted in a single large cell (Figure 46) made of Pyrex tubing 10 cm in diameter and 18 cm long. The ion gauge parts were taken from a conventional ion gauge and sealed into the cell. One of the tungsten filaments was replaced with a BaO-SrO-coated rhodium filament (low work function) to minimize pumping of hydrogen by thermal decomposition. The cell was connected to a standard ultrahigh vacuum system through

a magnetically operated ground-glass valve.

Preliminary investigations with hydrogen adsorption on a tungsten filament showed a thyratron (type 5720 electronic vacuum tube, mercury-filled) to be superior to a mechanical relay for closing the circuit to discharge the capacitor. For reasons that will become evident below, it was found advantageous to be able to discharge two capacitors in succession across the filament.

To this end, an electronic unit (MF-305) was constructed to specifications by the electronics shop. A block diagram of the circuitry is shown in Figure 47, and Figure 48 shows location of controls on the front panel of the unit. The letters inscribed in squares in the block diagram correspond to the labels shown on the front panel diagram. Underlined labels in the block diagram are found on the front panel itself.

The circuitry incorporates two capacitors--Cap. 1 (60 μF) and Cap. 2 (140 μF)--each connected to a thyratron for discharge. An external power supply (see Figure 49), connected via rear panel jacks, supplied 500 volts for charging the capacitors. The voltages, displayed on meters B and C, were adjustable with pots PB and PC, respectively. Either capacitor was capable of raising the filament temperature several hundred degrees with a rise time (capacitor discharge time) of less than 2 msec.

A time-delay circuit activated by push button P applied firing pulses to the two thyratrons at a time interval t_1 seconds apart (variable from 20 to 500 msec, pot F). After a second time interval (variable from 50 to 500 msec, pot G) the timing circuit activated a relay (K1) which disconnected the filament from the discharge circuit and connected it to a current source preselected by switch N. The outgas current was used for cleaning the filament ($\sim 2800^{\circ}$ K), desorb current for desorbing ($\sim 1000^{\circ}$ K) any hydrogen not removed by the discharges. The monitor circuit furnished a 0-25 mA current (negligible filament heating) for calibration of filament resistance and following the temperature after heating. (As in conventional flash filament, temperature was determined from the resistance between the sensing leads of the filament.) The monitor circuit incorporated known resistors in series (with the filament) and the voltage drop across them could be taken out to a recorder through switch O. Any one of these current sources could be connected to the filament by pushing switch S, without activating the timing circuit.

Jacks U connect to a set of relay contacts (K4) used for initiating recorder sweep (in time sweep mode) and pen lowering. The X-Y recorders were used for monitoring temperature following flash and (in some cases) the final desorption pressure. The relay contacts could be closed

independently of the timing circuit by pushing switch Q.

Normally to measure filament temperature following flash, the monitor current (e.g., 20 mA) was switched in (through relay K2) and the resultant voltage drop across the sensing leads was followed on the recorder. To avoid overloading the recorder during discharge, and to minimize pen travel (for faster response) following flash, a voltage (0 to 1.35 v) approximately equal to the anticipated filament IR drop was applied to the recorder input prior to and during flash.

Data were obtained with the system shown in Figure 49. A typical set of pressure (ion current)-time curves obtained from a photograph of the oscilloscope screen is shown in Figure 50a. Figure 50b illustrates the two capacitor discharges followed by a heating current. The oscilloscope trace was triggered by the voltage pulses, and usually the transients arising when switching in the heating current were also sufficiently large to trigger a trace (the horizontal trace in Figure 50a). The tailing seen at the beginning of the desorption traces is due to interaction of the ion gauge circuit with the discharge circuit in the cell.

Figure 51 shows a family of curves--each obtained at constant coverage (θ)--plotting the rate of desorption against the reciprocal of the desorption temperature. The

plots represent data from five isothermal desorption curves at temperatures ranging from 445 to 850° K. H_2 was dosed ($\sim 10^{-7}$ torr) to saturation at 300° K in each case. The filament was then heated by capacitor discharge to the temperature of interest and then to a second temperature high enough to give complete desorption on the second discharge, giving curves similar to the lower two in Figure 50a. P_{max} was taken as the limiting value of the upper, and $d\theta/dt$ values were measured on the lower curve by graphical differentiation. Surface coverage θ was calculated from $\theta = 1 - P/P_{max}$ with P and P_{max} in arbitrary units. (Pumping was negligible.)

If the Polanyi-Wigner equation is valid, these plots should be linear (regardless of variation of ΔH with θ). It was concluded that because of the evident nonlinearity, the pressure measured on the ion gauge was not a valid measure of the gas desorbed at these desorption rates. Presumably the gas density is higher near the filament than it is at the ion gauge; in other words, the ideal gas law was not valid under these conditions, and the ordinates of the points in Figure 51 are really not $- d\theta/dt$.

Theoretically, one should by proper selection of desorption temperature be able to achieve a suitable rate of desorption at which the pressure will be essentially equilibrated during desorption. In practice, however, pumping

(of walls, ion gauge, etc.) and the variation of ΔH with θ puts very severe restrictions on the temperatures that can be used.

If a suitable detector could be devised which would measure gas flux directly (e.g., a cryostated cell where the adsorption coefficient on the cell would be nearly unity) rather than an equilibrated pressure, the technique could yet prove viable.